UNIVERSITY OF CALIFORNIA, SAN DIEGO

Effects of non-linear processing on information transfer in the lateral geniculate nucleus

A dissertation submitted in partial satisfaction of the

requirements for the degree Doctor of Philosophy

in

Biology / Specialization in Computational Neurobiology

by

Kate Denning

Committee in charge:

Professor Daniel E. Feldman, Chair
Professor Jeffry S. Isaacson
Professor Richard Krauzlis
Professor Pamela Reinagel
Professor Jack Wolf

2006

The dissertation of Kate Denning is approved, and it is acceptable in quality and form for publication on microfilm:

_____

_____

_____

_____

_____
Chair

University of California, San Diego

2006

Table of Contents

List of Figures

Acknowledgements

I was fortunate to have the experience of being the first student to join the lab of Pam Reinagel. Not only was I able to learn about how to collect and analyze data, write papers, and give effective presentations, but I was able to observe the development of the lab. I sincerely appreciate all of the time, effort, and creative ideas that Pam has offered me during graduate school.

I would also like to thank members of my thesis committee, Dan Feldman, Rich Krauzlis, Jack Wolf, and Jeff Isaacson for their contributions to my research and their support.

Samar Mehta offered continuous help throughout graduate schools, enabling me to quickly progress through projects that would have easily taken much longer. I am very grateful for his help, patience, and time. Erik Flister and Philip Meier joined the lab two years after me, and they have made great intellectual and social contributions to the lab.

All experimental data could not have been attained without the help of our outstanding technician, Pam Magoffin. Her long hours, meticulous work, and support were very valuable.

Special thanks to my parents, Tom and Deb Denning, who have always supported me and have provided educational opportunities that enabled me to be where I am today. Finally, I am grateful for the daily support that I receive from my fiancé, Quentin Gaudry. His advice and encouragement has helped me get through both the exciting and frustrating days in graduate school.

Chapter 2, in full, is a republication of the material as it appears in Denning, K.S., Reinagel, P., Visual control of burst priming in the anesthetized LGN. *J Neurosci.* 25, 3231-3238 (2005). The dissertation author was the primary investigator and first author of this paper.

Chapter 4, in full, is a republication of the material submitted in June of 2006. K.S., Reinagel, P., Functional benefits of contrast normalization demonstrated in neurons and model cells. (2006). The dissertation author was the primary investigator and first author of this paper.

Chapter 5, in full, is a republication of the material submitted in June of 2006. K.S., Reinagel, P., Contrast adaptation in a non-adapting LGN model. (2006). The dissertation author was the primary investigator and first author of this paper.

Vita

2000 B.S., Physics, *cum laude*, Fort Hays State University

2006 Ph.D., Biology / Specialization in Computational Neurobiology,
University of California, San Diego

Publications

Peer reviewed competitive journals:

Denning KS, Reinagel P., Functional benefits of contrast normalization demonstrated in neurons and model cells. Nature. Submitted.

Denning KS, Reinagel P., Contrast adaptation in a non-adapting LGN model. J Neurosci. In preparation.

Denning KS, Reinagel P., Visual control of burst priming in the anesthetized LGN. J Neurosci. 25, 3231-3238 (2005).

Kenyon GT, Moore B, Jeffs J, Denning KS, Stephens GJ, Travis BJ, George JS, Theiler J, Marshak DW. A model of high-frequency oscillatory potentials in retinal ganglion cells. Vis Neurosci. 20(5), 465-480 (2003).

Anto RJ, Mukhopadhyay A, Denning K, and Aggarwal BB., Curcumin (diferuloylmethane) induces apoptosis through activation of caspase-8, BID cleavage and cytochrome C release: its suppression by ectopic expression of bcl-2 and bcl-xL. J Carcinogenesis. 23, 143-150 (2002)

Awards

National Science Foundation Fellow
National Physical Science Consortium Fellow
Vision and Learning in Humans and Machines: Integrative Graduate Education and Research Traineeship Fellow

ABSTRACT OF THE DISSERTATION

Effects of nonlinear processing on information transfer

in the lateral geniculate nucleus

by

Kate Denning

Doctor of Philosophy in Biology / Specialization in Computational Neurobiology

University of California, San Diego, 2006

Professor Daniel E. Feldman, Chair

Visual neurons' spike trains represent a large variety of visual stimuli. The local contrast varies across natural scenes, and the absolute luminance changes that define visual features during low-contrast stimuli are much smaller than during high-contrast stimuli. The contrast of the scene can remain relatively stable for an extended period of timing, suggesting that it would be advantageous for the neuron to adjust its coding strategy to the stimulus contrast. However, the contrast can also rapidly change. If the neuron utilizes different coding strategies during different stimulus conditions, it is imperative that the neuron be able to recognize when the statistics of the stimulus have changed. We propose that neurons in the lateral geniculate nucleus (LGN) utilize nonlinear properties in order to encode visual information across a variety of stimulus conditions. In Chapters 2 and 3, we find that bursts and single

spikes represent distinct stimuli, such that distinguishing between the bursts and single spikes provides information about the stimulus. Because bursts only occur following prolonged hyperpolarization, this suggests a means by which the neuron can encode the stimulus context: bursts may provide information about whether a stimulus is surprising given the recent stimulus history. In Chapter 4, we report the contrast normalization allows LGN neurons to encode information about stimuli across a wide range of local contrasts. Cells exhibiting strongest contrast normalization are best able to preserve information across stimuli. Furthermore, both the contrast normalization and the associated preservation of information could be reproduced by a non-adapting LGN model. In Chapter 5, we report other contrast-dependencies of the model, show transient changes in the model responses following a contrast change, and describe why the model is able to exhibit contrast normalization.

Chapter 1

Introduction

Natural scenes

Visual systems must be able to encode information about natural stimuli, but this is a difficult task, as there are a broad range of natural stimuli, characterized both by a wide range of light intensities and long temporal correlation (Figure 1.1A and Dong and Atick, 1995). In Figure 1.2A, the range of intensities and the temporal correlations are shown for one time-varying natural-scene stimulus from (van Hateren, 1997). These stimuli were obtained by a person walking in natural environments wearing a photodetector with spatial resolution similar to a human cone. We calculated the temporal contrast of this stimulus using 500-ms, non-overlapping bins, where contrast is defined as the standard deviation of the luminance divided by the mean. We note that by this definition of contrast, the contrast is always positive and can be greater than 100%. The correlations in addition to the rapid transitions in the stimulus intensity result in a variety of contrasts throughout the stimulus.

Across nine hours of time-varying natural stimuli from van Hateren (1997), we calculated the distribution of contrasts (Figure 1.2A). Most stimulus epochs were characterized by contrasts between 11% and 100% (Figure 1.2B). This measurement depended slightly on the window size used to calculate the contrast: higher contrasts were more probable when longer windows were used (Figure 1.2C).

This analysis suggests that in order to effectively visualize natural scenes, neurons must be able to represent stimuli across a variety of luminance values and contrasts. If the neuron uses a different coding strategy to represent stimuli of different statistics (i.e., contrast or luminance), then the neuron must be able to quickly recognize when the statistics of the stimulus has changed.

Detecting stimulus changes

As neurons' integration time is short (approximately 50 ms), one might imagine that it would be difficult to detect a change in stimulus. However, thalamic relay cells have voltage-gated T-type calcium channels. The state of these channels is influenced by longer stimulus epochs, and the state determines the type of spiking response that the neuron will elicit.

At depolarized membrane potentials, these channels are inactive, and the cell will respond to a reasonably large depolarization, such as a retinal EPSP, with a single spike. After sustained hyperpolarization, the channels are de-inactivated, and the same depolarization will cause a calcium spike. This calcium spike causes a high-frequency burst of sodium spikes (Jahnsen and Llinas, 1984).

Thus, thalamic relay cells are equipped with a channel which enables downstream neurons to determine some details about the more extended stimulus history merely by recognizing whether the spiking response was a burst or a single spike. If the response was a burst, then it could be inferred that the depolarizing activity occurred after an extended period of inactivity. Perhaps the function of bursts is to ensure that information about excitatory stimuli (high luminance or high contrast) is transmitted when these stimuli are preceded by less-excitatory stimuli (low luminance or low contrast). In this regard, it has been hypothesized that bursts may serve as a "wake-up call" (Sherman, 2001).

Indeed, the different response types are associated with different synaptic efficacies (Swadlow and Gusev, 2001), suggesting the existence of parallel pathways.

In the lateral geniculate nucleus (LGN), it seemed plausible that visual stimuli would influence the channel's state, but only 10% of synapses onto an LGN relay cell are from retinal ganglion cells, with the remainder coming from cortical feedback, interneurons, and non-visual sub-cortical areas (Erisir et al., 1997). Although the timing of bursts had been shown to encode visual information (Reinagel et al., 1999), this may simply be the result that both bursts and spikes were triggered by retinal EPSPs. Therefore, spikes and bursts may not encode distinct visual information.

In order to investigate this possibility, we recorded extracellularly in the cat LGN to determine whether bursts and single spikes are reliably elicited by different visual stimuli. In Chapter 2, we report that bursts are more frequent when natural stimuli are presented than when white noise stimuli are presented. Additionally, we report that bursts and single spikes do occur at distinct times within the stimuli and distinguishing between the responses does provide visual information. In Chapter 3, we further investigate the state-information measure presented in Chapter 2, and discuss the information associated with distinguishing bursts from other, related patterns.

Effective coding across stimulus conditions

Because natural scenes include a variety of contrasts (Figure 1.2), it is important to be able to encode fluctuations in both situations. Fluctuations in luminance can be caused by objects entering or exiting visual fields. Contrast depends on the magnitude of the absolute variations in luminance within the stimuli: in high-

contrast stimuli, large fluctuations occur, whereas in low-contrast stimuli, small fluctuations occur.

The reason that it is difficult for one neuron to encode stimuli at both contrasts can be illustrated by the following example. Suppose that a cell responds to different luminance values by eliciting a different number of spikes. At the lowest luminance value (Luminance=0), suppose it fires no spikes, and at the highest (Luminance=100), suppose is fires 25 spikes a second. Suppose that the cell can never fire more than 25 spikes a second. For all intermediate values, the cell fires an intermediate number of spikes. At high contrast, suppose the luminance values range from 0 to 100 and the cell's spiking rate can be used to differentiate the luminance values into 25 categories. At low contrast, suppose the luminance values range from 45 to 55. The more limited luminance range means that, at best, the cell would only fire three different spiking rates during the low-contrast stimulus. Therefore, the cell's spiking response could not capture much of the structure in the low-contrast stimulus.

Conversely, if the cell's spiking range matched that of the low-contrast stimulus, such that it fired no spikes when Luminance=45 and 25 spikes a second when Luminance=55, then the spiking rate would be informative about the low-contrast stimulus. During the high-contrast stimulus, however, the spiking rate would be equal to zero for all luminance values below 45 and saturated at 25 spikes a second for all luminance values above 55. Therefore, the cell's spiking response could not capture much of the structure in the high-contrast stimulus.

Contrast normalization is one mechanism that addresses this problem in the early visual system (Enroth-Cugell and Robson, 1966; Shapley and Victor, 1978;

Shapley and Victor, 1979; Shapley and Victor, 1981; Shapley and Enroth-Cugell, 1984; Ohzawa et al., 1985; Shapley, 1997; Benardete and Kaplan, 1999; Sanchez-Vives et al., 2000a, b; Chander and Chichilnisky, 2001; Kim and Rieke, 2001; Rieke, 2001; Baccus and Meister, 2002; Kim and Rieke, 2003; Solomon et al., 2004; Zaghloul et al., 2005). The dependence of neurons' spiking rates on luminance values varies with the stimulus contrast. Although this seemed to be an advantageous strategy to encode multiple contrasts, no study had quantified how beneficial contrast normalization is. Because spike timing can be as important as the firing rate (Reinagel and Reid, 2000), there is no guarantee that simply adjusting the dependence of the neuron's firing rate on the stimulus would in fact improve the information that the neuron was able to encode about the stimulus. The information rates depend on the reliability and precision of responses, in addition to the firing rate. In Chapter 4, we show that LGN cells do exhibit contrast normalization. Although the reliability and precision decrease as the contrast decreases across all cells, cells described by stronger contrast normalization are better able to preserve their information across contrasts.

Although there has been some investigation on active adaptive mechanisms that cause contrast normalization (Sanchez-Vives et al., 2000b; Kim and Rieke, 2001, 2003), theoretical studies have also emphasized that stationary nonlinear properties of neurons can account for some properties of contrast normalization and adaptation (Borst et al., 2005; Yu and Lee, 2005; Yu et al., 2005). In Chapter 4, we demonstrate that a non-adapting model exhibits contrast normalization, and the extent of contrast normalization is correlated with the degree of information preservation.

In Chapter 5, we determine how contrast normalization depends on model parameters and explore how the non-adapting model is able to exhibit contrast normalization. We also show that the reliability, precision, and latency of the responses exhibit similar contrast-dependencies to those found in LGN neurons. Finally, we report that transient changes in responses following a contrast change do not imply an active adaptation process: our non-adapting model can exhibit transient changes in both its firing rate and information rate.

Conclusions

In my thesis, I have shown that intrinsic nonlinearities in LGN cells could enable cells to encode information about natural scenes, which are characterized by a variety of rapidly-varying stimulus contrasts. I analyze in detail the information made available by state of the T-type calcium channels, which determines whether spiking responses will be single spikes or bursts of spikes (Chapter 2 and 3). This channel may provide a mechanism by which downstream neurons are able to compare present stimuli to recent stimulus history. I quantify the effect of contrast on reliability, precision, and information, and report that the degree of contrast normalization in LGN cells is correlated with information preservation across contrasts (Chapter 4). Finally, I found that both the contrast normalization and the information preservation can be described, at least in part, without any active adaptation (Chapter 4 and 5).

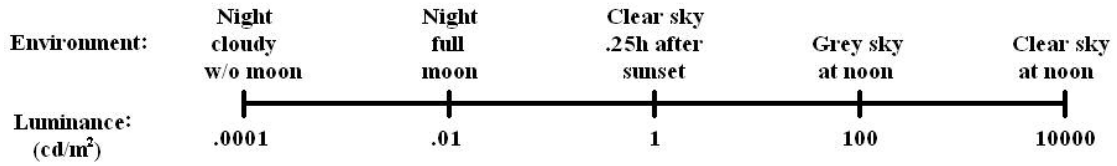

Figure 1.1: Range of luminance values observed in natural scenes.

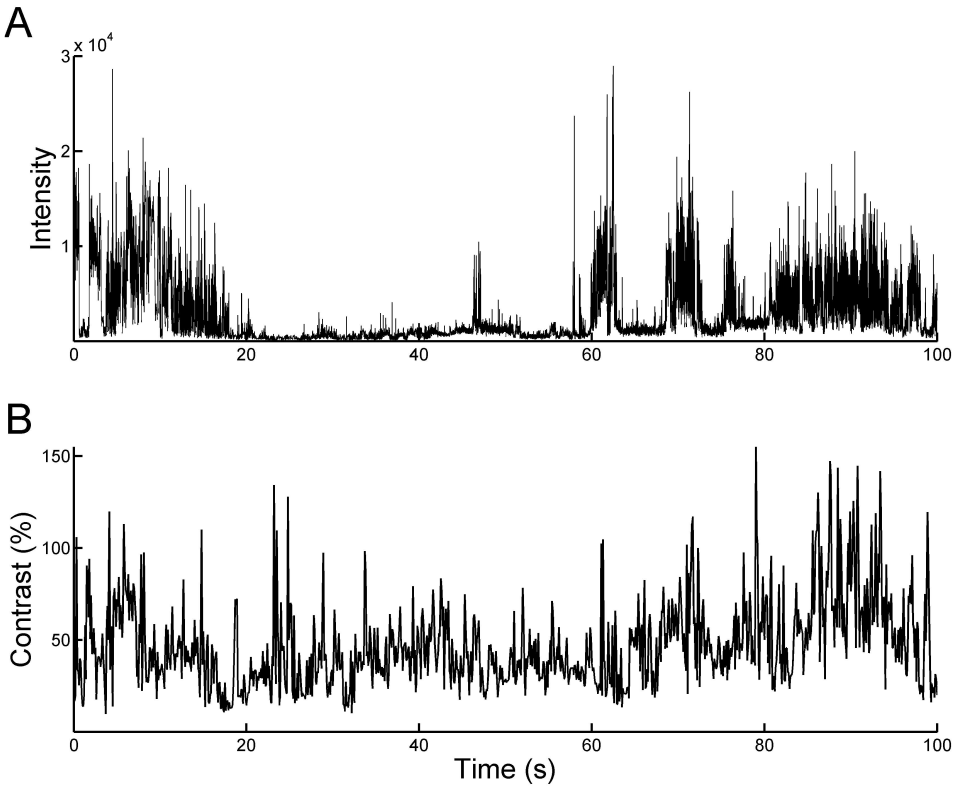

Figure 1.2: Natural-scene time course. A, A representative example of the time-varying intensity of a natural scene stimulus from (van Hateren, 1997). B, The contrast was calculated within 500-ms non-overlapping windows, where contrast was defined as the standard deviation of the intensity divided by the mean.

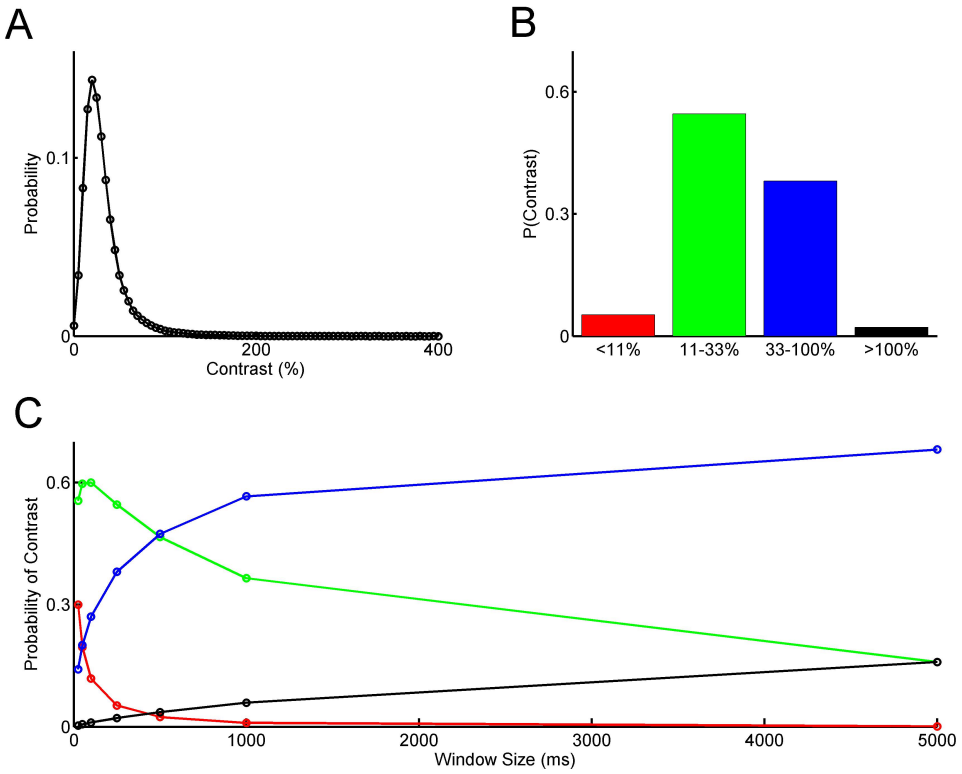

Figure 1.3: Distributions of contrasts in natural scenes. A, The probability of contrast across all natural-scene stimuli from (van Hateren, 1997), where contrast was calculated for 500-ms windows. B, The probability across stimuli that the contrast, calculated for 500-ms windows, was less than 11% (red bar), between 11% and 33% (green bar), between 33% and 100% (blue bar), or greater than 100% (black bar). C, The probability that the contrast was less than 11% (red curve), between 11% and 33% (green curve), between 33% and 100% (blue curve), or greater than 100% (black curve) when contrast was calculated using a variety of window sizes.

References

Baccus SA, Meister M (2002) Fast and slow contrast adaptation in retinal circuitry. Neuron 36:909-919.

Benardete EA, Kaplan E (1999) Dynamics of primate P retinal ganglion cells: responses to chromatic and achromatic stimuli. J Physiol 519 Pt 3:775-790.

Borst A, Flanagin VL, Sompolinsky H (2005) Adaptation without parameter change: Dynamic gain control in motion detection. Proc Natl Acad Sci U S A 102:6172-6176.

Chander D, Chichilnisky EJ (2001) Adaptation to temporal contrast in primate and salamander retina. J Neurosci 21:9904-9916.

Dong D, Atick J (1995) Statistics of natural time-varying images. Network 6:345-358.

Enroth-Cugell C, Robson JG (1966) The contrast sensitivity of retinal ganglion cells of the cat. J Physiol (Lond) 187:517-552.

Erisir A, Van Horn SC, Sherman SM (1997) Relative numbers of cortical and brainstem inputs to the lateral geniculate nucleus. Proc Natl Acad Sci U S A 94:1517-1520.

Jahnsen H, Llinas R (1984) Ionic basis for the electro-responsiveness and oscillatory properties of guinea-pig thalamic neurones in vitro. J Physiol 349:227-247.

Kim KJ, Rieke F (2001) Temporal contrast adaptation in the input and output signals of salamander retinal ganglion cells. J Neurosci 21:287-299.

Kim KJ, Rieke F (2003) Slow Na+ inactivation and variance adaptation in salamander retinal ganglion cells. J Neurosci 23:1506-1516.

Ohzawa I, Sclar G, Freeman RD (1985) Contrast gain control in the cat's visual system. J Neurophysiol 54:651-667.

Reinagel P, Godwin D, Sherman SM, Koch C (1999) Encoding of visual information by LGN bursts. J Neurophysiol 81:2558-2569.

Reinagel P, Reid RC (2000) Temporal coding of visual information in the thalamus. J Neurosci 20:5392-5400.

Rieke F (2001) Temporal contrast adaptation in salamander bipolar cells. J Neurosci 21:9445-9454.

Sanchez-Vives MV, Nowak LG, McCormick DA (2000a) Membrane mechanisms underlying contrast adaptation in cat area 17 in vivo. J Neurosci 20:4267-4285.

Sanchez-Vives MV, Nowak LG, McCormick DA (2000b) Cellular mechanisms of long-lasting adaptation in visual cortical neurons in vitro. J Neurosci 20:4286-4299.

Shapley R (1997) Retinal physiology: adapting to the changing scene. Curr Biol 7:R421-423.

Shapley R, Victor JD (1979) The contrast gain control of the cat retina. Vision Res 19:431-434.

Shapley R, Enroth-Cugell C (1984) Visual adaptation and retinal gain control. Progress in Retinal Research 3:263-346.

Shapley RM, Victor JD (1978) The effect of contrast on the transfer properties of cat retinal ganglion cells. J Physiol 285:275-298.

Shapley RM, Victor JD (1981) How the contrast gain control modifies the frequency responses of cat retinal ganglion cells. J Physiol 318:161-179.

Sherman SM (2001) A wake-up call from the thalamus. Nat Neurosci 4:344-346.

Solomon SG, Peirce JW, Dhruv NT, Lennie P (2004) Profound contrast adaptation early in the visual pathway. Neuron 42:155-162.

Swadlow HA, Gusev AG (2001) The impact of 'bursting' thalamic impulses at a neocortical synapse. Nat Neurosci 4:402-408.

van Hateren JH (1997) Processing of natural time series of intensities by the visual system of the blowfly. Vision Res 37:3407-3416.

Yu Y, Lee T (2005) Adaptive contrast gain control and information maximization. Neurocomputing 65-66:111-116.

Yu Y, Potetz B, Lee TS (2005) The role of spiking nonlinearity in contrast gain control and information transmission. Vision Res 45:583-592.

Zaghloul KA, Boahen K, Demb JB (2005) Contrast adaptation in subthreshold and spiking responses of mammalian Y-type retinal ganglion cells. J Neurosci 25:860-868.

Chapter 2

Visual control of burst priming in the anesthetized lateral geniculate nucleus

Abstract

Thalamic relay cells fire bursts of action potentials. Once a long hyperpolarization primes (de-inactivates) the T-type calcium channel, a depolarizing input will trigger a calcium spike with a burst of action potentials. During sleep, bursts are frequent, rhythmic, and non-visual. Bursts have been observed in alert animals, and burst timing is known to carry visual information under light anesthesia. We extend this finding by showing that bursts without visual triggers are rare. Nevertheless, if the channel were primed at random with respect to the stimulus, then bursts would have the same visual significance as single spikes. We find, however, that visual signals influence when the channel is primed. First, natural time-varying stimuli evoke more bursts than white noise. Second, specific visual stimuli reproducibly elicit bursts whereas others reliably elicit single spikes. Therefore visual information is encoded by the selective tagging of some responses as bursts. The visual information attributable to visual priming (as distinct from the information attributable to bursts' visual triggering) was 2 bits/burst on average. Although bursts are reportedly rare in alert animals, this must be investigated as a function of visual stimulus. Moreover, we propose methods to measure the extent of both visual triggering and visual priming of bursts. Whether or not bursts are rare, our methods could help determine whether bursts in alert animals carry a distinct visual signal.

Introduction

Distinctive bursts of action potentials were noted in the earliest recordings in the LGN (Hubel and Wiesel, 1961). LGN relay cells fire isolated action potentials during wakefulness or REM sleep, and burst rhythmically during slow-wave sleep (Livingstone and Hubel, 1981; Hirsch et al., 1983; McCarley et al., 1983). Slow-wave sleep was also characterized by suppression of visual responses in cortex (Livingstone and Hubel, 1981) and hyperpolarization of LGN relay cells (Hirsch et al., 1983). Hyperpolarization de-inactivates ("primes") the calcium channel that underlies bursts in these cells (Jahnsen and Llinas, 1984). Several studies reported that bursts are rare in alert animals, comprising between 1-5% of spikes in the LGN (Guido and Weyand, 1995; Ramcharan et al., 2000; Weyand et al., 2001). These results suggest that bursts are not relevant to the transmission of visual information (Steriade, 2001).

Much of the evidence for a visual function of bursts has come from anesthetized animals. The state of the LGN under anesthesia differs from either sleep or wakefulness. The LGN cells fire bursts, but unlike sleep, these bursts are arrhythmic and intermingled with single spikes (Guido et al., 1992; Guido et al., 1995; Guido and Weyand, 1995; Mukherjee and Kaplan, 1995; Reinagel et al., 1999). These arrhythmic bursts do not occur at random times; they are triggered by visual stimuli. The receptive-field properties of bursts and single spikes are similar but distinct, both temporally and spatially (Guido et al., 1992; Reinagel et al., 1999; Kepecs and Lisman, 2003; Rivadulla et al., 2003; Lesica and Stanley, 2004; Alitto et al., 2005). Bursts provide better signal detection, while single spikes provide better signal discrimination (Guido et al., 1995). Bursts also transmit visual information with higher

coding efficiency than single spikes, though at higher metabolic cost (Reinagel et al., 1999). Therefore bursts may be important when signal-to-noise ratio is low, or may emphasize stimuli that are surprising in a given context (Sherman, 2001a). These results suggest a visual function of bursts in alert animals, even if bursts are infrequent (see also Discussion).

LGN bursts are caused by calcium spikes via the T-type calcium channel. The channel is primed by prolonged hyperpolarization, but the calcium spike occurs only when triggered by a depolarizing input (reviewed in Perez-Reyes, 2003). Both priming and triggering may depend on both visual and non-visual inputs: only 10% of the synapses on an LGN relay cell come from retinal ganglion cells, the remainder coming from interneurons, cortical feedback, and non-visual sub-cortical areas (Erisir et al., 1997). Previous studies have established that bursts can be visually triggered, and suggest that bursts can also visually primed. Here we explicitly separate the question of visual priming from that of visual triggering.

We find that natural stimuli evoke more bursts than other stimuli, suggesting that visual inputs can influence priming. This paper examines the extent, specificity and reliability of the visual control of priming. Using information theory we estimate the visual information specifically attributable to the visual control of priming. Our results support a visual function for bursts, and suggest how this hypothesis could be better tested in alert animals. Preliminary results of this study have been reported in abstract form (Denning et al., 2003)

Methods

Surgical preparation. Cats were initially anesthetized with ketamine HCl (20 mg/kg, intramuscular) followed by sodium pentothal (2-4 mg/kg/hr intravenous, supplemented as needed). The animals were then ventilated through an endotracheal tube. EKG, EEG, temperature and expired CO_2 were monitored continuously. Animals were paralyzed with Norcuron (0.3 mg/kg/hr, intravenous). Eyes were refracted, fitted with appropriate contact lenses, and focused on a tangent screen. Electrodes were introduced through a 0.5 cm diameter craniotomy over the LGN. All surgical and experimental procedures were in accordance with NIH and USDA guidelines and were approved by the Harvard Medical Area Standing Committee on Animals.

Electrical recording. Single LGN neurons in the A laminae of the LGN were recorded with either Parylene-coated tungsten electrodes (AM Systems, Everett, WA), or Quartz- coated platinum/tungsten electrodes (System Eckhorn, Thomas Recording, Marburg, Germany). Recorded voltage signals were amplified, filtered, and passed to a PC running DataWave Discovery software (Longmont, CO) and spike times were determined to 0.1 ms resolution. Preliminary spike discrimination was done during the experiment, but analysis is based on offline spike sorting after the experiment using custom software. Only well isolated single units were analyzed. All cells used in this analysis were classified as X cells. All further analysis was performed with custom programs written in the Matlab programming environment (Mathworks, Inc., Natick, MA).

Visual stimulation. Both natural and white-noise stimuli were spatially-uniform (full-field) visual stimuli, modulated in time. Natural luminance time-series were obtained from (van Hateren, 1997). White-noise stimuli were obtained by drawing independent random samples from the distribution of luminance values in the natural stimulus, thereby eliminating the temporal correlations of the natural stimulus but preserving the distribution of the stimulus intensities. Stimuli were 8-32 seconds long and were repeated 128 times. Stimuli were presented either on a CRT monitor (128 frames/s, 8-bit grayscale, N=9 cells) or on a custom-made LED display (1200 frames/s, 15-bit grayscale, N=6 cells). All results reported here were the same for both CRT and LED data, so both are shown and both are included in all averages we report. In particular, stimulus presentation method was not correlated with burst frequency in these experiments.

Burst classification. We define a "burst" as a group of 2 or more action potentials separated by $\leq$4 ms, preceded by a period of >100 ms without spiking activity. This criterion was previously shown to reliably identify bursts that are due to low threshold (T-type) calcium spikes in LGN relay cells of the cat (Lu et al., 1992). Subsequent studies (Lu et al., 1993; Ramcharan et al., 2000) have found these classification criteria to be conservative. We repeated our analysis with a less stringent burst criteria (preceding interval <50 ms, internal interval <6 ms); this increased our estimated burst frequency only slightly and did not qualitatively change any of the results reported here.

Event classification. We presented the same dynamic stimulus repeatedly for 128 trials, and accumulated a PSTH, which represents the probability of firing as a

function of time. We divided this PSTH into discrete firing events by the method of Berry et al, 1997. Briefly, the PSTH was smoothed by a Gaussian filter with σ=10 ms, which approximated the trial-to-trial jitter of spike timing for the most precise events. In this smoothed PSTH, minima that were deep compared to adjacent maxima were taken as boundaries between distinct events. Specifically, our algorithm required that the minimum was $\leq$2/3 of the square root of the product of the adjacent maxima. These boundaries were then used to divide to the original, unsmoothed PSTH into discrete intervals, such that all spikes were assigned to one and only one interval. We excluded from further analysis any interval that contained spikes in fewer than 10% of the trials. We fit a Gaussian curve to each peak individually, and defined the time window of the event as the mean time $\pm 2\sigma$ of this best-fit Gaussian. Spikes that did not fall within any event so defined, were classified as non-visual responses. In the analysis of Figure 2.2D only, we separately identified reliable firing events using the same method, but including only events that contained spikes in at least 80% of trials.

Burst probability and priming probability. We define the burst probability within a visual firing event as the percentage of trials containing a burst within the event time window. Conceptually we define the probability of priming within a firing event as the fraction of trials in which the T-type calcium channel was de-inactivated at the time of the event. Operationally, we estimated this from the fraction of all responding trials that contained a burst.

To determine reproducibility of burst probability, we divided the data from each cell and stimulus into two non-overlapping sets: the 64 odd-numbered trials and

the 64 even-numbered trials. For each visual firing event as defined above, we determined the burst probability for each half of the data. These two independent estimates are compared in Figure 2.4E. We also computed the probability of priming separately in the two data sets; the estimates were similarly well correlated (not shown).

In Figure 2.5B and 2.5D, the priming probability was determined as a function of the preceding inter-spike interval, without reference to identified firing events. In this case, priming probability is defined as the percentage of all of the responses with a given preceding ISI that were bursts.

Information calculations. Our recorded neural data were represented as time-binned spike trains; in this study a fixed bin size of $\delta\tau$= 2 ms was used. The value in a time bin was set to 0 if no spikes occurred during that time interval, 1 if a single spike occurred during that time interval, or 2 if the first spike of a burst occurred during that time interval. Only the first spike of each burst was represented. Due to the refractory period of the cells, the occurrence of two spikes in the same time bin was so rare as to be negligible.

We calculated the visual information in spike trains by the direct method (Strong et al., 1998), implemented exactly as by Reinagel and Reid (2000). Briefly, we analyzed the information contained in words (short strings of bins), and varied the number of bins in the words, L. For each word length, we measured two forms of word entropy: the average noise entropy, $<H_{noise}>$, which reflects the trial-to-trial variability of words when the stimulus was fixed, and the average total entropy, $<H_{total}>$, which reflects the variability of words across all stimuli in the ensemble.

$H_{noise}(t)$ was calculated from the distribution of words at a fixed time t relative to stimulus onset, in 128 repeats of the same sample of the stimulus. We performed a separate calculation of H_{noise}(t) for many different values of t (separated by one bin) within the 8 or 32 sec stimuli. We then averaged over t to get the average noise entropy $<H_{noise}>$. We performed equally many separate calculations of $H_{total}(i)$, but the set of words was instead selected using a different time t from each trial. We used 256 words for each single estimate of H_{total}(i), to compensate for the approximately twofold difference in entropy. We averaged over i get the average total entropy $<H_{total}>$. Finally, the mutual information between the visual stimulus and the spike train is defined as $I = <H_{total}> - <H_{noise}>$. We computed information as a function of word length. We extrapolated to infinite word length from the linear part of the curve H versus $1/L$ as described by (Strong et al., 1998).

Extrapolation to infinite word length should in principle provide the best estimate of the total information, but the linear part of the curve was difficult to identify in some of our data. Therefore we show results using a fixed word length of L=8. We obtained similar results for infinite word lengths using L=[6,8,12] as the basis for extrapolation.

Data adequacy for entropy calculations. For all entropy estimates that we computed, we determined how our estimate of H converged as we used increasing fractions of the data and then corrected for finite data size according to the method of (Strong et al., 1998). The correction is obtained by fitting a second-order polynomial to 1/(fraction of data) versus estimate. We are confident of our estimates when the total correction for finite data size was <10% and the second-order term of this

correction was negligible, <1%. Results that passed these criteria are shown with filled symbols in Figure 2.6. For completeness we also show our results from cells that did not pass the criteria, open symbols in Figure 2.6.

Results

We recorded from fifteen neurons in the LGN of barbiturate-anesthetized cats during presentation of two different full-field visual stimuli: one that varied according to a naturally recorded time sequence (natural); and one that flickered randomly (white noise).

Throughout our analysis we will refer to a simplified model in which the T-type calcium channels of a given LGN relay cell are either fully inactivated or fully primed. Each relay neuron can therefore be described as having a binary state that is defined at each moment in time. In the unprimed state, if a depolarizing input (trigger) causes the neuron to cross threshold, the LGN cell will fire a single action potential. In the primed state, the same depolarization would trigger instead a calcium spike via the T-type calcium channel, and thus a burst of action potentials (Figure 2.1). Although this is an oversimplification, it allows us to clearly separate the question of the visual control of priming from the visual control of triggering.

Bursts occur and are visually triggered

Other studies have shown that bursts can be visually triggered. In LGN responses to white noise flicker, the average stimulus preceding a burst (the burst-triggered average) reveals that bursts occur in response to luminance transients. Bursts and single spikes are triggered by similar features, with some significant differences (Reinagel et al., 1999; Kepecs and Lisman, 2003; Rivadulla et al., 2003; Lesica and Stanley, 2004; Alitto et al., 2005). While reverse correlation can establish that many bursts are visually triggered, in general this method cannot exclude the presence of

additional, non-visual bursts. To determine what fraction of bursts are visually triggered it is necessary to determine for each individual burst whether it was visually evoked or random.

To answer this question we made use of the fact that we repeated the identical visual stimulus 128 times. We defined a visual firing event as a discrete time interval relative to the stimulus during which spikes occurred in at least 10% of trials (both open and closed diamonds in Figure 2.2A, 2.2B; see Methods). We identified putative T-type calcium bursts in our recordings by conventional inter-spike interval criteria (Methods). In this paper we will use the term response to refer either to a single spike or an entire burst. In accordance with other studies in anesthetized animals, we found stereotyped bursts intermingled among single action potentials (Figure 2.2A,2.2B).

Averaging over both stimuli, 86±18% (mean±SD) of bursts occurred during a visual firing event as defined by our criterion (Figure 2.2C). Similarly, 80±16% of single spikes occurred during a visual firing event. Given that visual firing events comprised only 22±14 % of the time in the trial, we would expect only about 22% of bursts to fall in visual firing events by chance.

In the data shown in Figure 2.2A,2.2B, all of the bursts occurred during particularly reliable firing events. To test the generality of this finding, we determined what fraction of bursts and single spikes were restricted to the most reliable visual firing events (stimulus-locked activity that occurred in >80% of trials, closed diamonds). For every cell in our sample, regardless of the visual stimulus, we consistently found that bursts were more likely than single spikes to occur during a high-reliability firing event (Figure 2.2D).

Burst frequency depends on visual stimulus

LGN cells fired more bursts per second during the natural visual stimulus than during the white noise stimulus (Figure 2.3A). A similar result was found by others comparing spatio-temporal natural movies to spatio-temporal white noise (Lesica and Stanley 2004). The increase in bursts during our natural stimulus was not due to a general increase in firing rate: a higher fraction of all responses were bursts when the natural stimulus was shown (Figure 2.3B). The fact that some types of stimuli elicit more bursts than others is strong evidence that visual inputs can influence the priming of the channel and thus the state of the cell, at least on average.

The burst state is primed at reproducible times

If the probability of priming is determined only by average stimulus properties, it should be roughly constant over time within a stimulus. Alternatively, if priming is determined by specific temporal features in the visual stimulus, we would expect that burst probability would vary across firing events. In our data we found that bursts occurred in a specific subset of firing events (Figure 2.4A, red curve; see also Figure 2.2A,2.2B, red points).

Most firing events had a zero probability of a primed burst state at the time of the visual trigger. For example, the cell shown in Figure 2.4A,2.2B responded with 163 stimulus-locked firing events over 8 seconds. Of these events, 104 excluded bursts (no bursts in 128 trials). In other firing events, the same cell had as high as 83% chance of being in the primed state when the visual trigger occurred (106 of 128 trials

had a burst within the time window of a single firing event). Other visually triggered events had an intermediate, but reproducible, probability of the primed state (compare Figure 2.4A and Figure 2.4B). Our findings are in agreement with other studies using different visual stimuli (Lesica and Stanley, 2004; Alitto et al., 2005). This result shows that the recent stimulus can reproducibly set the probability that the cell will be primed at the time of each visual trigger.

To summarize the result for all cells in our population, we estimated the probability of the primed state during a given firing event by the proportion of the responses that were bursts (the number of trials that burst during the event divided by the number of all trials with any spikes during the event). Across all cells, most firing events had 0% probability of the primed state, but this probability was as high as 94% for some individual firing events (Figure 2.4D). As expected, more firing events contained bursts in the natural stimulus experiment (compare the two curves in Figure 2.4D). The absolute probability of firing a burst within a firing event ranged from 0 to 89% (Figure 2.4E). Two independent subsets of the data gave highly-correlated estimates of the burst probability (symbols lie near the line x=y in Figure 2.4E). The probability of the primed state (Figure 2.4D) was also reproducible in independent samples (not shown).

Relation of burst rate to the frequency of long silences

Biophysically, priming of the T-type channel requires a prolonged hyperpolarization (50-100 ms without any action potentials). Operationally, our definition of a "burst" requires >100 ms with no spikes before the burst. The simplest

explanation for the increase of bursting during natural stimuli would be that the required long silences occurred more often. Alternatively, one could imagine that long inter-spike intervals were equally likely under both stimulus conditions, but that the probability of priming during that interval is higher during natural stimuli, for example because the cell was hyperpolarized more deeply and/or more continuously. A mixture of both causes is also possible. To test each of these possibilities, we examined the probability of long intervals as well as the conditional probability of priming given that a long interval has occurred.

Our population of cells could be divided into three groups according to their burst frequency. The first group of cells had the highest burst frequencies in our population ($0.75 < x < 1.08$ bursts/s; N=4 cells). This group of cells was also distinguished by the fact that responses to natural stimuli had significantly more long inter-spike intervals than responses to white noise (average shown in Figure 2.5A). For these cells, the higher frequency of long intervals could explain the higher burst frequency observed with natural stimuli.

The second group of cells had intermediate burst frequencies ($0.095 < x < 0.75$ bursts/s; N=7 cells). In every cell in this group, the probability of long inter-spike intervals was similar under both stimulus conditions (average shown in Figure 2.5C). Therefore the frequency of long intervals could not explain the higher burst frequency of responses to natural stimuli. Instead, we found that under natural stimulation, these cells had a greater probability of bursting after a long silence (Figure 2.5D). We observed a similar trend in the first (high-bursting) group, but the result was statistically significant only for a few interval lengths (Figure 2.5B). Shorter intervals

are not expected to show an effect (compare to Figure 2.5D) whereas longer intervals were too rare in white-noise responses (Figure 2.5A) to allow an accurate estimate.

Finally the third group consisted of the 4 cells with the lowest burst frequencies in our population (<0.095 bursts/s for our natural stimulus). This group was heterogeneous with respect to the relative likelihood of long inter-spike intervals in the two stimulus conditions (not shown). The conditional probability of bursting after a long interval could not be determined due to the rarity of the bursts.

Visual information encoded by priming

The results presented above show that visual stimuli influence the probability of priming of the T-type channel in the LGN. It follows that some extra visual information is transmitted by the LGN as a result of having two states (primed and unprimed) with distinguishable outputs (bursts and single spikes). To estimate how much visual information is specifically due to priming, we asked how much information is present in the LGN spike train when bursts and single spikes are distinguished, versus when they are not.

First we identified the bursts in our recorded spike trains. We created a surrogate spike train in which each single spike was denoted by one symbol at the time of the spike, and each identified burst was denoted by a different symbol at the time of the first spike in the burst (Methods). This identified response train retains information about the time of the triggers, as well as information about the state of the neuron at the time of the trigger (i.e. which responses were bursts), but it contains no further information about the structure of the burst (number of spikes or inter-spike intervals

within the burst). For purposes of this analysis, we will neglect any additional information that might be contained in burst structure. We will consider the information in the identified response train to be the total information in the LGN spike train, I_{total}.

We created a second control response train by randomizing which of the responses were labeled with the burst symbol. The control response train is matched for the frequencies of the two symbols and thus has the same overall burst rate. The control response train lacks any temporal information about the cell's state (primed or unprimed), but retains all information about when responses occurred, i.e., when the triggering inputs occurred. Therefore we interpret the information rate in this control response train as the information due to triggering alone, which we denote $I_{trigger}$.

We define the state information as the amount of visual information that was lost when the distinction between single spikes and bursts was removed: $I_{state} = I_{total} - I_{trigger}$. This is the information potentially transmitted to cortex solely by virtue of the ability of bursts to reveal the sub-threshold state of an LGN neuron, information that could not have been transmitted if bursts did not occur.

We found that the state information I_{state} depended on the overall burst rate: cells with more bursts transmitted more information through the state variable (Figure 2.6A: larger symbols are farther from the origin). The state information, I_{state}, was as high as 3.7 bits/s in experiments using the more natural stimuli. We emphasize that this is the visual information bursts transmitted by reporting the state of the LGN cell (primed vs. unprimed), independent of and in addition to the information that bursts carried about triggering stimulus (response vs. no response).

For most cells I_{state} was greater for natural stimuli than white noise stimuli (most symbols are above the diagonal; $p<0.05$ by Wilcoxon sign rank test). The fraction of the total information carried by state (I_{state} / I_{total}) was also greater for the natural stimuli ($p<0.001$). We find that the state information I_{state} measured in bits/burst was comparable to the trigger information $I_{trigger}$ measured in bits/response (Figure 2.6B).

Discussion

It has long been suggested that thalamic bursts may have a role in gating the flow of visual information to cortex (Singer, 1977; Crick, 1984; Sherman and Koch, 1986; McCormick and Feeser, 1990; Guido and Lu 1995). It has remained controversial whether bursts occur or function during visual awareness (Steriade, 2001; Sherman, 2001b). In this study we have analyzed the visual properties of bursts that occur intermingled with single spikes under conditions of light anesthesia.

Almost all bursts are visually triggered

Previous studies have shown that the average spike and the average burst are visually triggered, as opposed to being triggered by non-visual inputs or noise (Reinagel et al., 1999; Kepecs and Lisman, 2003; Rivadulla et al., 2003; Lesica and Stanley, 2004; Alitto et al., 2005). Using binary white-noise visual stimuli, reverse-correlation analysis revealed that almost every burst is preceded by a specific stimulus value at the peak spatial location and temporal delay, implying that few if any bursts are triggered by non-visual inputs (Alitto et al., 2005). In our study we used low-contrast grayscale stimuli, and the average stimulus preceding a spike or burst was always an intermediate luminance at all latencies. In this case the spike-triggered average does not reveal the fraction of bursts that were visually triggered. Instead we defined a response as visually triggered if it occurred during a brief time window that contained reliable stimulus-locked firing events (Figure 2.2). For both natural temporal flicker and white noise, most bursts were visually triggered by this criterion. Indeed bursts were even more likely than single spikes to occur within a visual firing

event. This result further demonstrates that these bursts are not driven by anesthesia-induced rhythms.

Visual stimuli influence the average probability of priming

Even if every burst were triggered by a visual stimulus, bursts could be merely interchangeable with single spikes. But if the priming of the T-type calcium channel is visually controlled, a decoder could extract visual information by selectively responding to bursts. Thus, bursting could allow LGN neurons to multiplex two different streams of visual information in a single spike train.

Consistent with the second possibility, other studies found average burst frequencies to depend on parameters of simple stimuli such as sinusoidal gratings (Grubb and Thompson, 2004) or flashing squares (Weyand et al., 2001). We report that LGN neurons are more likely to burst when visual stimuli contain temporal structure of natural scenes (Figure 2.3), compared to white noise stimuli (see also Lesica and Stanley, 2004). Although we only tested one example of a natural stimulus, its spectrum was typical of natural stimuli in that power was inversely proportional to frequency (van Hateren, 1997). Random stimuli with a 1/f power spectrum caused intermediate burst frequencies (data not shown), showing that the phase alignment found in natural stimuli is important for the efficiency of priming. Our interpretation is that temporal stimulus features that prime the burst state (i.e., de-inactivate the T-type calcium channel) are more prevalent in at least some natural scenes. The fact that some stimuli evoke more bursts than others is strong evidence that priming is visually controlled.

Visual control of the timing of state transitions

For both stimuli tested, we found that bursts occurred during specific firing events and not others (Figure 2.4). We conclude that specific temporal sequences in the visual stimuli determine the probability of the primed state. Thus, downstream cortical neurons could detect the internal state of pre-synaptic LGN neurons by detecting the stereotyped inter-spike intervals of bursts, just as we have done in our analysis.

An integrate-and-fire or -burst model predicts time-varying firing rates in the LGN relatively well, compared to a model that lacks bursts (Lesica and Stanley, 2004). Nevertheless, we still cannot accurately predict the probability of priming at each firing event. This will probably require taking into account additional nonlinear dependencies on the visual stimulus.

Our experiment does not address the spatial information encoded by bursting (but see Rivadulla et al., 2003; Alitto et al., 2005). We also have not determined the specific temporal stimulus features that predict the probability of priming. Others have shown that the average stimulus preceding a burst has a longer and stronger inhibitory phase preceding the excitatory trigger, consistent with the idea that inhibitory visual stimuli prime the T-type calcium channel (Lesica and Stanley, 2004; Alitto et al., 2005). Our approach is complementary to reverse-correlation analysis, which cannot separate whether bursts are visually primed, or whether the cell in the primed state has different triggering requirements.

The length of the preceding interval is not sufficient to predict priming

Prolonged hyperpolarization is required to prime the burst state. All cells in our study burst more during natural stimuli than white noise stimuli. We wondered if this could be accounted for by a higher likelihood of long periods without spikes during the more slowly modulated natural stimuli.

For all cells with high burst rates, natural stimuli evoked responses with more long silences (periods without spikes) (Figure 2.5A,2.5B). In cells with low burst rates, however, long silences were equally likely for both stimuli; instead the conditional probability of a burst given a long silence was higher if the stimulus had a natural time course (Figure 2.5C,2.5D). We conclude that the length of the preceding interval is not always sufficient to predict when bursts occur. We speculate that the natural stimulus either hyperpolarized the cells more deeply on average during the silent interval, or hyperpolarized them more continuously. A direct test of this hypothesis will require in vivo intracellular recording of the LGN during visual stimulation.

Several cells essentially never fired bursts, regardless of the preceding interval's duration. We cannot exclude the possibility that these units are inhibitory interneurons, though we have no specific reason to think so. Relay cells vary in their intrinsic tendency to burst (Weyand et al., 2001), perhaps due to different expression levels of the T-type calcium channel.

Information carried by state

Given that some visual stimulus sequences reliably prime the channel and others reliably prevent priming, the cell's state necessarily encodes visual information. We found that up to 3.7 bits/s of visual information was carried by state as such, as distinct from and in addition to the information carried by the times of triggered spikes and bursts (Figure 2.6). This information is accessible for decoding because cortical neurons can differentially respond to bursts (Usrey et al., 2000; Swadlow and Gusev, 2001).

Not surprisingly, cells with higher burst frequencies carried more state information. Responses to natural scenes had more bursts, and a greater fraction of the total visual information was carried in the state information compared to the responses to white noise.

Our analysis made the simplifying approximation that the neuron's state is binary (Figure 2.1). Intermediate priming states could be revealed by variability in burst structure (Kepecs and Lisman, 2003), potentially encoding even more information. Our cells, however, had relatively little variability in burst structure.

The state presumably encodes information about the visual history preceding the triggering stimulus feature, as others have suggested. Some information about visual history is encoded in the length of the preceding inter-spike interval. Still, it may be easier for downstream cortical cells to detect bursts than to keep track of long silences. Moreover, the preceding interval is not sufficient to determine whether an LGN cell will fire a burst (Figure 2.5). Therefore the state can encode additional information about the visual stimulus that could not be determined from the duration of the previous interval.

Are bursts important for vision?

Our results do not settle whether bursts are used for visual processing. At least some bursts occur in the LGN of alert animals (Guido and Weyand, 1995; Ramcharan et al., 2000; Ramcharan et al., 2001; Weyand et al., 2001; Martinez-Conde et al., 2002). Bursts have also been observed in thalamic relays of other sensory pathways in alert animals (Fanselow et al., 2001; Massaux et al., 2004). Although bursts are less frequent in alert than anesthetized animals, our results show that natural stimuli may be especially likely to elicit bursts. Therefore it will be important to measure burst frequency in alert animals during natural visual stimulation. Even if bursts are rare, they could be important signals when they occur.

We addressed only the visual information encoded by state. State could also encode behaviorally relevant non-visual information. Burst frequency correlates with global levels of arousal (Livingstone and Hubel, 1981; Hirsch et al., 1983; McCarley et al., 1983; Guido and Weyand, 1995; Weyand et al., 2001), but burst timing also correlates with specific behavioral states or events (Ramcharan et al., 2001; Martinez-Conde et al., 2002).

The fact that bursts are visually triggered only establishes that the T-type calcium channel does not interfere with visual transmission. To claim that bursts serve a distinctive function, it must also be shown that bursts and single spikes represent distinct visual inputs or behavioral conditions. Our data show that visual stimuli can control the priming of T-type calcium channels in LGN relay cells of anesthetized

animals. If the same proves true in alert animals, bursts could serve a visual function by relaying information to cortex about sub-threshold states in the thalamus.

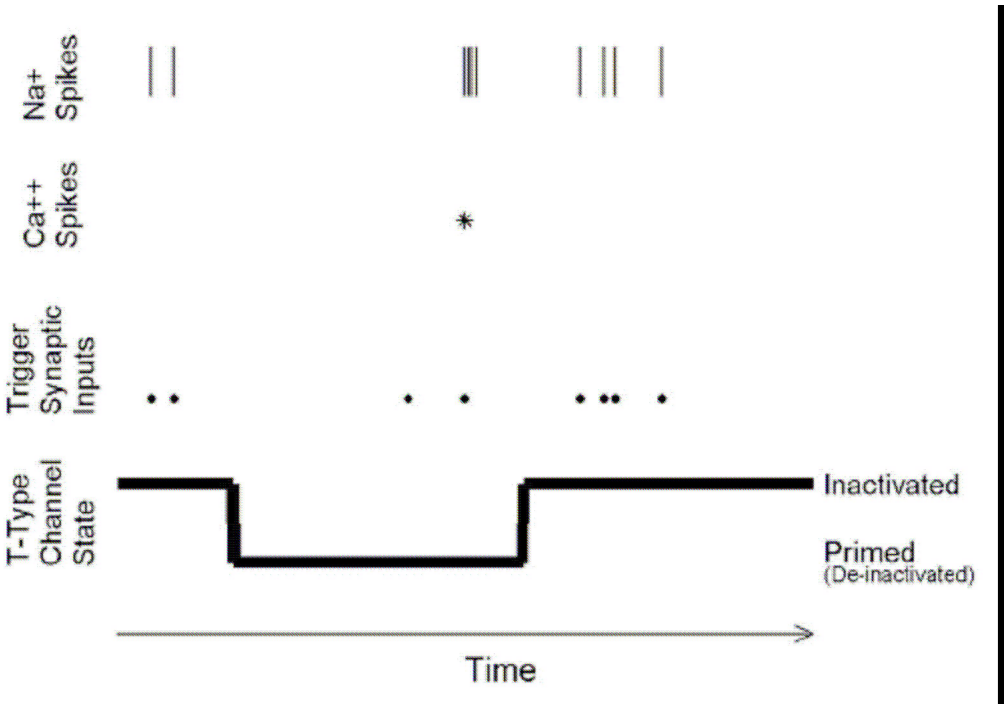

Figure 2.1: A simplified conceptual model of LGN firing modes. Each LGN neuron at any given time is assumed to be in one of two binary states depending on whether the T-type calcium channels are primed or inactivated. When we observe an isolated action potential in an extracellular recording, we infer that a retinal synaptic input most likely triggered the response, and that the T-type calcium channels in the LGN cell were inactivated at the time. When we observe a burst of appropriate structure, we infer that a retinal input triggered a calcium spike, and therefore the T-type calcium channels must have been primed. We note that we are ignorant of both retinal inputs and the state of the T-type calcium channels at other times.

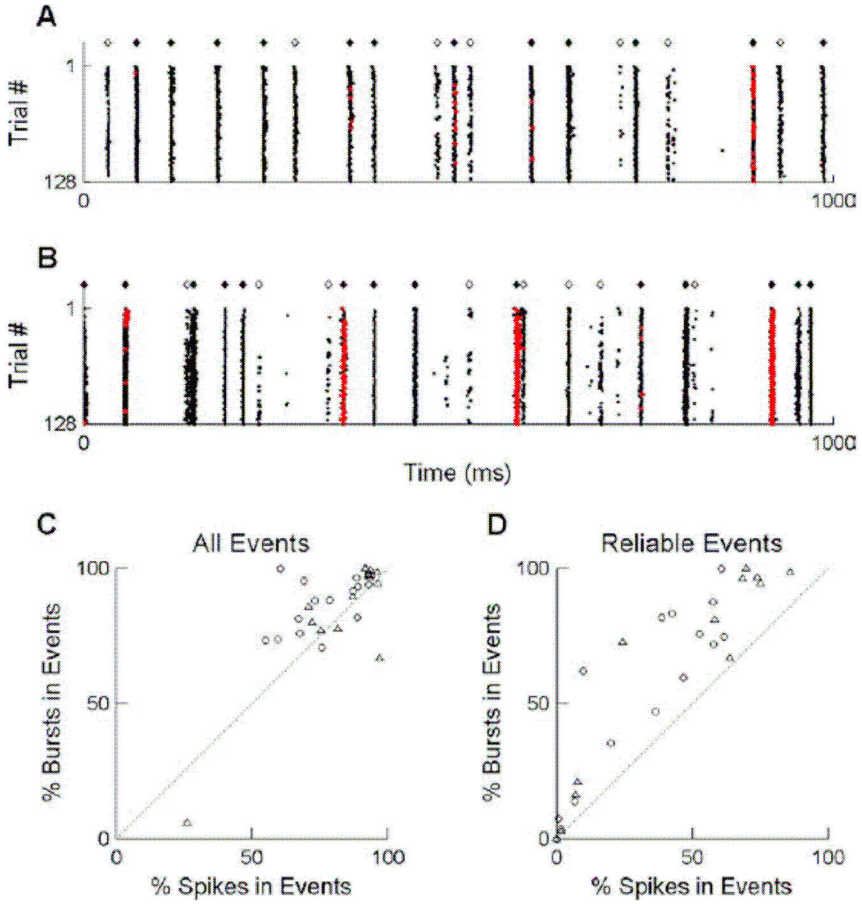

Figure 2.2: Visually triggered bursts. A, Raster plot of responses of an LGN neuron to 128 repeats of the same full-field white noise stimulus. Each row represents a trial; each point represents the time of an action potential in that trial. Red points indicate the action potentials that were classified as being part of a burst (see Methods). A representative 1-s from the middle of an 8-s trial is shown. Diamonds indicate the times at which we classified the response as a visually evoked firing event (cell responded in >10% of trials; see Methods). Filled diamonds indicate the subset of firing events that were highly reliable (cell responded during the event in >80% of trials). B, Responses of the same neuron to 128 repeats of a full-field stimulus with a time course recorded in nature, all symbols as in panel (A). C, Percent of isolated spikes (x axis) vs. percent of bursts (y axis) that occurred during a visually evoked firing event, ◊ in panels (A) and (B). Each symbol represents results for a single cell's response to either the natural stimulus (○) or the white noise stimulus (Δ). Dashed line indicates x=y. D, Percent of isolated spikes (x axis) vs. bursts (y axis) that occurred in a highly reliable visual event (♦ in panels A and B). Symbols as in panel (C).

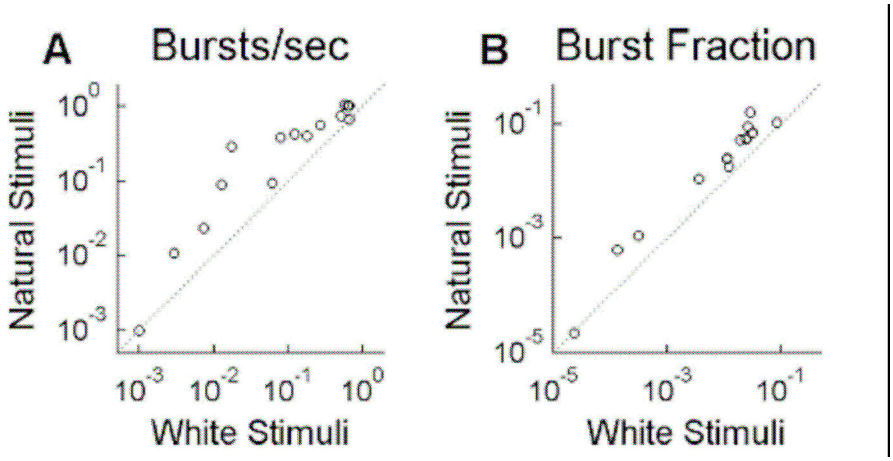

Figure 2.3: Burst rate is higher for naturalistic stimulus. Fifteen LGN neurons were presented two different stimulus ensembles, one having a natural temporal modulation (Natural Stimuli) and the other having a random modulation (White Stimuli). Both stimuli were spatially uniform across the visual field. Each symbol represents results for a single cell under the two stimulus conditions. A, Burst rate, in bursts per second. B, The fraction of all responses that were bursts, where a response is defined as either a single spike or an entire burst.

Figure 2.4: Discrete firing events have reproducible, intermediate burst probabilities. A, PSTH of all spikes (thin, black curve) and of the subset of spikes that were classified as bursts (thick, red curve), derived from the 64 odd-numbered trials of the raster shown in Figure 2.2B. B, PSTH as in panel (A), but from the 64 even-numbered trials. Events have a similar probability of bursting in both independent estimates. C, Luminance time course of the visual stimulus corresponding to the responses shown in (A) and (B). The stimulus was drawn from the natural ensemble, and the cell was an ON cell with a 29 ms latency to peak response. D, Distribution of priming probabilities of firing events, pooled over all cells (N=15). For each visual firing event (PSTH peak), the priming probability was defined as the probability of a burst given that any response was observed, P(Burst|Response) (see Methods). Results are shown for both the natural stimulus (○, N=3444 events) and the white noise stimulus (Δ, N=2342 events). The broken axis and dashed lines are used to show the fraction of events with P(Burst|Response)=0, which cannot be shown on the log scale. E, The absolute probability of bursting for each firing event, P(Burst), is defined as the probability across trials of observing a burst within the time of the event. Independent estimates from the odd trials (x axis) and even trials (y axis) are compared to assess reproducibility of our estimates. If burst probability were perfectly reproducible, points would lie on the identity line (dotted line). The majority of firing events had no bursts in 128 trials and therefore are plotted at the origin (N=2575 events for natural, N=2087 events for white noise).

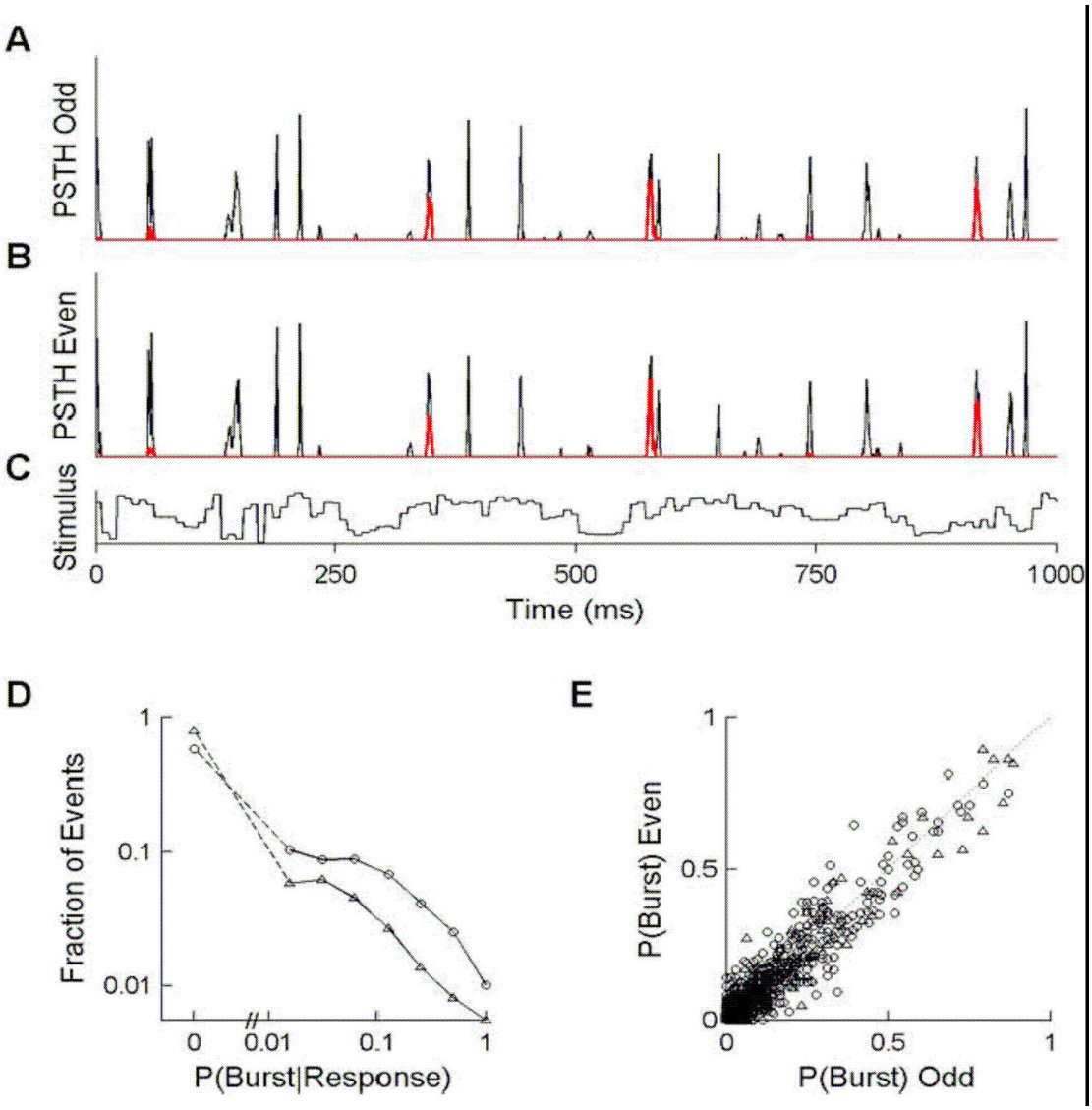
A
PSTH Odd
B
PSTH Even
C
Stimulus
0
250
500
750
1000
Time (ms)
D
Fraction of Events
1
0.1
0.01
0
0.01
0.1
1
P(Burst|Response)
E
P(Burst) Even
1
0.5
0
0
0.5
1
P(Burst) Odd

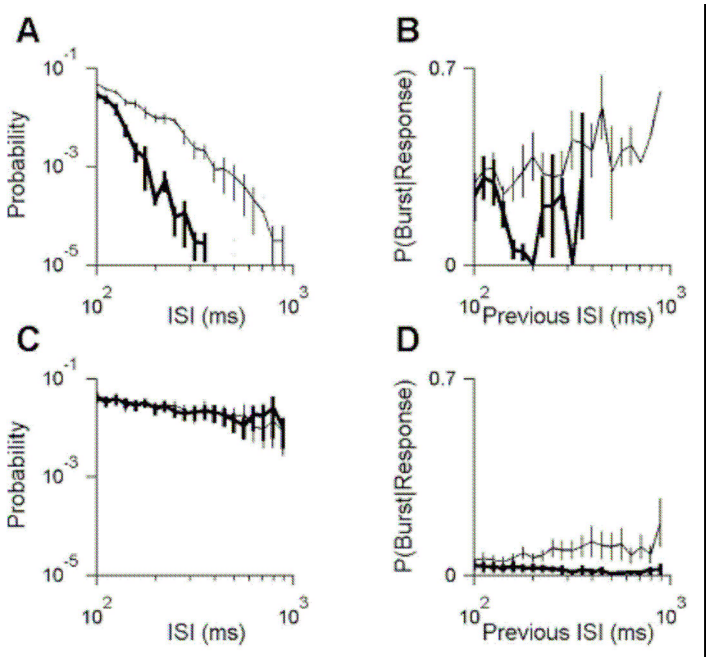

Figure 2.5: Stimulus-dependent burst rate is explained by two causes. A, The inter-spike interval (ISI) distribution for all cells with high burst rates (N=4 cells with burst rates between 0.75 and 1.08 bursts/s in response to natural stimuli). Probability is defined as the absolute probability of a given interval length among all intervals, excluding within-burst intervals. Distributions were averaged across cells for either natural stimuli (thin curve) or white noise stimuli (thick curve). Only long intervals (>100 ms) are shown. Short intervals (≤100 ms) constituted 79% and 92% of intervals during the natural and white noise stimuli respectively. Responses to natural scenes had many more of the long intervals required to prime the channel. B, The probability of priming as a function of the previous ISI, for the cells shown in (A) (see Methods). C, ISI distribution as in panel (A) but for the group of all cells with intermediate burst rates (N=7 cells with burst rates between 0.095 and 0.75 bursts/s). Short inter-spike intervals (≤100 ms, not shown) constituted 54% and 53% of intervals during natural and white noise stimuli respectively. There is no difference in ISI distribution to explain why the natural stimuli evoked more bursts. D, The probability of priming as a function of the previous ISI, as in panel B but for the cells shown in (C). These cells were more likely to prime the T-type calcium channel after a given period of inactivity if the stimulus had natural temporal structure, as opposed to white noise.

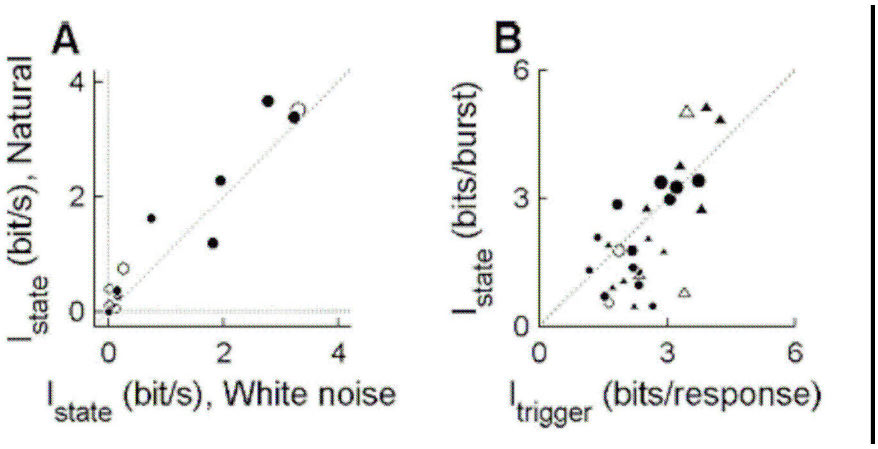

Figure 2.6: Visual information encoded by the cell's state. A, The state information I_{state} is that visual information which can only be decoded by identifying which of the visually triggered responses were bursts (see Methods). Each symbol shows I_{state} in units of bits/s for one cell's responses to the white noise stimulus (x-axis) versus the natural stimulus (y-axis). The symbol size is proportional to the burst rate of the cell, averaged across the two stimulus conditions. Dotted lines indicate x=0, y=0, and x=y. Information rate estimates were empirically corrected for finite data size (see Methods). Filled symbols indicate cells for which this correction was small and linear under both stimulus conditions. Open symbols indicate cells which did not pass this criterion. Results shown are for spike trains binned at 2ms resolution and words of length 8 bins; extrapolating to infinite word length gave qualitatively similar results. B, The state information expressed in bits/burst (I_{state} in bits/s divided by burst rate in bursts/s), compared with the trigger information expressed in bits/response ($I_{trigger}$ in bits/s divided by response rate in responses/s, where a response is either a single spike or an entire burst). Each symbol represents a single cell's response to either the natural stimulus (○) or the white noise stimulus (Δ). The symbol size is proportional to the burst rate of the cell for that stimulus. Filled and open symbols defined as in (A). Calculation parameters as in (A).

Chapter 2, in full, is a republication of the material as it appears in Denning K.S., Reinagel P., Visual control of burst priming in the anesthetized lateral geniculate nucleus. *J Neurosci.* 25, 3531-3538 (2005). The dissertation author was the primary researcher and first author of this paper.

Acknowledgements: This work was supported in part by National Institutes of Health Grant R01-EY10115. P.R. acknowledges support from the Sloan Foundation. K.S.D. acknowledges support from the National Science Foundation. We are indebted to R. Clay Reid for allowing the use of these previously unpublished data, which were collected by P.R. in the Reid laboratory for an unrelated analysis.

References

Alitto HJ, Weyand TG, Usrey WM (2005) Distinct properties of stimulus-evoked bursts in the lateral geniculate nucleus. J Neurosci 25:514-523.

Berry MJ, Warland DK, Meister M (1997) The structure and precision of retinal spike trains. Proc Natl Acad Sci U S A 94:5411-5416.

Crick F (1984) Function of the thalamic reticular complex: the searchlight hypothesis. Proc Natl Acad Sci U S A 81:4586-4590.

Denning KS, Reid RC, Reinagel P (2003) LGN burst state is controlled by visual signals. In: Society for Neuroscience Abstract. New Orleans, LA.

Erisir A, Van Horn SC, Sherman SM (1997) Relative numbers of cortical and brainstem inputs to the lateral geniculate nucleus. Proc Natl Acad Sci U S A 94:1517-1520.

Fanselow EE, Sameshima K, Baccala LA, Nicolelis MA (2001) Thalamic bursting in rats during different awake behavioral states. Proc Natl Acad Sci U S A 98:15330-15335.

Grubb MS, Thompson ID (2004) Visual response properties of burst and tonic firing in the mouse dorsal lateral geniculate nucleus. J Neurophysiol.

Guido W, Weyand T (1995) Burst responses in thalamic relay cells of the awake behaving cat. J Neurophysiol 74:1782-1786.

Guido W, Lu SM, Sherman SM (1992) Relative contributions of burst and tonic responses to the receptive field properties of lateral geniculate neurons in the cat. J Neurophysiol 68:2199-2211.

Guido W, Lu SM, Vaughan JW, Godwin DW, Sherman SM (1995) Receiver operating characteristic (ROC) analysis of neurons in the cat's lateral geniculate nucleus during tonic and burst response mode. Vis Neurosci 12:723-741.

Guido W, Lu SM (1995) Cellular bases for the control of retinogeniculate signal transmission. Int J Neurosci 80:41-63.

Hirsch JC, Fourment A, Marc ME (1983) Sleep-related variations of membrane potential in the lateral geniculate body relay neurons of the cat. Brain Res 259:308-312.

Hubel DH, Wiesel TN (1961) Integrative action in the cat's lateral geniculate body. J Physiol 155:385-398.

Jahnsen H, Llinas R (1984) Ionic basis for the electro-responsiveness and oscillatory properties of guinea-pig thalamic neurones in vitro. J Physiol 349:227-247.

Kepecs A, Lisman J (2003) Information encoding and computation with spikes and bursts. Network 14:103-118.

Lesica NA, Stanley GB (2004) Encoding of natural scene movies by tonic and burst spikes in the lateral geniculate nucleus. J Neurosci 24:10731-10740.

Livingstone MS, Hubel DH (1981) Effects of sleep and arousal on the processing of visual information in the cat. Nature 291:554-561.

Lu SM, Guido W, Sherman SM (1992) Effects of membrane voltage on receptive field properties of lateral geniculate neurons in the cat: contributions of the low-threshold Ca2+ conductance. J Neurophysiol 68:2185-2198.

Lu SM, Guido W, Sherman SM (1993) The brain-stem parabrachial region controls mode of response to visual stimulation of neurons in the cat's lateral geniculate nucleus. Vis Neurosci 10:631-642.

Martinez-Conde S, Macknik SL, Hubel DH (2002) The function of bursts of spikes during visual fixation in the awake primate lateral geniculate nucleus and primary visual cortex. Proc Natl Acad Sci U S A 99:13920-13925.

Massaux A, Dutrieux G, Cotillon-Williams N, Manunta Y, Edeline JM (2004) Auditory thalamus bursts in anesthetized and non-anesthetized states: contribution to functional properties. J Neurophysiol 91:2117-2134.

McCarley RW, Benoit O, Barrionuevo G (1983) Lateral geniculate nucleus unitary discharge in sleep and waking: state- and rate-specific aspects. J Neurophysiol 50:798-818.

McCormick DA, Feeser HR (1990) Functional implications of burst firing and single spike activity in lateral geniculate relay neurons. Neuroscience 39:103-113.

Mukherjee P, Kaplan E (1995) Dynamics of neurons in the cat lateral geniculate nucleus: in vivo electrophysiology and computational modeling. J Neurophysiol 74:1222-1243.

Perez-Reyes E (2003) Molecular physiology of low-voltage-activated t-type calcium channels. Physiol Rev 83:117-161.

Ramcharan EJ, Gnadt JW, Sherman SM (2000) Burst and tonic firing in thalamic cells of unanesthetized, behaving monkeys. Vis Neurosci 17:55-62.

Ramcharan EJ, Gnadt JW, Sherman SM (2001) The effects of saccadic eye movements on the activity of geniculate relay neurons in the monkey. Vis Neurosci 18:253-258.

Reinagel P, Godwin D, Sherman SM, Koch C (1999) Encoding of visual information by LGN bursts. J Neurophysiol 81:2558-2569.

Rivadulla C, Martinez L, Grieve KL, Cudeiro J (2003) Receptive field structure of burst and tonic firing in feline lateral geniculate nucleus. J Physiol 553:601-610.

Sherman SM, Koch C (1986) The control of retinogeniculate transmission in the mammalian lateral geniculate nucleus. Exp Brain Res 63:1-20.

Sherman SM (2001a) Tonic and burst firing: dual modes of thalamocortical relay. Trends Neurosci 24:122-126.

Sherman SM (2001b) A wake-up call from the thalamus. Nat Neurosci 4:344-346.

Singer W (1977) Control of thalamic transmission by corticofugal and ascending reticular pathways in the visual system. Physiol Rev 57:386-420.

Steriade M (2001) To burst, or rather, not to burst. Nat Neurosci 4:671.

Strong SP, de Ruyter van Steveninck RR, Bialek W, Koberle R (1998) On the application of information theory to neural spike trains. Pac Symp Biocomput:621-632.

Swadlow HA, Gusev AG (2001) The impact of 'bursting' thalamic impulses at a neocortical synapse. Nat Neurosci 4:402-408.

Usrey WM, Alonso JM, Reid RC (2000) Synaptic interactions between thalamic inputs to simple cells in cat visual cortex. J Neurosci 20:5461-5467.

van Hateren JH (1997) Processing of natural time series of intensities by the visual system of the blowfly. Vision Res 37:3407-3416.

Weyand TG, Boudreaux M, Guido W (2001) Burst and tonic response modes in thalamic neurons during sleep and wakefulness. J Neurophysiol 85:1107-1118.

Chapter 3

Basis of burst-specifics tate information in LGN neurons

Abstract

Neurons in the lateral geniculate nucleus (LGN) can respond to depolarization either with a single spike or a burst of spikes. The response type depends on the state of the T-type calcium channel. Strong hyperpolarization de-inactivates the channels and causes cells to respond to excitatory stimuli with a burst of spikes. It has been shown that bursts and spikes occur at distinct times within visual stimuli, indicating that visual stimuli can influence the state of the T-type calcium channel (Lesica and Stanley, 2004; Alitto et al., 2005; Denning and Reinagel, 2005). Therefore, distinguishing between bursts and single spikes provides additional information about the visual stimuli. In Denning and Reinagel (2005), we introduced a state-information measure to quantify this additional information. Here, we first examine why this technique is superior to other information measures that could be used to examine the same question. Secondly, we begin to investigate whether time-varying firing rates independent of the T-type calcium channel could reproduce the bursting patterns and the state information found in LGN neurons. Thirdly, we and others identify putative low-threshold bursts from extracellular recordings by two inter-spike interval criteria: bursts must follow a long silence and spikes within the burst must be separated by short intervals. We show that bursts convey visual information that is distinct from patterns identified using only one of the above criteria. Finally, we report that the number of spikes within a burst is influenced by the stimulus, such that distinguishing between bursts of different sizes provides additional visual information. We conclude that visual stimuli can influence the state of the T-type calcium channel, such that distinguishing between response types can provide additional visual information.

Introduction

Sustained hyperpolarization will de-inactivate LGN cells' T-type calcium channel. When the channel is de-inactivated, an excitatory stimulus will then cause a burst of action potentials, whereas if the channel is inactive, an excitatory stimulus will cause a single action potential (Jahnsen and Llinas, 1984). Several studies have reported that bursts are rare in alert animals (Guido and Weyand, 1995; Ramcharan et al., 2000; Weyand et al., 2001; Ruiz et al., 2006), which has caused speculation as to whether bursts are important for visual processing. However, the information value provided by the T-type calcium channel can not be determined merely by the frequency of bursts. Just as spikes act as a sparse code, bursts may provide an additional sparse code.

If the activation state of the T-type calcium channel was not influenced by visual stimuli, then the channel would be de-inactivated at random times with respect to the visual stimuli. Although bursts would be triggered by visual inputs, such that the timing of bursts and spikes would still convey visual information, identifying responses as either bursts or spikes would provide no additional visual information. This does not appear to be the case. In anesthetized animals, bursts and spikes are reliably elicited by distinct stimuli (Alitto et al., 2005; Denning and Reinagel, 2005). In Denning and Reinagel (2005), we modified the direct method of Strong et al. (1998) in order to determine whether distinguishing between bursts and spikes provides additional information about visual stimuli.

The initial description of the state-information measure in Denning and Reinagel (2005) was brief and did not include a full analysis of the properties of the measure. Here we explore differences between our state-information measure and other possible state-information measures, and we explain why our state-information measure is superior to other potential analyses.

In addition, we address two possible concerns about the measure. The first is that by replacing all bursts by a single symbol, the analysis in Denning and Reinagel (2005) eliminates information within burst structure. An ROC analysis performed on model data suggests that the number of spikes in a burst corresponds to the slope of the stimulus (Kepecs et al., 2002; Kepecs and Lisman, 2003). Additionally, LGN bursts consisting of a large number of spikes are more likely to follow a micro-saccade (Martinez-Conde et al., 2002). Results in the primary visual cortex led Martinez-Conde et al. (2002) to speculate that the number of spikes in a burst would also be sensitive to other stimulus characteristics. Here, we show that burst size does convey additional information about the stimulus.

Secondly, we investigate what aspect of the burst criteria is necessary for our results. Bursts are identified using inter-spike interval (ISI) criteria (Lu et al., 1992, 1993; Ramcharan et al., 2001). A long interval of silence is required before the burst (>50-100 ms), and the spikes within a burst must have short ISI (<4-6 ms). Therefore, perhaps although bursts are informative, they are no more informative than any high-frequency spiking epoch or than any spike preceded by a long silence. Or perhaps bursts are simply an epiphenomena explained by a time-varying stimuli, in which case

a time-varying Poisson spike train would encode the same amount of “state” information. Here, we explore allof these possibilities.

Methods

Surgical preparation. Cats were first anesthetized with ketamine HCl (20 mg/kg, i.m.), then by sodium pentothal (2– 4 mg • kg^{-1} • h^{-1}, i.v., supplemented as needed). They were ventilated through an endotracheal tube. Electrocardiogram, electroencephalogram, temperature, and expired CO_2 were continuously monitored. Animals were paralyzed with Norcuron (0.3 mg • kg^{-1} • h^{-1}, i.v.). (Data in Figures 3.6 and 3.7 was collected on un-paralyzed cats.) The eyes were refracted, fit with appropriate contact lenses, and focused on a tangent screen. Electrodes were inserted through a 0.5 cm diameter craniotomy over the LGN. Surgical and experimental procedures were in accordance with National Institutes of Health and United States Department of Agriculture guidelines. Procedures involving data from Figures 3.6 and 3.7 were approved by the UCSD Institutional Animal Care and Use Committee; procedures involving data of all other figures were approved by the Harvard Medical Area Standing Committee on Animals.

Electrical recording. Either parylene-coated tungsten electrodes (AM Systems, Everett, WA) or Quartz-coated platinum/tungsten electrodes (System Eckhorn; Thomas Recording, Marburg, Germany) were inserted through a 0.5 cm diameter craniotomy over the LGN. Recordings were amplified, filtered, and passed to a personal computer running either DataWave Technologies (Longmont, CO) Discovery software or Spike2, ver. 5.12a (Cambridge Electronic Design, Cambridge, UK); spike times were recorded with 0.1 ms resolution. Waveforms were analyzed offline to isolate single unit responses (Fee et al., 1996). Only well-isolated single unit responses with absolute refractory periods were analyzed further. Figures 3.6 and 3.7

contained both X (n=3) and Y cells (n=3), while all other figures contained only X cells. Additional analysis was performed using custom programs written in the Matlab programming environment (Mathworks, Natick, MA).

Visual stimulation. Stimuli in Figures 3.6 and 3.7 were 5-second spatially uniform, binary, white-noise stimuli. These stimuli were presented on a custom-built LED array (125 frames per second) at 100% contrast, and were repeatedly presented between 53 and 128 times. All other stimuli were spatially uniform and presented either on a cathode ray tube (CRT) monitor (128 frames per second; eight-bit grayscale; n = 9 cells) or a custom-built LED array (1200 frames per second; 15-bit grayscale; n = 6 cells). These stimuli were obtained by drawing independent random samples from the distribution of luminance values in natural luminance time series from van Hateren (1997), thereby eliminating the temporal correlations of the natural stimulus but preserving the distribution of the stimulus intensities. Stimuli were 8–32 s long and repeated 128 times. Results reported here were the same for both CRT and LED data, so both are shown and both are included in all averages we report.

Burst classification. We define a "burst" as a group of two or more action potentials separated by ≤6 ms, preceded by a period of >50 ms without spiking activity. This criterion was shown previously to reliably identify bursts that are attributable to low-threshold (T-type) calcium spikes in LGN relay cells of the cat (Lu et al., 1992, 1993; Ramcharan et al., 2001). We repeated our analysis with a more stringent burst criteria (preceding interval, >100 ms; internal interval, ≤4 ms); this decreased our estimated burst frequency only slightly and did not qualitatively change any of the results reported here.

Information calculations. Our recorded neural data were represented as time-binned spike trains; in this study, a fixed bin size of $\delta\tau$ = 2 ms was used. State information values were calculated from binned representations of the actual spike trains ($I_{identified}$) and compared to those calculated from binned representations of the response-shuffled spike trains ($I_{randomized}$). Because the state of the T-type calcium channel determines whether a response will be a burst or a single spike, if distinguishing the bursts from the spikes is advantageous, then I_{state} should be positive.

$$I_{state} = I_{identified}, - I_{randomized}$$

For calculations of $I_{identified}$, the value of a time bin was set to 0 if no spikes occurred during that time interval, 1 if a single spike occurred during that time interval, or 2 if a burstoccurred in that time interval. Each observed occurrence of a burst was represented by a single 2 the time of the first spike within the burst. This procedure was implemented both when calculating the noise entropy and the total entropy for $I_{identified}$.

For state-information calculations, used to determine whether it is informative to distinguish a burst from other spikes, we calculate the noise and total entropy as above, but we first shuffle the 2's and 1's across all non-0 bins, thereby preserving the number of patterns and spikes. $I_{randomized}$ is again the difference between the total and noise entropies. If bursts were interchangeable with single spikes, this shuffling should not change the information of the spike train.

Entropy calculations. Once the spikes and patterns are in a binned representation, we calculated the visual information in spike trains by the direct method (Strong et al., 1998), implemented exactly as by Denning and Reinagel

(2005). Briefly, we analyzed the information contained in words (short strings of bins) and varied the number of bins in the words, *L*. For each word length, we measured two forms of word entropy: the average noise entropy, $<H_{noise}>$, which reflects the trial-to-trial variability of words when the stimulus was fixed, and the average total entropy, $<H_{total}>$, which reflects the variability of words across all stimuli in the ensemble. $H_{noise}(t)$ was calculated from the distribution of words at a fixed time t relative to stimulus onset, in all repeats of the same sample of the stimulus. We performed a separate calculation of $H_{noise}(t)$ for many different values of t (separated by one bin) within the 8 or 32 s stimuli. We then averaged over t to get the average noise entropy $< H_{noise}>$.We performed equally many separate calculations of $H_{total}(t)$, but the set of words was instead selected using a different time t from each trial. When estimating $H_{total}(t)$, we used twice the number of words used to estimate $H_{noise}(t)$ in order to compensate for the approximately twofold difference in entropy. We averaged over t get the average total entropy $< H_{total}>$. Finally, the mutual information between the visual stimulus and the spike train is defined as $I = < H_{total}>-< H_{noise}>$.We computed information as a function of word length. We extrapolated to infinite word length from the linear part of the curve H versus $1/L$ as described by Strong et al. (1998).

Data adequacy for entropy calculations. For all entropy estimates that we computed, we determined how our estimate of H converged as we used increasing fractions of the data and then corrected for finite data size according to the method of Strong et al. (1998). The correction is obtained by fitting a second-order polynomial to 1/(fraction of data) versus estimate. We are confident of our estimates when the total correction for finite data size was <10% and the second-order term of this correction

was negligible, <1%. Results that passed these criteria are shown with filled symbols. For completeness, we also show our results from cells that did not pass the criteria. For these cells, we estimated the entropy by fitting a first-order polynomial to 1/(fraction of data) versus estimate.

Results

Overview

In Denning and Reinagel (2005), we concluded that bursts reliably occur at distinct times within stimuli. In the LGN cell shown in Figure 3.1A, a white-noise, time-varying, full-field, 8-second stimulus was repeatedly presented 128 times. In Figure 3.1A, single spikes are identified by black symbols and bursts of spikes by red symbols. As reported in Denning and Reinagel (2005), specific stimuli nearly always result in bursting responses, while other stimuli nearly always result in single-spiking responses. We then shuffle the responses' identity (as either a burst or single spike), in which case, the reliability of burst labels is eliminated (Figure 3.1B), indicating that the symbol identity is no longer informative about the stimulus.

The reliable occurrence of response types suggests that distinguishing between the response types can provide information about the stimulus. One method used to quantify the information available within spike trains is the direct method (Strong et al., 1998). The Direct Method begins by converting continuous spike trains into binary, binned responses. Time bins are set to 1 if a spike occurred within the bin and 0 if no spike occurred. These binary representations are then divided into words, consisting of a binary string defined by the values of consecutive bins. The mutual information between spike trains and visual stimuli is calculated by comparing the variability in the words when presented with the same, repeated stimulus (H_{noise}), and the variability in the words when presented with many different stimuli (H_{total}).

Because, as words get longer, it is exponentially more difficult to estimate the probability of any given word, these calculations are typically performed using short

words. Throughout this paper, we define the duration of our time bins ($\delta\tau$) as 2ms and the length of our words (L) as 8 bins (16ms). Although the utilization of short words removes information about longer spiking responses, one might imagine a decoding cell to only be sensitive to spiking responses along a similarly short timescale.

Distinguishing bursts and spikes provides visual information

We want to calculate the difference between the information available when bursts and single spikes can be correctly identified and the information available when the spiking responses cannot be correctly identified. We define this difference as the state information, because the state of the T-type calcium channel (either de-inactivated or inactivated) determines the response type (either a burst or a single spike, respectively). When the voltage trace is binned into the original spiking response (Figure 3.2), not only can bursts be correctly identified, based on ISI criteria, but burst structure (e.g., ISIs within the burst and the number of spikes within the burst) is preserved. Perhaps the simplest state-information calculation would be to calculate the information from the original representation and subtract from that the information from the unidentified representation (Figure 3.2), in which all bursts are replaced by single spikes. Figure 3.3B illustrates that, indeed, the information from the original representation is greater than that from the unidentified representation, suggesting that distinguishing between bursts and single spikes is informative. However, because the original representation contains more spikes than the unidentified representation, it will be more difficult to estimate the probability distributions of words, subjecting the two calculations to a different bias.

In Denning and Reinagel (2005), we define the identified representation as one in which each burst is replaced by a single symbol (Figure 3.2). (In the binned representation, each burst is replaced by a 2 at the time of the first spike within the burst.) This representation eliminates any information within burst structure, but preserves any information within the response identity. Because in this data set, there was little variability within the burst structure, the information rates from the original representation, $I_{original}$, and the information rates from the identified representation, $I_{identified}$, are approximately equal (Figure 3.3A). Again, we could compare the information from this representation and the information from the unidentified representation, $I_{unidentified}$, (Figure 3.3C), but a larger number of words are still present in the identified representation due to the inclusion of the extra symbol; therefore, the biases are still different.

If, instead, we merely shuffle the identity of the spiking responses to create a randomized representation (Figures 3.2 and 3.1B), then information within the response identity is lost, but the bias from the identified and randomized representations are roughly equal. We define the state information, I_{state}, as the difference in the mutual information between the stimulus and the identified spike train, $I_{identified}$, and the mutual information between the stimulus and the randomized spike train, $I_{randomized}$. Because the information from the randomized spike train is less than that from the identified spike train (Figure 3.3D), the state information is positive, and we conclude that it is informative to distinguish between bursts and single spikes.

Entropy contributions to state information

Positive state information values could be explained if the variability of words during unique stimuli was greater for the identified representation than the randomized, if the variability during repeated stimuli was less for the identified representation than the randomized, or a combination of the two. Spike trains during both repeated and unique stimuli are converted to either identified or randomized representations in order to estimate the total (H_{total}) and noise (H_{noise}) entropies for both conditions (see Methods). We first calculate the total entropy, H_{total}. This value measures the variability in words when many different stimuli are presented. Shuffling the burst symbols (2) amongst the spikes' symbols increased H_{total} by a negligible amount (Figure 3.4A). This small increase in entropy likely occurs because the randomized representation can contain words that are never observed in the identified representation. For example, if two responses are separated by 10ms, the second response could never be a burst in the identified representation, as a burst must be preceded by long silence, but in the randomized representation, a burst symbol may be assigned to the second response.

Next, we calculate the noise entropy, H_{noise}. This value measures the variability in words across trials when the same stimulus is repeatedly presented. In addition to the effect noted above for H_{total}, H_{noise} will increase to the extent that the response symbol is consistent across trials. Shuffling the patterns' symbol among the spikes' symbols increased H_{noise} (Figure 3.4B). In addition to the effect noted above for H_{total}, H_{noise} increases to the extent that the response symbol is consistent across trials. The null hypothesis that bursts are a random subset of responses predicts that H_{total} and H_{noise} will change by similar amounts.

The amount of visual information, I, is equal to the total entropy, H_{total}, minus the noise entropy, H_{noise}, (see Methods). Because the randomized representations were characterized by lower noise entropy values than the identified representation, the identified responses' information, $I_{identified}$, is larger than the randomized responses' information, $I_{randomized}$ (Figure 3.3D).

The state information, $I_{state,}$ is equal to the difference of the identified responses' information, $I_{identified}$, and the randomized responses' information, $I_{randomized}$. In other words, how much more could a decoder know about the visual stimulus by knowing which responses are bursts, compared to one that only knows what fraction of responses are bursts. As shown in Denning and Reinagel (2005), I_{state} depends on the frequency of bursts (Figure 3.4C). The positive values of I_{state} indicate that it is informative to distinguish the bursts from single spikes. The state information can contribute a substantial amount of information, up to 11% in this data set.

Contributions of time-varying firing rate to state information

One could imagine that a time-varying stimulus could be constructed such that a cell will frequently respond with a particular spiking pattern. If the cell only fired one spike every time an excitatory stimulus was presented, then by presenting excitatory stimuli at precise times, a spiking pattern would be evident in the cell's response.

If apparent bursts were merely an artifact of time-varying firing rates, then a Poisson spike train should exhibit similar state information to that found in LGN cells. Therefore, for each LGN cell, we created rate-varying Poisson spike trains to match

the observed PSTH of the cell. "Bursts" were identified by ISI criteria. We observed more patterns meeting the burst criteria in the Poisson spike trains than in LGN data (Figure 3.5A). We notice this difference to be particularly evident during imprecise firing events that contain only one spike in the majority of trials. The imprecision of the events causes a broad peak in the probability of firing, causing multiple spikes within single trials of the Poisson spike trains.

We measure I_{state} as described above, and find that, for most cells, I_{state} in bits per second is greater for LGN cells than for Poisson spike trains (Figure 3.5B). This is surprising, because in LGN cells we find that I_{state} increases as the burst frequency increases (Figure 3.5D and Denning and Reinagel, 2005).

When I_{state} is measured in bits per burst, LGN state information is greater than Poisson spike trains' state information for all cells (Figure 3.5C). This indicates that the bursting pattern conveys more information than would be expected merely by the time-varying firing rate, and although I_{state} depends on the burst rate for both LGN data and Poisson data, the information rate corresponding to any given burst rate is greatest for LGN data (Figure 3.5D). We note that many "burst" patterns observed in Poisson data arise since actual bursts provide burst-like structure to the time-varying firing rate. Therefore, we believe that the Poisson comparison over-estimates the contribution of the state information that is due only to spiking patterns not caused by the T-type calcium channel.

Contributions of single-ISI criterion patterns to state information

Bursts are identified by two inter-spike interval criteria: the burst must consist of at least two spikes, separated by short ISIs (≤6ms) and the burst must be preceded by a long ISI (≥ 50ms). Alitto et al. (2005) reported that, although bursts and single spikes differed in the average stimulus preceding the responses, the average stimulus preceding responses that satisfied only the long ISI criteria also differed from all other spikes. Perhaps it is equally informative to distinguish between any response following a long ISI (regardless of whether or not it was a burst) and other spikes as it is to distinguish between bursts and single spikes.

In order to test whether bursts are merely a random sub-set of long-ISI responses, we begin by calculating the state information, I_{state}, as described above. Next, instead of shuffling the burst symbols (**2**) amongst all responses, as was described above, we only shuffle the bursts amongst the sub-set of responses (either bursts or single spikes) that were preceded by a long-ISI. We define the information rate of this response representation as $I_{long\ ISI\ shuf}$. The long-ISI information rate, $I_{long\ SI}$, is equal to $I_{identified}$ minus $I_{long\ ISI\ shuf}$. If similar stimuli cause bursts and spikes preceded by a long ISI, then $I_{long\ ISI}$ should be equal to zero. Instead, we find that information is lost when bursts are shuffled amongst long-ISI responses (symbols to the right of the x=0 line in Figure 3.6A), indicating that it is informative to distinguish bursts and long-ISI single spikes. However, not as much information is lost as when bursts are shuffled amongst all spikes (symbols above y=x line in Figure 3.6A), indicating that long-ISI responses are a distinct sub-set of other spikes and that some of the information obtained by distinguishing spikes from bursts (I_{state}) is due to the fact that bursts follow long-ISIs.

Similarly, we investigate whether bursts are a random subset of all responses satisfying the other short-ISI criterion. This required the extra step of collapsing high-firing rate epochs into singular "events" analogous to burst events. First, we represent all bursts with a 2. Next, we represent all other high-firing rate epochs (multiple spikes separated by short ISIs but not preceded by a long ISI) with a single 1. All other spikes are represented by a 1. The modified identified information, $I_{identified}$', is then calculated in the same manner as described above, and this is compared to the information rate when the burst symbols are shuffled amongst all non-0 symbols, $I_{randomized}$'. I_{state}' is then defined as $I_{identified}$'minus $I_{randomized}$'. Next, we shuffle the correctly-identified burst symbols amongst only responses satisfying the second, short-ISI criteria. That is, the burst symbols are shuffled amongst the 2's and the 1's that represented the high-firing rate epochs and this shuffled information rate, $I_{short\ ISI\ shuf}$, is calculated. The short-ISI information rate, $I_{short\ ISI}$, is equal to $I_{identified}$' minus $I_{short\ ISI\ shuf}$. As before, we find that information is lost when bursts are shuffled amongst short-ISI responses (symbols to the right of the x=0 line in Figure 3.6B), indicating that it is informative to distinguish putative low-threshold bursts from other short-ISI spikes. However, not as much information is lost as when bursts are shuffled amongst all spikes (symbols above y=x line in Figure 3.6B), indicating that short-ISI responses are a distinct sub-set of other spikes and that some of the information obtained by distinguishing spikes from bursts (I_{state}) is due to the fact that bursts include short-ISI spikes.

Burst size encodes information

The state-information method represents all bursts by a 2, thereby removing any information encoded by burst size (the number of spikes within a burst). However, in vitro studies have shown that the number of action potentials within a burst depends on the degree of hyperpolarization (Bevan et al., 2002). This suggests that the burst size (the number of spikes within a burst) could encode information about the stimulus. Additionally, theoretical results have suggested that the burst size is related to the magnitude of the slope of the input signal.

In the data used in Denning and Reinagel (2005) and in most of the LGN cells that we have recorded from, there was little variability in burst structure (data not shown). However, for six cells, we observed a variety of burst sizes (Figure 3.7A). (We required at least 200 bursts with more than three spikes within the bursts in order for cells to be included in this analysis.) This allowed us to determine whether burst size

We calculated the spike-triggered averages for bursts of different sizes (Figure 3.7B). Across cells, as the burst size increased the magnitude of the suppressive phase increased, and the time to the excitatory maximum decreased (data not shown across cells). This suggests that different stimuli trigger bursts of different sizes, and therefore burst size could encode information.

In order to explore this hypothesis, we represented each burst with an integer value equal to the burst size. All other spikes were represented by a 1. The information rate of these responses was calculated; we subtracted from that the information rate obtained when the burst symbols were shuffled amongst all response symbols. This difference was defined as $I_{State\ Burst\ Size}$.

We wanted to compare this information rate to that if bursts were not distinguished by their burst size. In order to keep constant any bias introduced by the larger number of symbols, instead of representing all bursts by the same symbol, we shuffled all burst symbols amongst each other. We calculated the information rate of these responses and subtracted from that the information rate obtained when burst symbols were shuffled amongst all response symbols, as before. This difference was defined as $I_{State\ Burst\ Size\ Shuf}$.

If burst size conveys information about the stimulus, then shuffling the burst symbols amongst each other will reduce the information, meaning that $I_{State\ Burst\ Size\ Shuf}$ will be less than $I_{State\ Burst\ Size}$. Indeed, $I_{State\ Burst\ Size\ Shuf}$ was less than $I_{State\ Burst\ Size}$ for all cells (Figure 3.7C and 3.7D).

We compared the first ISI within a burst across bursts of different sizes. We find that short ISIs are more probable if the burst contains many spikes (Figure 3.8). Therefore, we suspect that distinguishing between bursts with different ISIs would similarly provide visual information.

Discussion

Bias and the state-information measure

Above, we demonstrate a technique which quantifies how informative it is to distinguish bursts from single spikes. In Figures 3.2 and 3.3, we describe several methods by which this information value could be calculated. Our method replaces the bursts and single spikes by two different symbols, calculates the information, and then calculates the information lost if the bursts' symbols are shuffled amongst symbols from all responses. An alternative method might calculate the information from the original binned representation and compare that to the information from a binned representation that replaces all burst spikes with a single spike. In the latter method, the two information values compared in the latter method will include a different sampling bias; more words are possible within the original binned representation, thereby increasing the bias. The state-information measure reduces the difference biases by including the burst symbol in both representations.

Our measure does not equalize the bias in both the identified and randomized representation. By shuffling the burst symbol amongst all symbols in the randomized representation, some words are possible that could never exist in the identified representation. For example, two spikes could be separated by 10 milliseconds. In the identified representation, the second spike could never be identified as the first spike of a burst, as the preceding ISI is too short, given the burst criteria. During the randomized representation, the second spike is as likely as any other to be assigned to a burst symbol. Separate calculations revealed that if we restricted the randomly-

assigned bursts to responses that would not result in "impossible words", results presented above are unchanged (not shown).

Information in burst structure

In Figure 3.4, we show that specific visual stimuli trigger bursts containing different numbers of spikes. The spike-triggered averages in Figure 3.7B suggest that when a cell is more hyperpolarized (by longer or stronger inhibitory stimuli), bursting responses will contain more spikes. This is consistent with the in vitro study that has shown that the number of action potentials within a burst depends on the degree of hyperpolarization (Bevan et al., 2002). We hypothesize that these cells contained multiple T-type calcium channel molecules and stronger inhibitory stimuli de-inactivated more of these channels, resulting in larger calcium influx during the calcium spikes and therefore burst sizes. Most other cells did not show much heterogeneity in burst size: bursts typically consisted of just two spikes. We suspect that these cells did not have as many T-type calcium channels.

Information explained by time-varying firing rate

We found that Poisson spike trains generated from cells' time-varying firing rate are characterized by positive "state" information (Figure 3.5). This may suggest that some "state" information is merely because we are identifying spiking patterns caused by the stimulus and not the T-type calcium channel. Unfortunately, bursts' patterns contribute to the time-varying firing rate, such that many "bursts" in the Poisson data likely reflect real bursts in the LGN data.

In order to better test the above hypothesis, one might generate time-varying Poisson data using the unidentified representation. This approach is slightly complicated by the fact that not all spikes within bursts may be correctly identified by ISI criteria, but increases the probability that all "bursts" within the Poisson data are artifactual bursts due to patterns not caused by the T-type calcium channels.

Secondly, both this proposed analysis and the analysis presented in Figure 3.5 should be repeated using time-varying Poisson data that incorporates a refractory period. If the Poisson-refractory data of the unidentified representation is also characterized by positive "state" information, this could reveal a bias in our analysis, as many "bursting" patterns may be identified as T-type calcium bursts when, in fact, they were merely spiking patterns caused by the stimulus.

Information in long-ISI spikes and high-firing rate epochs

It is informative to distinguish both spikes following long-ISIs and high-firing rate epochs from single spikes. However, bursts are not interchangeable with either of these patterns (Figure 3.6). It remains to be determined whether the information associated with distinguishing bursts and single spikes can be explained by a combination of the information rates associated with the long-ISI spikes and high-firing rate epochs. These two patterns may encode redundant information, therefore adding the information values associated with each pattern

Future directions

Lesica and Stanley (2004) reported that a bursting mechanism had to be added to an integrate-and-fire model in order to accurately model LGN responses. Here, we extend findings from Denning and Reinagel (2005) that bursts and single spikes respond to distinct stimuli. Furthermore, in Figure 3.4, we illustrate that specific stimuli can elicit bursts of different sizes. Because the integrate-and-fire-or-burst model can accurately reproduce much of the LGN responses, it would be interesting to apply our state-information measure to model data and compare the state information from LGN cells to that from their respective model data. This should further our understanding of the influence of visual stimuli on de-inactivating the T-type calcium channel.

Other applications

We speculate that our state-information measure could be applied to other spiking patterns besides those caused by T-type calcium channels. Instead of replacing bursts with a specific symbol, any arbitrary pattern could be replaced, and then calculations could proceed as above.

For example, visual cortex neurons, prefrontal cortex neurons, superior colliculus neurons, lateral posterior nucleus neurons, lateral geniculate nucleus (LGN) neurons, mitral cells, and retinal ganglion cells (Strehler and Lestienne, 1986; Lestienne and Strehler, 1987; Mandl, 1993; Lestienne et al., 1999; Li et al., 2003) can exhibit distinct epochs of high-frequency spiking. These high-frequency spiking epochs can include doublet or triplet spikes, depending on the cell type, but importantly, the same spiking pattern can be repeatedly observed throughout the cell's

spiking response. Although these patterns are observed more frequently than expected either by a Poisson-like process or a renewal process with the same inter-spike interval distribution as the cells (Lestienne and Tuckwell, 1998), it is unknown whether it is informative to distinguish these patterns from individual spikes.

Not only could the measure determine whether it is informative to distinguish the spiking pattern from single spikes, but one could evaluate whether two spiking patterns are equivalent. For example, we concluded that bursts of different sizes are not equivalent, as more information was present when bursts of different sizes were correctly and differently identified, versus when their identity was randomized. The measure could be used to determine whether several different spiking rates are equivalent.

Finally, some analyses have suggested that spike correlations across neurons provides information about the stimulus (Eckhorn et al., 1988; Gray et al., 1989; Gray and Singer, 1989; Meister et al., 1995; Vaadia et al., 1995; deCharms and Merzenich, 1996; Dan et al., 1998; Steinmetz et al., 2000; Hirabayashi and Miyashita, 2005), while other analyses have suggested that these correlations carry little to no information about the stimulus (Nirenberg et al., 2001; Oram et al., 2001; Panzeri et al., 2001; Petersen et al., 2001; Levine et al., 2002; Panzeri et al., 2002b; Panzeri et al., 2002a; Petersen et al., 2002; Averbeck et al., 2003; Averbeck and Lee, 2003; Golledge et al., 2003). We speculate that this technique may be able to determine whether correlated spikes in the retina are distinct from other non-correlated spikes.

Conclusion

We demonstrate a state-information measure that indicates that distinguishing between bursts and single spikes in the LGN provides visual information. Although in principle, our measure is equivalent to other measures, our measure is less sensitive to biases induced by finite data. We find that the state information cannot be explained by structure caused by time-varying firing rate, and we find that bursts are not interchangeable with spikes following long silences or with spikes separated by short intervals. Finally, we provide experimental evidence that different visual stimuli cause bursts with various numbers of spikes. Therefore, burst size can also provide visual information. We conclude that visual stimuli influence the T-type calcium channel, and the response type is able to provide additional information about the stimulus to downstream neurons.

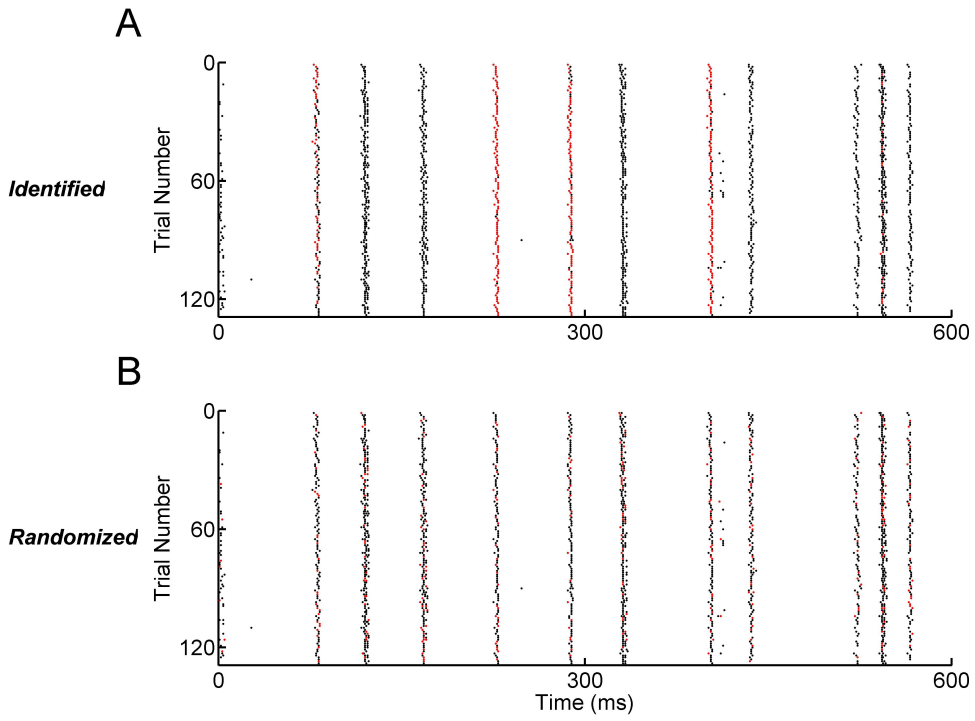

Figure 3.1: Binned representation of spikes and patterns. A, Identified representation of a raster plot from a representative LGN neuron to 128 repeats of the same white-noise stimulus. Each row represents a trial; each point represents the time of an action potential within that trial. A 600ms segment from the middle the 8s trials is shown. The red points indicate bursts, defined as a group of spikes following a silence of at least 50 ms and with inter-spike intervals less than or equal to 6 ms. Black points indicate single spikes. B, Randomized representation of the raster: the spike-pattern symbols are shuffled among the spikes. That is, the red points in (A) are shuffled among the black points.

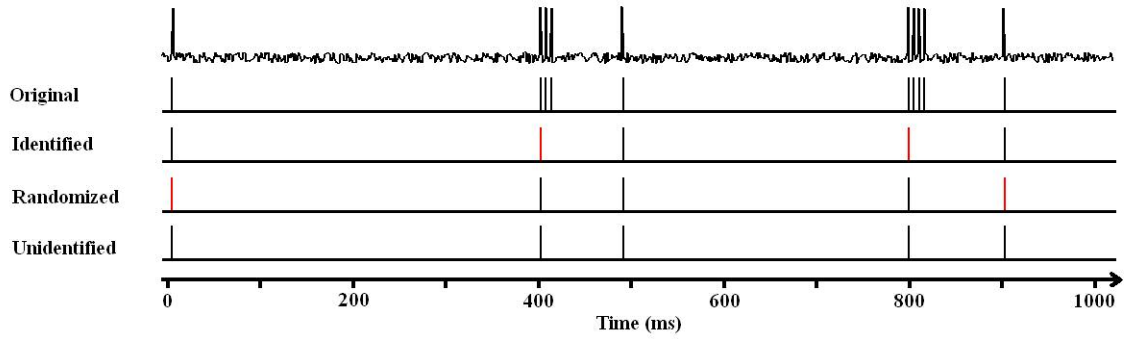

Figure 3.2: Illustration of spike-train representations. The top row shows a fake voltage trace. The original representation (second row) is the unprocessed spike train, such that the values of all time bins containing a spike (regardless of whether the spike was a single spike or part of a burst) are represented by a 1 (as shown with black lines). The identified representation (third row) replaces all bursts with a 2 (as shown with red lines). The randomized representation (fourth row) shuffles the 1 and 2 symbols amongst each other. The unidentified representation (fifth row) represents all bursts and all single spikes with a 1 (as shown with black lines).

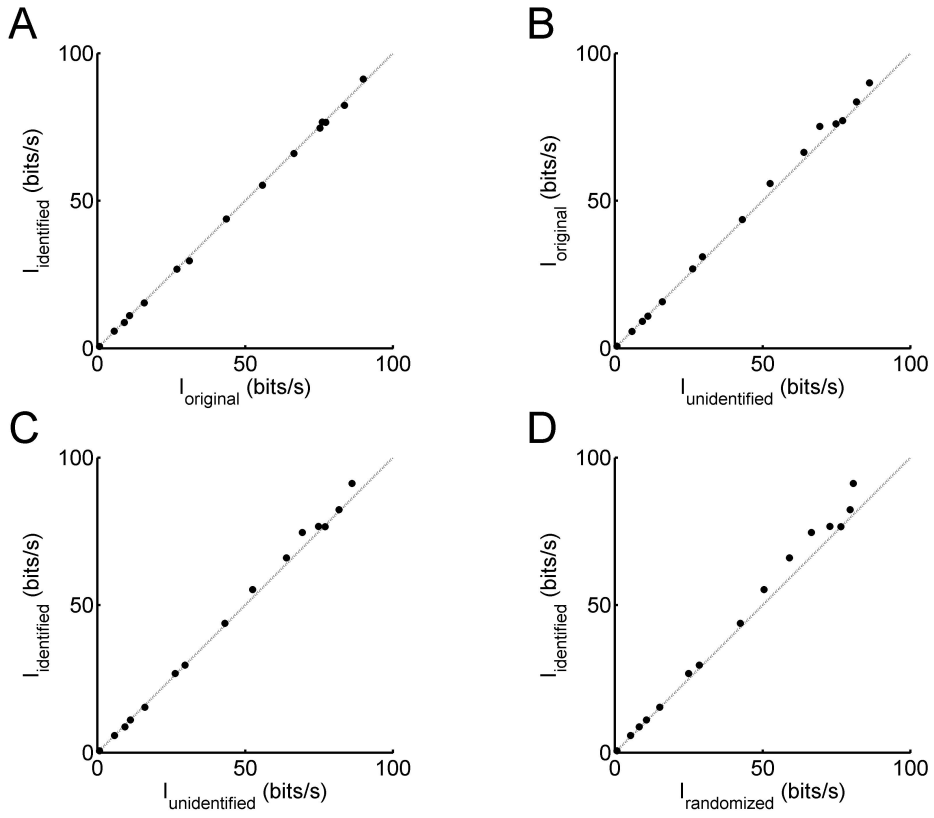

Figure 3.3: Information from different spike-train representations. A, Information rates in bits per second from the identified and original representations are not significantly different (p=.016). B, Information rates from the original and unidentified representations are significantly different ($p < 0.05$). C, Information rates from the identified and unidentified representations are significantly different ($p < 0.05$). D, Information rates from the identified and the randomized representations are significantly different ($p < 0.001$).

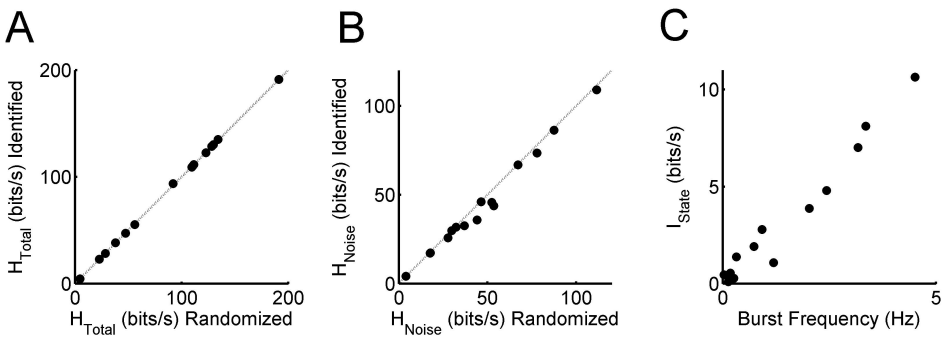

Figure 3.4: Entropies and information rates associated with distinguishing bursts and spikes. A, The noise entropy of cells' identified rasters is compared to that of cells' randomized rasters. Each symbol represents data from one cell. Entropies and information values were calculated using $\delta\tau$=2ms bins and L=8 bins. Entropy estimates were empirically corrected for finite data size (see Methods). Filled symbols indicate cells for which this correct was small and linear for both randomized and identified rasters. Open symbols indicate cells that did not pass this criterion. B, The total entropy is compared between cells' identified and randomized responses. Symbols as in (A). C, The state information rate, I_{state}, versus the burst frequency. Symbols as in (A).

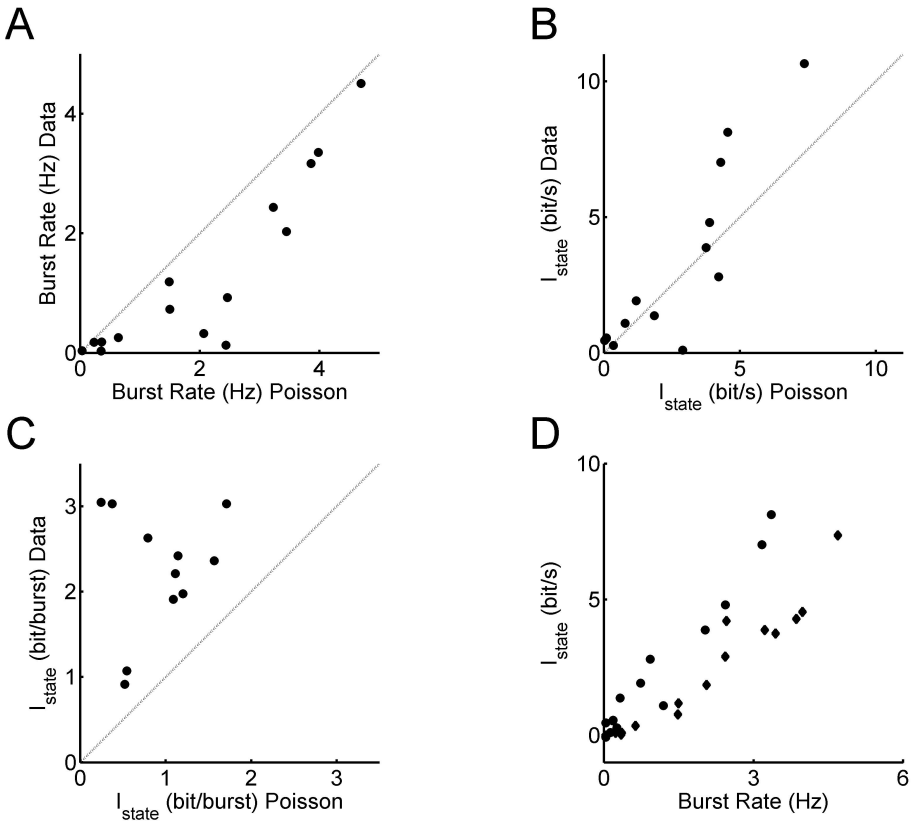

Figure 3.5: State information of time-varying Poisson spike trains. A, The burst rate of LGN cells compared to that from time-varying Poisson spike trains, where bursts were identified using standard ISI criteria. Each symbol compares data from one LGN cell to data from Poisson spike trains, generated from the post-stimulus time histogram of the respective cell. B, The information rate, measured in bits per second for LGN data versus Poisson data. Symbols as in (A). C, The information rate, measured in bits per burst for LGN data versus Poisson data. D, The information rate in bits per second versus the burst rate. Circles represent data from LGN cells, while diamonds represents data from Poisson spike trains.

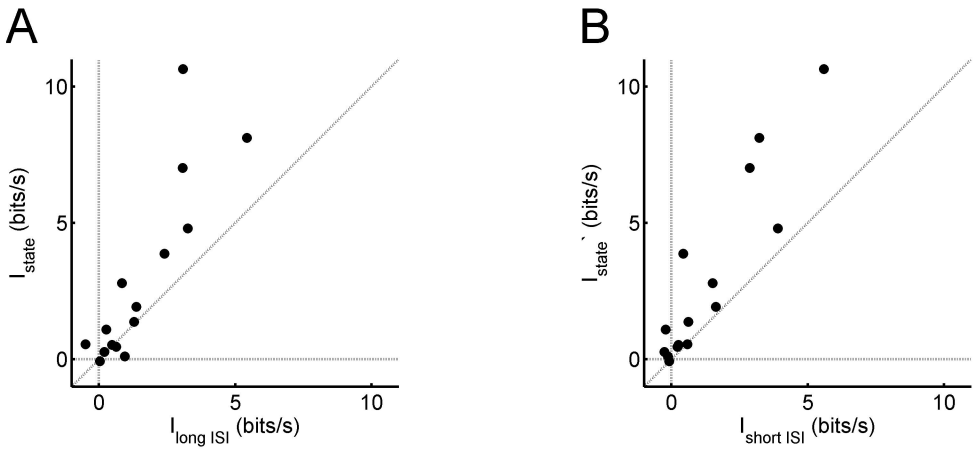

Figure 3.6: State information not explained by single ISI criterion. A, The state information, I_{state}, is compared to $I_{long\ ISI}$, as described in the text, in order to determine whether bursts were interchangeable with long-ISI responses. Each symbol represents data from one cell. B, The modified state information, I_{state}', is compared to $I_{short\ ISI}$, as described in the text, in order to determine whether bursts were interchangeable with short-ISI responses. Symbols as in (A).

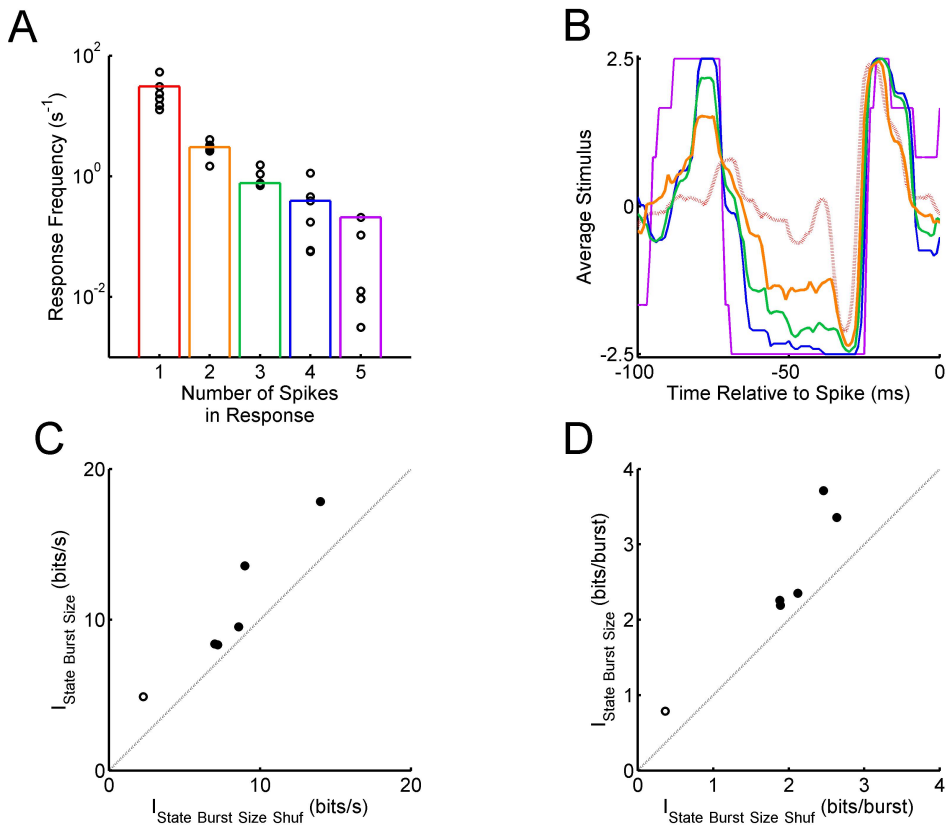

Figure 3.7: Information encoded by burst size. A, The frequency of responses with the shown number of spikes per response. A response is defined as either a burst or single spike, such that all responses with one spike in the response are defined as single spikes. The frequencies of bursts with 2-5 spikes are also shown. Six cells had sufficient data for this analysis. The average response frequency for each given number of spikes is shown by the bars. B, The average stimulus preceding single spikes (red dashed curve) or bursts from one representative LGN cell. The orange, green, blue, and purple spike-triggered averages correspond to the average stimulus preceding bursts consisting of 2, 3, 4, and 5 spikes, respectively. C, The state information, I_{state}, in bits/s when bursts were represented by an integer value corresponding to the number of the spikes per burst versus the state information when these integer values were randomly shuffled amongst all bursts. Cells above the diagonal line indicate that burst size encodes visual information. Information rates were corrected for finite data size (see Methods). Filled symbols indicate cells for which this correction was small and linear under both conditions. Open symbols indicate cells that did not pass this criterion. D, Same as (C), where the state information is shown in bits/burst.

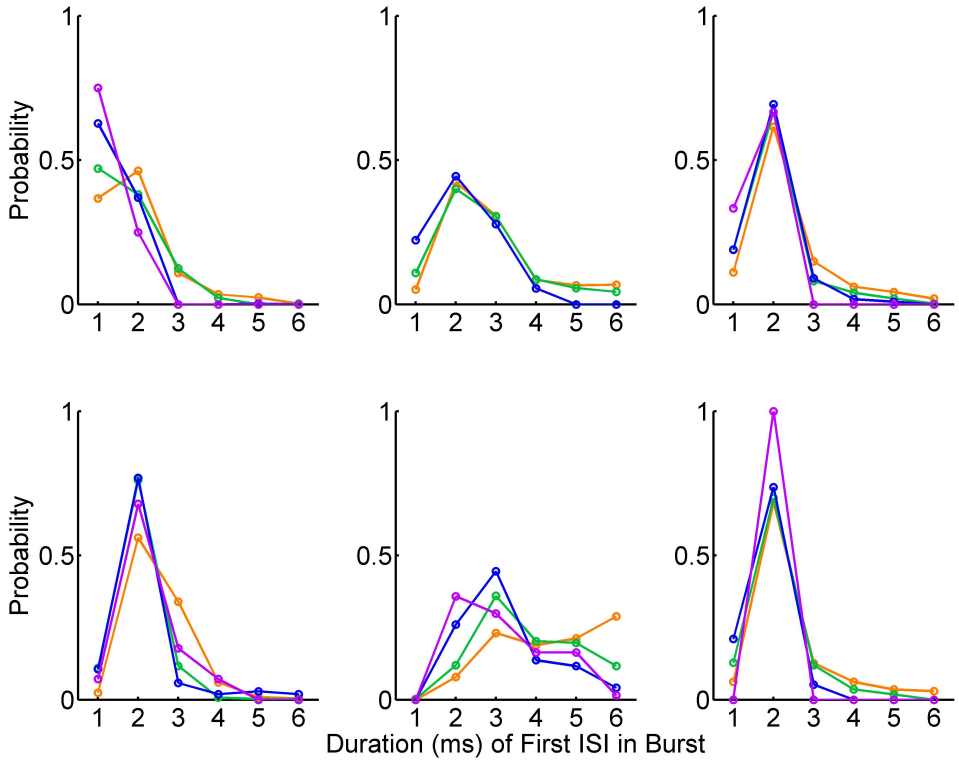

Figure 3.8: The probability of a burst with a given first inter-spike interval. Each panel represents data from a different cell. The orange, green, blue, and purple ISI-probability curves indicate the probability of the ISI within bursts containing two, three, four, or five spikes, respectively.

References

Alitto HJ, Weyand TG, Usrey WM (2005) Distinct properties of stimulus-evoked bursts in the lateral geniculate nucleus. J Neurosci 25:514-523.

Averbeck BB, Lee D (2003) Neural noise and movement-related codes in the macaque supplementary motor area. J Neurosci 23:7630-7641.

Averbeck BB, Crowe DA, Chafee MV, Georgopoulos AP (2003) Neural activity in prefrontal cortex during copying geometrical shapes. II. Decoding shape segments from neural ensembles. Exp Brain Res 150:142-153.

Bevan MD, Magill PJ, Hallworth NE, Bolam JP, Wilson CJ (2002) Regulation of the timing and pattern of action potential generation in rat subthalamic neurons in vitro by GABA-A IPSPs. J Neurophysiol 87:1348-1362.

Dan Y, Alonso JM, Usrey WM, Reid RC (1998) Coding of visual information by precisely correlated spikes in the lateral geniculate nucleus. Nat Neurosci 1:501-507.

deCharms RC, Merzenich MM (1996) Primary cortical representation of sounds by the coordination of action-potential timing. Nature 381:610-613.

Denning KS, Reinagel P (2005) Visual control of burst priming in the anesthetized lateral geniculate nucleus. J Neurosci 25:3531-3538.

Eckhorn R, Bauer R, Jordan W, Brosch M, Kruse W, Munk M, Reitboeck HJ (1988) Coherent oscillations: a mechanism of feature linking in the visual cortex? Multiple electrode and correlation analyses in the cat. Biol Cybern 60:121-130.

Fee MS, Mitra PP, Kleinfeld D (1996) Automatic sorting of multiple unit neuronal signals in the presence of anisotropic and non-Gaussian variability. J Neurosci Methods 69:175-188.

Golledge HD, Panzeri S, Zheng F, Pola G, Scannell JW, Giannikopoulos DV, Mason RJ, Tovee MJ, Young MP (2003) Correlations, feature-binding and population coding in primary visual cortex. Neuroreport 14:1045-1050.

Gray CM, Singer W (1989) Stimulus-specific neuronal oscillations in orientation columns of cat visual cortex. Proc Natl Acad Sci U S A 86:1698-1702.

Gray CM, Konig P, Engel AK, Singer W (1989) Oscillatory responses in cat visual cortex exhibit inter columnar synchronization which reflects global stimulus properties. Nature 338:334-337.

Guido W, Weyand T (1995) Burst responses in thalamic relay cells of the awake behaving cat. J Neurophysiol 74:1782-1786.

Hirabayashi T, Miyashita Y (2005) Dynamically modulated spike correlation in monkey inferior temporal cortex depending on the feature configuration within a whole object. J Neurosci 25:10299-10307.

Jahnsen H, Llinas R (1984) Ionic basis for the electro-responsiveness and oscillatory properties of guinea-pig thalamic neurones in vitro. J Physiol 349:227-247.

Kepecs A, Lisman J (2003) Information encoding and computation with spikes and bursts. Network 14:103-118.

Kepecs A, Wang XJ, Lisman J (2002) Bursting neurons signal input slope. J Neurosci 22:9053-9062.

Lesica NA, Stanley GB (2004) Encoding of natural scene movies by tonic and burst spikes in the lateral geniculate nucleus. J Neurosci 24:10731-10740.

Lestienne R, Strehler BL (1987) Time structure and stimulus dependence of precisely replicating patterns present in monkey cortical neuronal spike trains. Brain Res 437:214-238.

Lestienne R, Tuckwell HC (1998) The significance of precisely replicating patterns in mammalian CNS spike trains. Neuroscience 82:315 336.

Lestienne R, Tuckwell HC, Chalansonnet M, Chaput M (1999) Repeating triplets of spikes and oscillations in the mitral cell discharges of freely breathing rats. Eur J Neurosci 11:3185-3193.

Levine MW, Castaldo K, Kasapoglu MB (2002) Firing coincidences between neighboring retinal ganglion cells: inside information or epiphenomenon? Biosystems 67:139-146.

Li J, Bickford ME, Guido W (2003) Distinct firing properties of higher order thalamic relay neurons. J Neurophysiol 90:291-299.

Lu SM, Guido W, Sherman SM (1992) Effects of membrane voltage on receptive field properties of lateral geniculate neurons in the cat: contributions of the low-threshold Ca2+ conductance. J Neurophysiol 68:2185-2198.

Lu SM, Guido W, Sherman SM (1993) The brain-stem parabrachial region controls mode of response to visual stimulation of neurons in the cat's lateral geniculate nucleus. Vis Neurosci 10:631-642.

Mandl G (1993) Coding for stimulus velocity by temporal patterning of spike discharges in visual cells of cat superior colliculus. Vision Res 33:1451-1475.

Martinez-Conde S, Macknik SL, Hubel DH (2002) The function of bursts of spikes during visual fixation in the awake primate lateral geniculate nucleus and primary visual cortex. Proc Natl Acad Sci U S A 99:13920-13925.

Meister M, Lagnado L, Baylor DA (1995) Concerted signaling by retinal ganglion cells. Science 270:1207-1210.

Nirenberg S, Carcieri SM, Jacobs AL, Latham PE (2001) Retinal ganglion cells act largely as independent encoders. Nature 411:698-701.

Oram MW, Hatsopoulos NG, Richmond BJ, Donoghue JP (2001) Excess synchrony in motor cortical neurons provides redundant direction information with that from coarse temporal measures. J Neurophysiol 86:1700-1716.

Panzeri S, Golledge H, Zheng F, Tovée M, Young M (2001) Objective assessment of the functional role of spike train correlations using information measures. Vis Cogn 8.

Panzeri S, Pola G, Petroni F, Young M, Petersen R (2002a) A critical assessment of different measures of the information carried by correlated neuronal firing. Biosystems 67:177-185.

Panzeri S, Golledge H, Zheng F, Pola G, Blanche T, Tovée M, Young M (2002b) The role of correlated firing and synchrony in coding information about single and separate objects in cat V1. Neurocomputing 44-46:579=584.

Petersen RS, Panzeri S, Diamond ME (2001) Population coding of stimulus location in rat somatosensory cortex. Neuron 32:503-514.

Petersen RS, Panzeri S, Diamond ME (2002) The role of individual spikes and spike patterns in population coding of stimulus location in rat somatosensory cortex. Biosystems 67:187-193.

Ramcharan EJ, Gnadt JW, Sherman SM (2000) Burst and tonic firing in thalamic cells of unanesthetized, behaving monkeys. Vis Neurosci 17:55-62.

Ramcharan EJ, Gnadt JW, Sherman SM (2001) The effects of saccadic eye movements on the activity of geniculate relay neurons in the monkey. Vis Neurosci 18:253-258.

Ruiz O, Royal DW, Sary G, Chen X, Schall JD, Casagrande VA (2006) Low-Threshold Ca2+-Associated Bursts are Rare Events in the LGN of the Awake Behaving Monkey. J Neurophysiol.

Steinmetz PN, Roy A, Fitzgerald PJ, Hsiao SS, Johnson KO, Niebur E (2000) Attention modulates synchronized neuronal firing in primate somatosensory cortex. Nature 404:187-190.

Strehler BL, Lestienne R (1986) Evidence on precise time-coded symbols and memory of patterns in monkey cortical neuronal spike trains. Proc Natl Acad Sci U S A 83:9812-9816.

Strong SP, de Ruyter van Steveninck RR, Bialek W, Koberle R (1998) On the application of information theory to neural spike trains. Pac Symp Biocomput:621-632.

Vaadia E, Haalman I, Abeles M, Bergman H, Prut Y, Slovin H, Aertsen A (1995) Dynamics of neuronal interactions in monkey cortex in relation to behavioural events. Nature 373:515-518.

van Hateren JH (1997) Processing of natural time series of intensities by the visual system of the blowfly. Vision Res 37:3407-3416.

Weyand TG, Boudreaux M, Guido W (2001) Burst and tonic response modes in thalamic neurons during sleep and wakefulness. J Neurophysiol 85:1107-1118.

Chapter 4

Functional benefits of contrast normalization

demonstrated in neurons and model cells

Abstract

The large dynamic range of natural stimuli poses a challenge for neural coding: how is a neuron to encode large differences at high contrast while remaining sensitive to small differences at low contrast? Many sensory neurons exhibit contrast normalization: gain depends on the range of stimuli presented, such that firing-rate modulation is maintained across contrasts. Yet coding depends strongly on the precision of spike timing and the reliability of spike number, neither of which can be predicted from neural gain. We report that as contrast decreases, responses are more variable and encode less information. Nevertheless these changes can be small, and information transmission is even better preserved across contrasts than rate modulation. The preservation of information is correlated with the extent of contrast normalization, thereby establishing a functional consequence of normalization. We further show that a non-adapting model can exhibit both contrast normalization and the associated information preservation.

Introduction

Given that a neuron can only produce a limited range of firing rates, the sensitivity of its firing rate to stimulus strength will determine the range of stimuli it can effectively discriminate. There is a broad range of contrasts present in natural scenes (Ruderman and Bialek, 1994; van Hateren, 1997) (see Figure 1.3), suggesting that it would be advantageous to adapt sensitivity to the prevailing contrast (Atick and Redlich, 1992; Schwartz and Simoncelli, 2001). Contrast normalization has long been known to occur in the early visual system of mammals (Shapley and Victor, 1978, 1981; Shapley and Enroth-Cugell, 1984; Benardete et al., 1992; Shou et al., 1996; Benardete and Kaplan, 1997; Smirnakis et al., 1997; Brown and Masland, 2001; Chander and Chichilnisky, 2001; Kim and Rieke, 2001; Kremers et al., 2001; Baccus and Meister, 2002; Kim and Rieke, 2003; Solomon et al., 2004; Jin et al., 2005). Analogously, adaptation to the variance of higher-order stimulus features is found in visual cortex (Ohzawa et al., 1985; Bonds, 1991; Heeger, 1992; Kohn and Movshon, 2003) and many other sensory systems. For example, in the fly visual system, the sensitivity of H1 neurons to motion scales with motion contrast (Brenner et al., 2000; Fairhall et al., 2001; Heitwerth et al., 2005). Model simulations verify that this scaling optimizes the information available at the level of firing rate (Brenner et al., 2000).

The relationship between contrast normalization and neural coding remains unclear, however, because information is not coded only by firing rate. In the lateral geniculate nucleus (LGN), for example, the reliability and temporal precision of spikes are both essential for the encoding of high-contrast white-noise visual stimuli (Reich et al., 1997; Reinagel and Reid, 2000; Liu et al., 2001; Reinagel and Reid, 2002). As a

result of lower signal-to-noise ratio, one might expect responses to be less temporally precise, less reliable from trial to trial, and less informative as contrast decreases. It is difficult, however, to predict the magnitude and significance of these effects. Neural coding at low contrast could be either better or worse than predicted by contrast normalization alone.

It is also not known whether contrast normalization requires an active adaptation process. Response properties of neurons change gradually after a change in contrast, and the speed of these changes has attracted theoretical interest (DeWeese and Zador, 1998; Fairhall et al., 2001). The biophysical properties of neurons also change with stimulus contrast (Carandini and Ferster, 1997; Sanchez-Vives et al., 2000; Kim and Rieke, 2001; Baccus and Meister, 2002). On the other hand, there is experimental evidence that spike-generation mechanisms play a role in contrast normalization (Kim and Rieke, 2001, 2003; Zaghloul et al., 2005). Recent theoretical results show that nonlinear systems can exhibit contrast normalization without any active changes; fixed nonlinear properties of the cell (such as the threshold and saturation) can be sufficient to produce contrast normalization (Borst et al., 2005; Yu and Lee, 2005; Yu et al., 2005). In the models previously shown to exhibit contrast normalization, optimization of information transfer across contrasts was either not tested or not found (Yu and Lee, 2005). These studies used firing-rate models that do not consider the reliability and precision of real neurons, and information transmission was not analyzed at the level of spike timing.

Results

In order to address these open questions, we recorded responses of LGN neurons to full-field flickering binary white-noise stimuli with each of three contrasts: 100%, 33% or 11% (see Methods). We determined that this range is representative of temporal contrasts found in natural stimuli (see Figure 1.3). The responses of one representative cell are shown in Figure 4.1. Consistent with previous reports (Reinagel and Reid, 2000; Liu et al., 2001), the high-contrast white-noise stimulus elicited sparse responses with discrete firing events separated by periods with no spiking activity (Figure 4.1A). When the same stimulus sequence was scaled to lower contrasts, the firing events appear to be weaker and noisier, as expected (Figure 4.1B and 4.1C). Nevertheless, even at 11% contrast, there are discrete and precise peaks in the time-varying firing rate (Figure 4.1D). For this cell, both firing rate (Figure 4.1E) and rate modulation (Figure 4.1F) increase with contrast. Nevertheless LGN neurons' rate modulation does not increase linearly, consistent with classically-described contrast gain control (Shapley and Victor, 1978; Benardete et al., 1992).

Contrast normalization in LGN neurons

We measured the gain of LGN neurons by fitting the data to a Linear-Nonlinear cascade, in order to test whether cells matched their gain to the stimulus contrast. Contrast normalization in the retina has been extensively studied in this framework (Hunter and Korenberg, 1986; Chander and Chichilnisky, 2001; Chichilnisky, 2001; Kim and Rieke, 2001; Rieke, 2001; Baccus and Meister, 2002). In the analysis shown here, we estimated a linear filter $F(t)$ for each cell in each

contrast condition by the normalized spike-triggered average stimulus (see Methods). Filters obtained from one Y OFF cell during high-contrast stimuli (red) and medium-contrast stimuli (blue) are shown in Figure 4.2A. By scaling the linear filters to the same amplitude at all contrasts, we can estimate the gain, *G*, of the neuron from the slope of a sigmoidal input-output function (nonlinearity) that is empirically measured from the data (Figure 4.2B; see Methods). The gain indicates how much the neuron's probability of firing will increase for a given increase in stimulus strength. Therefore a higher gain corresponds to an increased neural sensitivity.

When the stimulus contrast was decreased, we found that the neurons' gain increased (all symbols are above unity line in Figure 4.2C), indicating that the sensitivity (slope of the input-output function) increased. Nevertheless, the gain changed by less than the change in contrast. In other words, a threefold drop in contrast was not compensated by an exactly threefold boost in gain (thin line, compare to circles and diamonds) and likewise for a 9-fold change in contrast (dotted line, compare to triangles). We defined a contrast normalization index, κ, such that $\kappa=0$ if there was no gain change and $\kappa=1$ if the neuron's gain increased by the same factor that the stimulus contrast decreased (see Methods). The average contrast normalization, κ, was around 0.5, consistent with previous reports in the retina and LGN (Shapley and Enroth-Cugell, 1984; Benardete et al., 1992; Chander and Chichilnisky, 2001; Kim and Rieke, 2001; Kremers et al., 2001; Baccus and Meister, 2002; Zaghloul et al., 2005). Some individual cells exhibited almost no gain change ($\kappa\approx0$), while others came close to compensatory scaling ($\kappa\approx1$). Even within cell type,

there was considerable variability across cells. The extent of gain change was comparable for X and Y subpopulations; OFF cells had significantly more contrast normalization than ON cells (see Supplementary Methods).

Variability in number and timing of spikes

Contrast normalization is thought to help maintain sensitivity under different contrast conditions. However the gain change (which reflects the firing rate) cannot predict changes in the temporal precision of responses or the trial-by-trial variability in spike number, both of which are important for determining the rate of information transmission in the LGN (Reich et al., 1997; Reinagel and Reid, 2000; Liu et al., 2001).

When a visual stimulus is presented repeatedly, there is some variability from trial to trial in the number of spikes within any time bin of the response. It is known that this spike-count variability is lower during high instantaneous firing rates, due to the regularizing effects of refractoriness (Berry and Meister, 1998; Keat et al., 2001; Uzzell and Chichilnisky, 2004; Zaghloul et al., 2005). Given that both mean rate (in some cells) and response modulation (in all cells) increased with contrast, we predicted a decrease in variability at high contrast. Nevertheless this was not guaranteed to be the case; changes in the refractoriness of the system could either enhance or reduce the expected change (Berry and Meister, 1998; Kara et al., 2000).

To quantify the variability in spike count we calculated the Allan Factor of neural responses in the high (100%), medium (33%), and low (11%) contrast conditions. Like the more familiar Fano Factor, the Allan Factor has a value of zero

for a deterministic process, increases as variability increases, and has a value of one for a Poisson process (see Supplementary Methods). Consistent with previous observations (Kara et al., 2000; Reinagel and Reid, 2000), most LGN neurons had sub-Poisson variability at high contrast (Allan Factor<1). Responses to lower contrast stimuli had more spike-count variability (Allan Factor increased in 80/82 comparisons, $p<0.001$ by Wilcoxon sign rank test). Nevertheless most cells remained sub-Poisson even at 11% contrast (Figure 4.3A). This finding, based on within-cell comparisons, is consistent with recent results based on population comparisons in the primate retina (Uzzell and Chichilnisky, 2004).

We measured the variability of spike timing by the temporal jitter of spikes across trials (see Supplementary Methods). In our data from 100% contrast stimuli, temporal jitter was less than 2 ms for 61% of cells and less than 1 ms for 29% of cells, comparable to the precision reported previously for high-contrast white-noise stimuli (Reinagel and Reid, 2002). As the contrast decreases, the decreasing signal-to-noise ratio might be expected to produce increasing jitter in spike timing. Compared to the jitter at high contrast, nearly all cells had more temporal jitter at 33% contrast (20/24 comparisons, $p<0.002$) and still more at 11% contrast ($p<0.002$) (Figure 4.3B). These results agree with those from the primate retina (Uzzell and Chichilnisky, 2004) that spike time precision increases with effective contrast at the population level. Note that in our data, most cells still had temporally precise responses (<10 ms jitter) even at the lowest contrast. In a few cells (7%) sub-millisecond precision was retained even at 11% contrast.

Contrast normalization preserves information

In most cells, responses to lower contrast had a lower firing rate and an increased variability in both spike timing and spike number. Thus one might expect a decrease in the information rate, as measured by the Mutual Information between a stimulus and a neural response (Berry et al., 1997; Reich et al., 1997; Reinagel and Reid, 2000; Liu et al., 2001; Freed, 2005). Depending on the detailed structure of the neural code, information transmission could be more or less robust to contrast changes.

Therefore we measured the mutual information *I* for each cell at all three contrasts (Strong et al., 1998; Reinagel and Reid, 2000) (see Supplementary Methods). The information rate was significantly lower at lower contrasts, whether measured in bits/s (not shown) or in bits/spike (symbols are below the solid diagonal line in Figure 4.4A). Yet the information rate did not decrease by the same factor as the contrast (symbols are above their respective dashed lines). The mutual information remained substantial at 11% contrast for some cells (as high as 30.8 bit/s or 3.1 bits/spike). The extent to which information was preserved at low contrast varied considerably in our population, with no correlation to cell type.

It has long been known that contrast normalization mitigates the effect of contrast at the level of firing rate, such that rate modulation does not decrease by the same factor that contrast decreases. We asked whether the information rate of each cell was more or less preserved than its firing-rate modulation as contrast changed. To compare the information rate of the same cell at two contrasts we used the ratio of the rate at the lower contrast condition divided by that at higher contrast condition

(*Information Ratio*). Similarly, to compare the firing rate modulation (see Figure 4.1F) we define a *Rate Modulation Ratio* between the two contrasts. We find that information rates were less sensitive to contrast changes than were firing rate modulations (most symbols are above the diagonal line in Figure 4.4B; $p<0.05$ for filled symbols). Thus, information is more preserved across contrasts than was predicted by firing rate effects alone.

It is widely assumed that contrast normalization serves to maintain the fidelity of neural coding across contrasts. This does not follow because information transmission depends strongly on the temporal precision and trial-by trial reliability of responses, which also change with contrast. We exploited the diversity among cells to test whether neurons with stronger contrast normalization were better able to preserve information transmission across contrasts. We find that the magnitude of contrast normalization, κ, is significantly correlated with the conservation of information across contrasts (Figure 4.4C; $R^2 = 0.67$ for filled symbols, $p<0.001$).

Normalization in a non-adapting model

The results presented above are consistent with the hypothesis that cells actively adapt their sensitivity in order to optimize information transfer, but nonlinear systems with fixed parameters can also exhibit contrast normalization (Borst et al., 2005; Yu and Lee, 2005; Yu et al., 2005). We implemented a nonlinear model (see Figure 4.3) that has been shown to successfully reproduce responses of LGN neurons to white noise stimuli (Keat et al., 2001). We created a large population of model cells by varying the model parameters (see Methods). We then presented the model with the

same stimuli presented to LGN neurons above. The parameters for each model cell remained fixed across all contrasts, in order to determine whether parameter changes were required for contrast normalization to occur.

We find that for this non-adapting model, the gain, *G*, increased as the contrast decreased (Figure 4.5A). Depending on parameters, some model cells showed little or no contrast normalization ($\kappa \approx 0$), whereas the gain of other model cells increased by nearly the same factor that the contrast decreased ($\kappa \approx 1$). Thus the range of contrast normalization we found in the LGN can also be produced by a fixed nonlinear system.

Like LGN cells, the model cells' information rate also decreased when the contrast decreased (Figure 4.5B). Again, the magnitude of this decline in information depended on the model parameters, such that some model cells lost nearly all information at low contrasts, while other model cells transmitted nearly the same information across contrasts. Across our population of model cells, we find that contrast normalization is correlated with the information ratio (Figure 4.5C; $R^2=0.86$, $p<0.0001$). This correlation is remarkably similar to the one observed in LGN cells (compare blue, black, and green symbols to grey symbols). Therefore, contrast normalization without active adaptation is a viable candidate mechanism for how LGN neurons preserve information transmission across contrasts. A detailed exploration of how contrast normalization arises in this model will be presented elsewhere (K.D. & P.R., in preparation).

Discussion

In conclusion, it is well known that contrast normalization exists in the early visual system and boosts responsiveness at low contrast. But in addition to firing rate, information transmission depends critically on the consistency of spike timing and spike number. It was not known how these properties would change with contrast, nor could these changes be predicted on the basis of gain changes. We show that both spike count and spike timing are more variable as contrast decreases. Nevertheless, many LGN cells have sub-Poisson variability and high temporal precision even at the lowest contrast tested. Average spike-timing jitter at low contrast was less than 2 ms in a third of our cells. Therefore reliable, precise spiking and efficient coding are not idiosyncratic to high-contrast visual stimuli.

It is often argued that neurons must adapt to contrast because they lack the dynamic range to discriminate both weak stimuli (low contrast) and strong stimuli (high contrast) simultaneously. Indeed our results show that contrast normalization is associated with maintenance of neural coding efficiency, as predicted on theoretical grounds. Moreover, information transmission is better preserved than rate modulation, perhaps due to the changes in neural dynamics that are also associated with Contrast Gain Control (Shapley and Victor, 1978; Victor, 1987, 1999). Nevertheless our modeling results challenge the assumption that an active process of adaptation is required for this function: at least one non-adapting model can exhibit normalization that is correlated with information preservation.

Methods

Surgical preparation. Cats were anesthetized initially with ketamine HCl (20 mg/kg, i.m.), followed by sodium pentothal (2-4 mg * kg^{-1} * h^{-1}, i.v., supplemented as needed). Animals were ventilated using an endotracheal tube. Electrocardiogram, electroencephalogram, temperature, expired CO_2, and oxygen in blood were continually monitored. All surgical and experimental procedures were in accordance with National Institutes of Health and United States Department of Agriculture guidelines and were approved by the UCSD Institutional Animal Care and Use Committee.

Electrical recording. We report results from 41 LGN relay cells recorded from the A laminae of the LGN of anesthetized cats. We sampled the four main cell classes: ON X, OFF X, ON Y, and OFF Y. Parylene-coated tungsten electrodes (AM Systems, Everett, WA) were inserted through a 0.5 cm diameter craniotomy over the LGN. Recordings were amplified, filtered, and digitized at 10kHz sampling rate (CED micro 1401 and Spike2, ver. 5.12a; Cambridge Electronic Design, Cambridge, UK). Waveforms were analyzed offline isolate single unit responses (Fee et al., 1996).

Visual stimulation. Stimuli were spatially uniform and presented on a custom-built LED array. To create matched stimuli at all contrasts, we began with a random binary stimulus of 125 frames/s for 10 s. The same binary sequence was scaled about the mean to obtain three contrast conditions (11%, 33%, and 100%, where contrast is defined as the standard deviation of the luminance over the mean.) Stimuli of the three contrasts were interleaved and presented between 10 and 128 times each. We

analyzed only the last five seconds of the response to each 10-s stimulus. The mean luminance was the same at all contrasts and was well within the photopic range. We also presented cells with a 1-second, binary stimulus at 10 different contrasts, repeated 40 times at each contrast (used in Figure 4.1E and 4.1F).

Measure of spike count variability. The trial-by-trial variability in spike count was measured by the Allan Factor (*AF*):

$$AF = \frac{< (N_i - N_{i-1})^2 >}{2\mu} \qquad \text{Eq. 1}$$

where N_i is the spike count in trial i, μ is the mean spike count over all trials, and < ... > denotes the average result over a sliding 5-ms window. See Supplementary Methods for additional details.

Linear-Nonlinear Cascade. For each cell at each contrast, we began by estimating the filter as the spike-triggered average. The filters for the three contrasts were normalized by the amplitude of their first peaks. The stimulus was convolved by the corresponding filter to create a generator potential, *g(t)*. We compared this generator potential to the observed probability of spiking at each time bin. For each cell, we fit the observed input-output function at 100% contrast to the following sigmoid equation:

$$y = \exp(A - e^{-Gx+S}) \qquad \text{Eq. 2}$$

In Eq. 2, the variables *A*, *G*, and *S* describe the amplitude, slope, and horizontal offset of the nonlinear function, respectively. We then fit the input-output functions at the other two contrasts holding the amplitude (*A*) constant for all contrast conditions for

each cell. We excluded a data set from our analysis if there were less than 100 spikes observed in the response, or if the R^2 value associated with the sigmoid fit was less than 0.90. For each cell at each contrast, we then define the Gain as *G* from Eq. 2. Our results did not depend critically on how the filters were scaled; similar results were found by normalizing by the peak-to-peak amplitude of the spike-triggered average. See Supplementary Methods for additional details.

Contrast Normalization Index. The greater the change in contrast, the larger change in gain (sensitivity) would be required to compensate. Thus we express the magnitude of gain change relative to the magnitude of contrast change and call this the contrast normalization index κ:

$$\kappa = \frac{G_{lower} / G_{higher} - 1}{C_{higher} / C_{lower} - 1} \qquad \text{Eq. 3}$$

where *G* is neural gain and *C* is stimulus contrast.

Non-adapting LGN Model. Model cells were implemented as described in Keat et. al. (2001) (see schematic in Figure 5.1). Briefly, the model first convolves the stimulus with a linear filter. The generator potential is equal to the convolved stimulus plus noise; the amplitude and time-constant of this noise are defined by the model parameters σ_a and τ_A, respectively. A spike is generated whenever the generator signal crosses a threshold, θ. Each time a spike occurs, a negative after-potential is added to the generator potential, such that the threshold is crossed repeatedly during sustained excitatory stimuli. The amplitude, time-constant, and variability in the amplitude of the negative after-potential are defined by the model parameters *B*, τ_P, and σ_b,

respectively. We generated a set of model cells using all possible combinations of the following parameters: $\theta = 0.1$; $B = 3$, 5, or 7; $\tau_P = 20$, 35, or 50; $\tau_A = 20$; $\sigma_a = 0.01$, 0.16, 0.31, or 0.61, $\sigma_b = 0.02$, 0.15, or 0.28; $F = F_X$ or F_Y. The filter functions, F_X and F_Y, were taken from the X ON and Y OFF cat LGN data in Figure 8C of Keat et. al. (2001).

Supplementary Methods

Comparisons between cell types. To classify cell types, spatiotemporal receptive fields were mapped using reverse correlations of responses to a white-noise (m-sequence) stimulus. Most cells were also classified as X or Y based on observations of null phases or frequency doubling of contrast reversing stimuli modulated at 1, 2 or 4 Hz. We used both contrast-reversing sine gratings and contrast-reversing bipartite field stimuli. The latter consisted of two hemifields sinusoidally modulated in counterphase; the vertical division between the hemifields was varied, presenting ten cycles for each location of the division.

Several studies have reported that different cell types of the early visual system differ in the degree of Contrast Gain Control. Experiments with sine grating stimuli found stronger Contrast Gain Control in Y cells than X cells of the cat retina (Shapley and Victor, 1978). Contrast Gain Control was reported to be stronger for OFF than ON cells in salamander retina, but stronger for ON cells in primate retina (Chander and Chichilnisky, 2001). Both rapid and slow forms of Contrast Gain Control were stronger in the primate magnocellular (M) pathway than in the parvocellular (P) pathway (Benardete et al., 1992; Benardete and Kaplan, 1999; Kremers et al., 2001; Solomon et al., 2004). In our data set, the distributions of contrast normalization indices were not significantly different between X and Y cells for any contrast combination. Contrast normalization did differ between ON and OFF cells when comparing the high-medium and high-low contrast combination ($p=0.028$ and $p=0.014$, respectively): the average contrast normalization index, κ, of OFF cells ($0.56\pm.25$ and $0.41\pm.20$, respectively) was higher than ON cells ($0.37\pm.20$ and

0.25±.12, respectively). Contrast normalization indices were not significantly different between ON and OFF cells when comparing the medium and low contrast conditions (p=0.12).

Unlike the primate retina (Uzzell and Chichilnisky, 2004), we did not find any significant difference between ON and OFF cells in the cat LGN with respect to spike count variability or its dependence on contrast, nor with respect to the precision or the dependence of precision on contrast.

Alternative method of estimating gain. We replicated our entire using an alternative framework for estimation of the gain, namely, fixing the nonlinear function at all contrasts and scaling the filters as needed to match the empirical relation between *g(t)* and the observed probability of spiking (Chichilnisky, 2001). The two approaches are conceptually similar but subject to different practical limitations. Our results were qualitatively the same in both analyses; we prefer scaling the filters because the measured nonlinear functions can differ in offset as well as in gain. In our population of cells, the horizontal offset (*S*) increased as contrast increased for some cells, decreased for others, and remained constant for still others. The offset change was not correlated with information preservation (not shown).

Spike-count Variability Measure. The trial-by-trial variability in spike count can be estimated by the Fano Factor, which is defined as the variance divided by the mean number of spikes within some time window. The Allan Factor is related to the Fano Factor, but instead of calculating the variance as the average squared difference in spike count with respect to the average spike count across all trials, the numerator is the average difference in spike count with respect to the spike count during the

preceding trial. The Allan Factor is preferred because it is less sensitive than the Fano Factor to slow changes in neural activity. All trends reported remained the same, however, if the Fano Factor was used instead of the Allan Factor (not shown).

Responses to repeated stimuli were divided into non-overlapping 5-ms bins. (Trends were the same using 10, 50, 100, 250, 500, and 1000-ms bins, not shown.) The Allan Factor was computed from the distribution of spike counts across trials separately in each time bin, and these values were averaged across time bins for each cell within each contrast condition.

We performed similar analysis using firing events (Berry et al., 1997), such that instead of calculating the Allan Factor from the number of spikes within each bin, the calculation was performed on the number of spikes within each PSTH peak. We either averaged the Allan Factors across firing events and compared the average across contrasts, or compared the Allan Factors between contrasts on a peak-by-peak basis (not shown). Both yielded similar results to the time-binned method.

To test whether the observed increase in mean firing rate (Figure 4.1E) or in rate modulation (Figure 4.1F) was sufficient to explain the observed decrease in variability at high contrast (Figure 4.3A), we also compared the Allan Factors for a subset of time bins from each contrast that fell within a narrow range of firing rates. This range was chosen separately for the high-medium and high-low contrast comparisons, as often there was one no firing rate sufficiently represented at all three contrasts. We required a minimum N=10 samples at each contrast. We used 5-ms bins, such that at most one PSTH peak was contained within a bin. Since the mean rates could not be perfectly matched between two contrasts, we erred in the direction of

including higher firing rate bins for the lower contrast, so that our bias if any would be to attribute less variability to low contrast responses. Even when firing rate was matched, the Allan Factor of the cells increased as contrast decreased ($p<0.0001$). We obtained similar results when comparing the variability of individual firing events (PSTH peaks) that contained the same average number of spikes.

A minority of cells had super-Poisson variability (Allan Factor >1) which was attributable to bursting (Kara et al., 2000). We use inter-spike interval criteria to identify these bursts which we attribute to low-threshold calcium channels (Lu et al., 1992). We define the burst probability as the ratio of the burst frequency over the response frequency, where a response is either a burst or a single spike. Across all our conditions (41 cells x 3 contrasts), 33/123 had burst probability >5%; this subset included all 20 conditions for which AF>1.05 (supra-Poisson variability).

Temporal precision measures. For each cell at each contrast condition, we measured the trial-to-trial jitter in spike trains by the width of the peak of the average cross-correlation between sequential trials. We defined precision as the half-width of this peak at half maximum. Thus if spike times had a normal distribution of σ about the mean time, our measure would assign a precision of $(-2\cdot\ln(.5)\cdot\sigma^2)^{1/}2$. We excluded conditions if the peak was not at t=0. Additionally, data was required to be at least 75% smooth, where smoothness was defined as the 1 minus cumulative square difference between the with and without smoothing by a 5-point moving average.

Our findings did not depend on the method used to measure temporal precision of responses: similar results were found by comparing the widths of PSTH peaks

across contrasts. In one analysis we determined the average width of firing events within contrast and compared the average across contrasts. In another analysis we compared the peak widths between contrasts on a peak-by-peak basis (not shown). Both yielded similar results to the cross-correlation method. We note that all these definitions of precision are sensitive to the duration of the firing event as well as the jitter in the time of onset. Thus our estimate is an upper bound on the precision in this latter sense.

Mutual Information measures. We calculated the visual information in spike trains by a direct entropy method (Strong et al., 1998), implemented exactly as by (Reinagel and Reid, 2000). Briefly, we represented LGN responses as time-binned spike trains. In our analysis we varied $\delta\tau$ from 1 to 16ms; results for $\delta\tau$ = 2ms are shown. The value in a time bin was set to zero if no spikes occurred during that time interval or one if a single spike occurred during that time interval. Because of the refractory period of the cells, the occurrence of two spikes in the same 2-ms time bin was so rare as to be negligible.

We analyzed the information in words (short strings of bins) and varied the number of bins in the words, *L*. For each word length, we measured two forms of word entropy: the average noise entropy, $\langle H_{noise} \rangle$, which reflects the trial-to-trial variability of words when the stimulus was fixed, and the average total entropy, $\langle H_{total} \rangle$, which reflects the variability of words across all stimuli in the ensemble. The mutual information between the visual stimulus and the spike train is defined as $I = \langle H_{total} \rangle - \langle H_{noise} \rangle$. Finally, we define the coding efficiency of the cell as the mutual information divided by the total entropy (H_{total} /*I*).

In detail, $H_{noise}(t)$ was calculated from the distribution of words at a fixed time t relative to stimulus onset across all repeated trials of the same sample of the stimulus. We performed a separate calculation of $H_{noise}(t)$ for many different values of t (separated by one bin). We then averaged over t to get the average noise entropy $<H_{noise}>$. We performed equally many separate calculations of $H_{total}(i)$, but the set of words was instead selected using a different time t from each trial. Twice the number of words were used for each single estimate of $H_{total}(i)$ to compensate for the approximately twofold difference in entropy. We averaged over i to get the average total entropy $<H_{total}>$. We computed information as a function of word length. Results are shown for a word length of 1 bin (2 ms), but all trends were the same at all word lengths tested. Specifically, the correlation between contrast normalization and information ratios was nearly identical when considering words of length 8 bins (16 ms) ($R^2 = 0.66$, $p<0.001$).

For each entropy estimate, we determined how our estimate of H converged as we used increasing fractions of the data, and then corrected for finite data size according to the method of Strong et al. (1998). We fit a second-order polynomial to 1/(fraction of data) versus the entropy estimate. We used this polynomial to extrapolate to infinite data only if the resulting correction was <10% and the second order term <1%. If data did not meet these criteria, a linear fit was used to correct for finite data size (maximum 15% correction), and we indicate our reduced confidence in these data by open symbols in Figures 4.4 and 4.5. All our results were qualitatively unchanged if we did not perform correction for finite data size (not shown).

The largest and most significant correlation in our data was between the Information Ratio and the Contrast Normalization Index (shown in Figure 4.4C). Some other relationships we considered are as follows: We also measured the coding efficiency, defined as the fraction of the cell's entropy that carries visual information (I /<H_{total}>). Coding efficiency declined significantly with contrast, but remained as high as 0.39 at low contrast for some cells. The coding efficiency of some cells declined only modestly with contrast (efficiency ratios of up to 0.93) while others declined dramatically (ratios as low as 0.18). The efficiency ratio was higher on average than the information ratio, indicating that efficiency was even more invariant to contrast. The information rate in bits/s was highly correlated with the firing rate modulation (R^2 = 0.92, $p<0.0001$). The spike-count variability (Figure 4.3A) was inversely related to firing rate, and therefore negatively correlated with information rate (R^2 = 0.61, $p<0.001$). The temporal jitter of spike times (Figure 4.3B) was not significantly correlated with information rate per second (R^2 = 0.21, $p=0.07$), but was significantly negatively correlated with both the information per spike (R^2 = 0.51, $p<0.001$) and the coding efficiency (R^2 = 0.51, $p<0.001$).

Appendix

In the early visual system of vertebrates, Contrast Gain Control is a classically defined phenomenon involving not only contrast normalization but also changes in temporal dynamics, including latency. In this chapter I focused on contrast normalization only. This appendix describes some additional observations that were not pursued in detail.

In this chapter I described our analysis of multiplicative contrast normalization (dependence of the neural gain on the input contrast). In our data we also found evidence for a second, additive form of contrast adaptation (lateral shifting of the input-output functions). The significance of this additive effect is still unclear, but differentially affected ON and OFF cells. Latency was also differentially affected in ON and OFF cells. The ON cells showed a surprising and previously undescribed increase in latency with an increase in contrast.

Shift in Input-Output Functions.

As described above, we calculate the gain at different contrasts by fitting LGN responses to a Linear-Nonlinear cascade at each contrast. We fit the input-output functions to sigmoid functions at each contrast (see Methods). The slope of the input-output function is related to the Gain, *G*, whereas the horizontal position of the function is related to the Offset, *S*. We reported that across LGN cells, the gain increased as the contrast decreased. Changes in the offset of the input-output functions were more diverse across cells.

In Figure 4.6, we show linear-nonlinear cascades fit to medium and high contrast data for one Y OFF cell (top row) and one X ON cell (bottom row). The filters were defined as the normalized spike-triggered averages (Figure 4.6A and 4.6D). For each contrast condition, the input to the cell was estimated by convolving the stimulus with the corresponding filter to produce a generator potential g(t). We then determined from our data the probability of firing as a function of this generator potential (symbols Figure 4.6B and 4.6F). The empirical input-output function was fit to a sigmoid nonlinearity for each cell and contrast condition (curves Figure 4.6B and 4.6F, see Methods). The parameters from this fit allowed us to estimate at each contrast both the gain (*G*), which is related to the slope of the sigmoid curve, and horizontal offset. Some cells' input-output functions differed across contrasts only in the gain (such as the Y OFF cell in Figure 4.6A-4.6D), while others differed in both the gain and offset (such as the X ON cell in Figure 4.6E-4.6I).

Gain differences are equivalent to a multiplicative scaling of the generator potential, whereas offset differences are equivalent to an additive shift of the generator potential. To illustrate this difference, we can scale the generator potential for one contrast such that the input-output functions for both contrasts have the same gain (Figure 4.6C and 4.6G). We can further shift the generator potential of one contrast such that the input-output functions also have the same offset (Figure 4.6D and 4.6H). In some cases, the input-output functions differed only by their gain (compare Figure 4.6C and 4.6D). In other cases, the input-output functions also differed in horizontal offset (compare Figure 4.6G and 4.6H). In principle, a change in amplitude of the sigmoid might have been required, or the data might have been poorly fit by any

sigmoid function, but we found that the input-output functions of a given cell at different contrasts could be accurately described by sigmoid functions that differed only in gain and horizontal offset.

Depending on the cell, the offset of the input-output functions either decreased (symbols below diagonal in Figure 4.7A), increased (symbols above diagonal), or remained constant (symbols on diagonal) as the contrast decreased. A decrease in offset when the contrast decreased indicates that the input-output function shifted to the left. Because the input-output functions were centered to the right of zero, this implies that at lower contrasts, smaller generator potentials could evoke spikes.

We found that shift in offsets for ON cells (average shift = -0.331 ± 0.324; green symbols in Figure 4.7B) differed significantly ($p < 0.0001$) from OFF cells (average shift = -0.0120 ± 0.242; purple symbols). We found no significant difference between X and Y cells (letter symbols in Figure 4.7B; $p=0.38$). Finally, we note that the shifts in offsets was significantly correlated with the contrast normalization ($R^2 = 0.55$; $p<0.0001$). When the input-output function shifted over to the left, less contrast normalization was observed.

Latency depends on contrast.

In both retinal ganglion cells and LGN cells, it has been shown that the phase of responses advance as the contrast of sinusoidal stimuli decreased (Shapley and Victor, 1978; Benardete et al., 1992; Kremers et al., 2001). Subsequently, other studies using white noise stimuli confirmed that latency in the retina decreases with contrast, where latency was defined as the time to first peak in the spike-triggered average

(Chander and Chichilnisky, 2001). Based on these results in the retina, we expected that in the LGN response latency would decrease with contrast. In some cells we observed the expected result (Figure 4.8A), but in other cells we found the opposite result (Figure 4.8B).

The latency trend in the LGN was correlated with the ON/OFF cell type. For OFF cells, the latencies from the high-contrast responses are significantly shorter than those from the medium- or low-contrast responses (purple symbols in Figure 4.8C; $p < 0.001$ for both comparisons). The decrease in latency from low to medium contrast was also significant ($p<0.01$). For ON cells, latency changed significantly in the other direction (green symbols in Figure 4.9C). The increase in latency from medium to high contrast was significant ($p<0.001$). Most cells also increased latency from low to high contrast, but this was not significant ($p>0.05$), because of a few exceptions in the low contrast condition.

We note that our latency results did not depend on our fitting of the Linear-Nonlinar Cascade to our data. We also compared the times of peaks in the time-varying firing rates across contrasts and obtained similar results. Additionally, we compared the times of the first spikes within the time-varying firing rate peaks and observed the same trends as reported above.

In Figure 4.8B we reported that ON and OFF cells showed another asymmetry: ON cells were more likely to shift their nonlinear function to the left as the stimulus contrast decreased. Within the linear-nonlinear cascade model this could approximate either an increase in the cell's membrane potential or a decrease in its spiking threshold. In either case, the cell's membrane potential would be closer to threshold

during lower contrast stimuli. We speculated that cells with this property could then take less time to reach threshold during lower contrast stimuli. Therefore, for each cell, we compared the difference in latency during two contrast conditions to the difference in offsets. (We excluded from this analysis data points in which over 20% of the responses were bursts, as bursts have different dynamics than tonic spikes.)

Despite the fact that differences in latency values will also depend on factors such as filter shapes, which are not accounted for in this analysis, across our population of cells, we found a significant correlation between these variables (R^2=0.43, p<.001). Cells whose latency was longer at higher contrasts (symbols below horizontal y=0 line) were also described by nonlinear functions that shifted to the left as contrast decreased (symbols to the left of vertical x=0 line).

Conclusion

Earlier studies found that response latency (phase of responses to sinusoidal gratings) decreased with increasing contrast in cat retinal ganglion cells of all types; no difference was found between ON and OFF cells (Shapley and Victor, 1978; Kremers et al., 2001). Similarly, primate LGN cells show phase advance with increasing contrast of grating stimuli (Kremers et al., 2001). The amount of phase advance for grating stimuli depends on temporal frequency, so it is difficult to extrapolate from these results to white noise stimuli. In experiments with white noise, response latency decreased with increasing contrast in primate and salamander retina for all cell types reported, although this effect was stronger in OFF cells (Chander and Chichilnisky, 2001). In the cat LGN, we find that OFF cells' latency decreased with

increasing contrast, as expected (Figure 4.8C). Past results suggested that latency changes in ON cells would either be the same as or weaker than OFF cells. We were surprised to find that ON cells' latency changed in the opposite direction: latency increased as contrast increased (Figure 4.8C). Additionally, we found that the horizontal shift in the input-output functions also exhibited an ON-OFF asymmetry (Figure 4.7B), and the shift was correlated with latency difference (Figure 4.8D). In the future it will be interesting to determine which of the many differences between ON and OFF pathways (Cohen, 1998, 2000; Chichilnisky and Kalmar, 2002; Zaghloul et al., 2003) can account for these reported asymmetries.

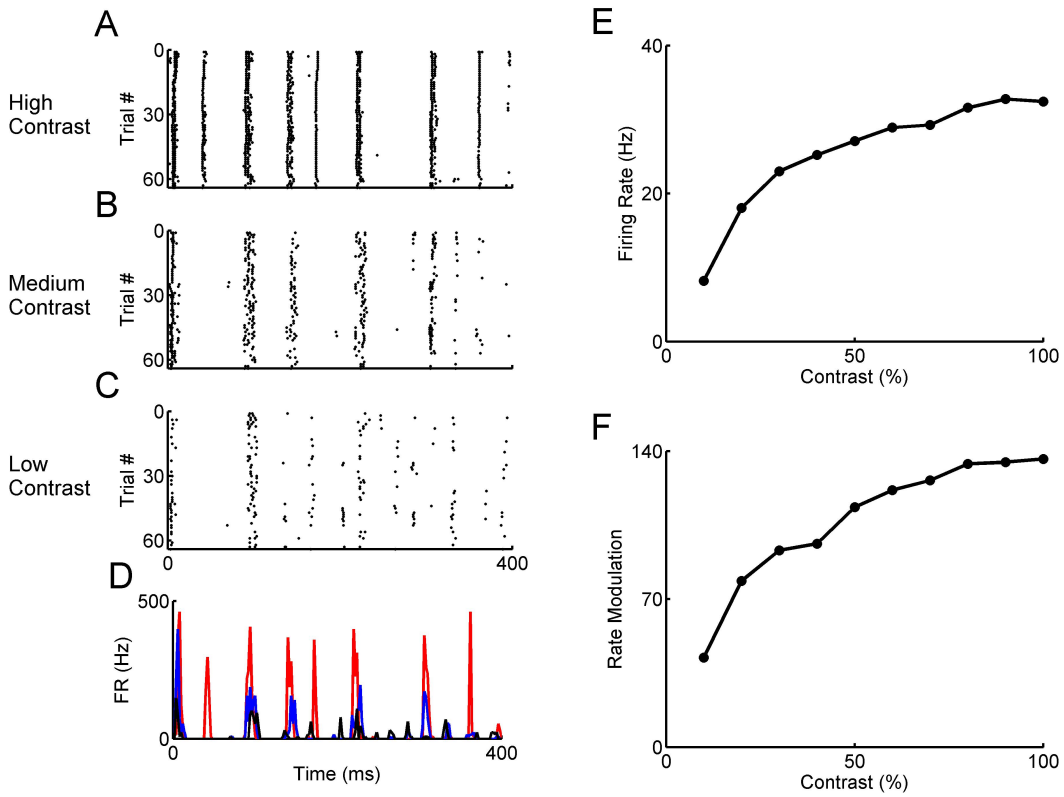

Figure 4.1: Response characteristics as a function of temporal contrast. Responses of one representative ON Y LGN cell to full-field binary white noise visual stimuli of different contrasts. A, Raster plot for 64 repeats of the same stimulus at 100% contrast. Each row represents a trial; each point represents the time of an action potential within that trial. A 400-ms segment is shown from the middle of the 5 s trials. B and C, Responses to 64 repeats of the same full-field binary stimulus sequence, which was scaled about the mean to 33% and 11% contrast, respectively. D, Time varying firing rate in 2ms time bins, derived from data in (A)-(C). E, Effect of contrast on firing rate. F, Effect of contrast on the modulation in firing rate (standard deviation of the firing rate across time bins, calculated in 1ms bins).

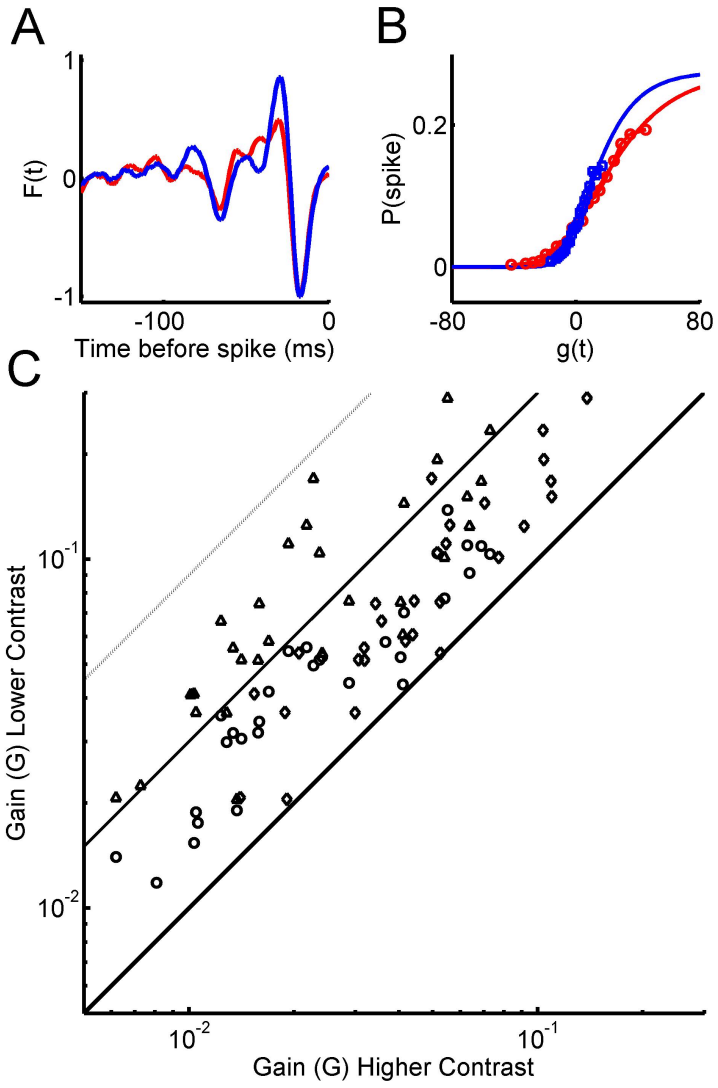

Figure 4.2: Gain changes with contrast. A, Linear filters from a Linear-Nonlinear cascade, fit to high (red curve) and medium (blue curve) contrast responses from one Y OFF cell. The filters were normalized by the amplitude of their first peak. B, Symbols indicate the observed probability of spiking versus the generator potential, g(t) for the same cell as in (A). The curves show the best-fit sigmoid functions. Based on these fits, the gain at the high contrast was 0.63 times that at medium contrast. C, Across cells, we compare the gain between 100% and 33% contrast (○), 33% and 11% contrast (◊), and 100% and 11% (Δ) contrast, where the gain at the higher contrast is always shown on the horizontal axis. In the absence of gain control, gain would be constant (x=y, thick, solid line). The thin, solid line indicates a threefold gain change (compare to threefold contrast changes: ○,◊). Dashed line indicates 9-fold gain change (cf. 9-fold contrast changes: Δ).

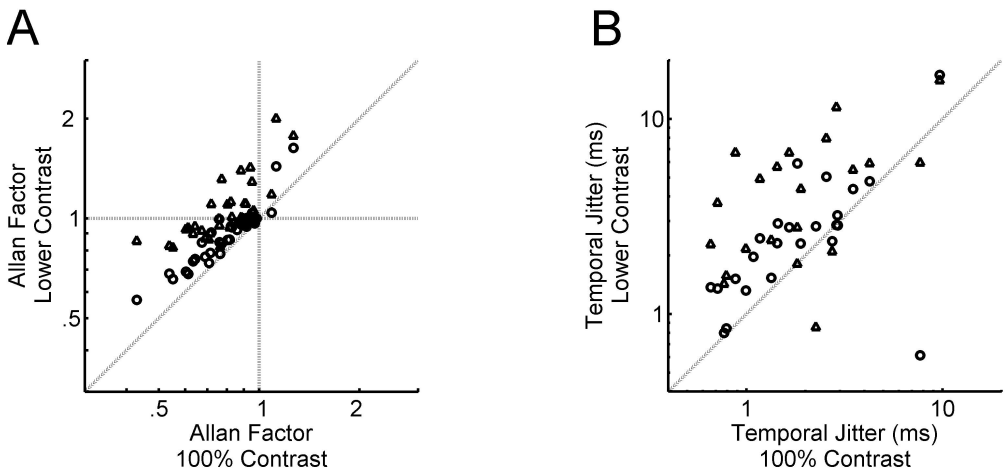

Figure 4.3: Variability in spike count and spike timing decrease with increasing contrast. A, Each point indicates the variability of responses of a single LGN neuron responding to 100% contrast (x-axis) compared to either 33% (○) or 11% (Δ) contrast (y-axis). In each case, Allan Factor was computed in 5ms bins and averaged across the 5-s trial. B, Each point indicates the temporal jitter of spike timing of a single LGN neuron responding to 100% contrast (x-axis) compared to either 33% (○) or 11% (Δ) contrast (y-axis). Jitter was measured by the half-widths at half-maxima of the cross-correlation peaks between trials from each LGN neuron, analyzed separately for each contrast condition.

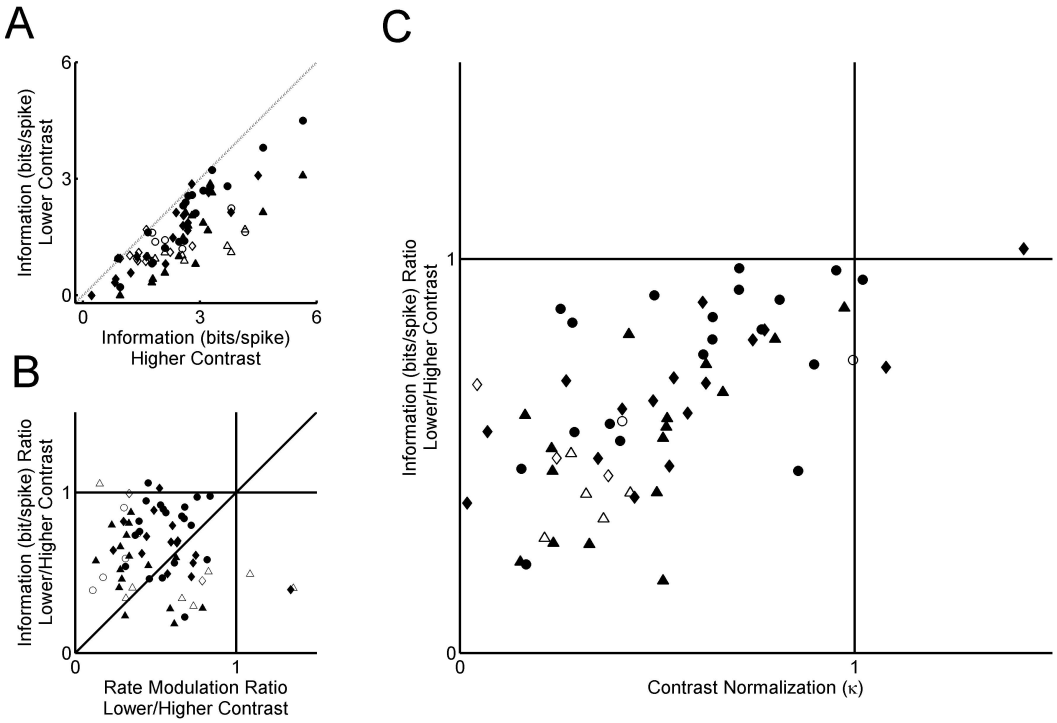

Figure 4.4: Mutual information between visual stimuli and LGN responses. A, The mutual information in units of bits per spike was determined for all contrast conditions for each cell. The results are compared between 100% and 33% contrast (○,●), 100% and 11% contrast (Δ,▲), and 33% and 11% contrast (♦,◊). Filled symbols indicate cases in which the correction for finite data size was small and linear for both contrasts (see Supplementary Methods); open symbols indicate remaining cases for which our estimate should be considered approximate. Information rates were significantly higher at higher contrast ($p<0.01$ for both 100% to 33% and 100% to 11% comparisons, whether we included all results or only those shown as filled symbols). B, Each symbol indicates a particular cell for a particular pair of contrasts, as defined in (A). The ratio of information rates (in bits per spike) is plotted against the ratio of rate modulation. C, Each symbol indicates the information ratio for a given cell versus the contrast normalization index (κ) in the same data. Symbols as in A.

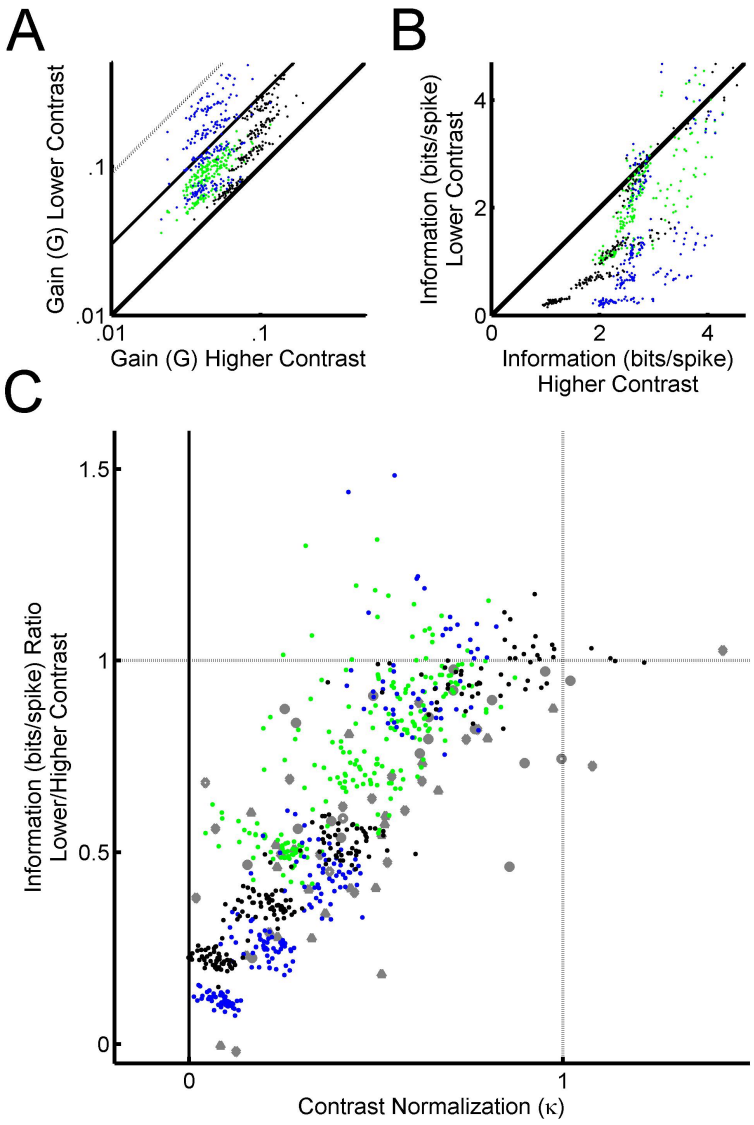

Figure 4.5: Contrast normalization and information preservation in a non-adapting model. A, Each symbol compares the gain of one model cell at two contrasts, where the gain at the higher contrast is always shown on the x-axis (cf. Figure 4.2C). Comparisons are between 100% and 33% contrast (green symbols), 33% and 11% contrast (black symbols), or 100% and 11% (blue symbols). B, Mutual information in units of bits per spike. Each symbol compares the information rates for one model cell at two contrasts, where the information rate at the higher contrast is always shown on the x-axis. Symbols as in (A). C, Each symbol indicates the information ratio versus the contrast normalization (κ) for one model cell for two contrasts. The green, black, and blue symbols as defined in (A). For comparison, results from LGN cells are shown in grey (replotted from Figure 4.4C).

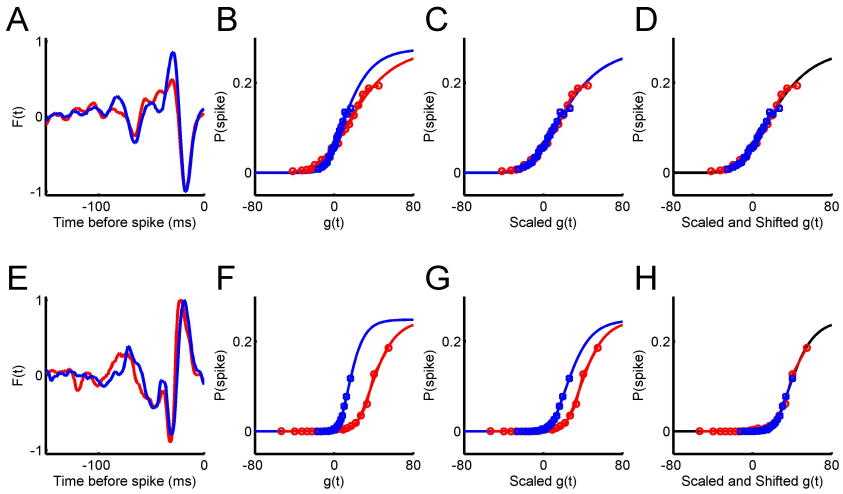

Figure 4.6: Using a Linear-Nonlinear model to estimate gain. A, Linear filters from a Linear-Nonlinear cascade model, fit to high (red curve) and medium (blue curve) contrast data from one Y OFF cell. The filters were normalized by the amplitude of their first peak. B, Symbols indicate the observed probability of spiking versus the generator potential, *g(t)*, for the same cell as in (A). The curves show the best-fit sigmoid functions. Based on these fits, the gain at the high contrast was 0.63 times that at medium contrast. C, Equivalently, we can scale the generator potential at medium contrast by a factor of 0.63 in order to set the gain of the two input-output functions to the value at high contrast. For this cell, the nonlinear functions are now quite similar. D, After shifting the blue curve horizontally to correct for horizontal offset (which differed by only 0.0068 units), the same sigmoid function (black curve) can now describe both the medium contrast's shifted and scaled nonlinear function (R^2 = 0.987) and the nonlinear function at high contrast (red symbols; R^2 = 0.992). E-H, Data from an X ON cell, plots as in (A)-(D). This cell's gain at the high contrast was also 0.63 times that at the medium contrast, panel (F), but in this case the input-output functions also differed by 0.97 units in horizontal shift, panel (G). Shifting the scaled curves reveals that the sigmoid function (black curve) was a good fit to the data from both medium contrast (R^2 = 0.996) and at high contrast (R^2 = 0.991).

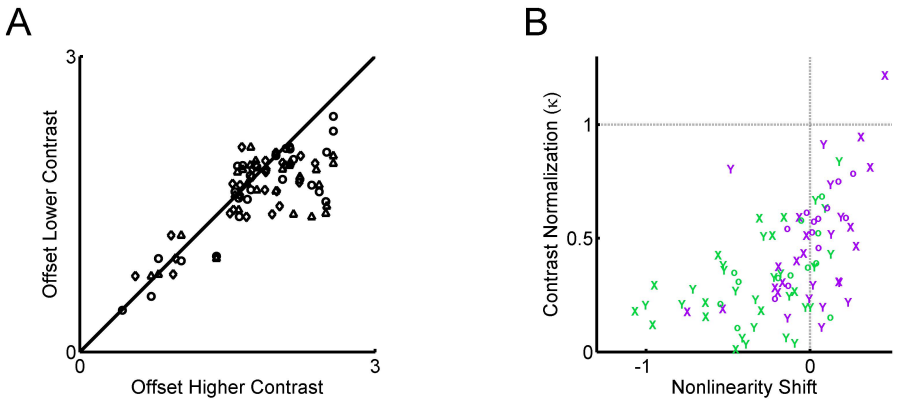

Figure 4.7: Multiplicative and additive changes to input-output functions. For each cell, nonlinear functions at all contrasts (Figure 4.7B and 4.7E) were fit to a sigmoid (see Methods). A, The offset of each cell at each contrast were defined as the factor that was added to the scaled generator potential of the sigmoid equation (see Methods), thereby describing the horizontal offset of the nonlinear function. Here, we compare the offset between 100% and 33% contrast (○), 33% and 11% contrast (◊), and 100% and 11% (Δ) contrast, where the gain at the higher contrast is always shown on the horizontal axis. If all differences in the nonlinearity were captured by changes in gain, offsets would be constant across contrasts (x-y, thick, solid line). Symbols below the line indicate the nonlinear function was shifted to the left at lower contrasts. B, Each symbol compares the contrast normalization index (κ) to the difference in offsets for a particular pair of contrasts for a single cell. The difference in offsets was defined as the offset, from (A), at the lower contrast minus that at the higher contrast. Therefore, neurons whose nonlinear functions shifted to the left as contrast decreased are described by a negative offset difference. The color of the symbols indicates whether the cell was an OFF cell (purple symbols) or an ON cell (green symbols). Symbols distinguish X cells (X), Y cells (Y), and unclassified cells (○).

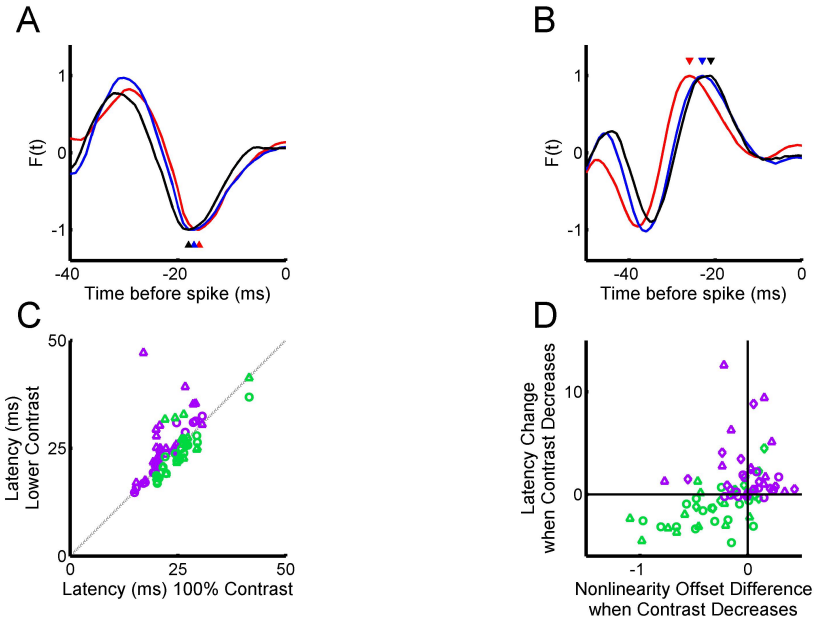

Figure 4.8: Effects of contrast on latency. A, The average stimulus preceding spikes, normalized by the amplitude of the first peak, from a representative OFF LGN neuron calculated in the three contrast conditions. The response latency of this cell was 24.7 ms (low contrast, black curve), 22.1 ms (medium contrast, blue curve), and 21.7 ms (high contrast, red curve). The arrows indicate the latency of the cell at each of the three contrasts. B, The average stimulus preceding spikes from a representative ON LGN neuron. The response latency of this cell was 21.7 ms (low contrast), 22.1 ms (medium contrast), and 24.7 ms (high contrast). C, Response latency across cells. Latency of responses at 100% contrast (horizontal axis) is compared to latency of the same cell at either 33% contrast (○) or 11% (Δ) contrast. ON and OFF cells are represented by green and purple symbols, respectively. Symbols above the diagonal indicate a latency decrease with contrast. D, Difference in latency, shown in (C), compared to the difference in offsets from the nonlinear functions (shown in Figure 4.8A). Both differences are calculated as the variable at the lower contrast minus the variable at the higher contrast. Therefore, symbols above the horizontal x=0 line indicate that latency increased as contrast decreased, and symbols to the left of the vertical y=0 line indicate that the nonlinear function at the lower contrast was shifted to the left of that at higher contrast. Each symbol represents a comparison between two contrast conditions for one cell. Symbol shapes indicate whether the comparison was between 100% and 33% contrast (○), 33% and 11% contrast (◊), or 100% and 11% (Δ). Symbol colors are as defined in (C).

Chapter 4, in full, is a republication of the material submitted in June of 2006. K.S., Reinagel, P., Functional benefits of contrast normalization demonstrated in neurons and model cells. (2006). The dissertation author was the primary investigator and first author of this paper.

Acknowledgements: The authors thank Pamela Magoffin for surgical assistance, Samar Mehta for assistance with spike sorting, and E.J. Chichilnisky for comments on earlier versions of the manuscript. This work was supported by NSF and NSF/IGERT (K.D.) and Alfred P. Sloan Foundation (P.R.).

References

Atick J, Redlich A (1992) What does the retina know about natural scenes? Neural Comput 4:196-210.

Baccus SA, Meister M (2002) Fast and slow contrast adaptation in retinal circuitry. Neuron 36:909-919.

Benardete EA, Kaplan E (1997) The receptive field of the primate P retinal ganglion cell, II: Nonlinear dynamics. Vis Neurosci 14:187-205.

Benardete EA, Kaplan E (1999) Dynamics of primate P retinal ganglion cells: responses to chromatic and achromatic stimuli. J Physiol 519 Pt 3:775-790.

Benardete EA, Kaplan E, Knight BW (1992) Contrast gain control in the primate retina: P cells are not X-like, some M cells are. Vis Neurosci 8:483-486.

Berry MJ, Meister M (1998) Refractoriness and neural precision. J Neurosci 18:2200-2211.

Berry MJ, Warland DK, Meister M (1997) The structure and precision of retinal spike trains. Proc Natl Acad Sci U S A 94:5411-5416.

Bonds AB (1991) Temporal dynamics of contrast gain in single cells of the cat striate cortex. Vis Neurosci 6:239-255.

Borst A, Flanagin VL, Sompolinsky H (2005) Adaptation without parameter change: Dynamic gain control in motion detection. Proc Natl Acad Sci U S A 102:6172-6176.

Brenner N, Bialek W, de Ruyter van Steveninck R (2000) Adaptive rescaling maximizes information transmission. Neuron 26:695-702.

Brown SP, Masland RH (2001) Spatial scale and cellular substrate of contrast adaptation by retinal ganglion cells. Nat Neurosci 4:44-51.

Carandini M, Ferster D (1997) A tonic hyperpolarization underlying contrast adaptation in cat visual cortex. Science 276:949-952.

Chander D, Chichilnisky EJ (2001) Adaptation to temporal contrast in primate and salamander retina. J Neurosci 21:9904-9916.

Chichilnisky EJ (2001) A simple white noise analysis of neuronal light responses. Network 12:199-213.

Cohen ED (1998) Interactions of inhibition and excitation in the light-evoked currents of X type retinal ganglion cells. J Neurophysiol 80:2975-2990.

Cohen ED (2000) Light-evoked excitatory synaptic currents of X-type retinal ganglion cells. J Neurophysiol 83:3217-3229.

DeWeese M, Zador A (1998) Asymmetric dynamics in optimal variance adaptation. Neural Comput 10:1179-1202.

Fairhall AL, Lewen GD, Bialek W, de Ruyter Van Steveninck RR (2001) Efficiency and ambiguity in an adaptive neural code. Nature 412:787-792.

Fee MS, Mitra PP, Kleinfeld D (1996) Automatic sorting of multiple unit neuronal signals in the presence of anisotropic and non-Gaussian variability. J Neurosci Methods 69:175-188.

Freed MA (2005) Quantal encoding of information in a retinal ganglion cell. J Neurophysiol 94:1048-1056.

Heeger DJ (1992) Normalization of cell responses in cat striate cortex. Vis Neurosci 9:181-197.

Heitwerth J, Kern R, van Hateren JH, Egelhaaf M (2005) Motion adaptation leads to parsimonious encoding of natural optic flow by blowfly motion vision system. J Neurophysiol 94:1761-1769.

Hunter IW, Korenberg MJ (1986) The identification of nonlinear biological systems: Wiener and Hammerstein cascade models. Biol Cybern 55:135-144.

Jin X, Chen AH, Gong HQ, Liang PJ (2005) Information transmission rate changes of retinal ganglion cells during contrast adaptation. Brain Res.

Kara P, Reinagel P, Reid RC (2000) Low response variability in simultaneously recorded retinal, thalamic, and cortical neurons. Neuron 27:635-646.

Keat J, Reinagel P, Reid RC, Meister M (2001) Predicting every spike: A model for the responses of visual neurons. Neuron 30:803-817.

Kim KJ, Rieke F (2001) Temporal contrast adaptation in the input and output signals of salamander retinal ganglion cells. J Neurosci 21:287-299.

Kim KJ, Rieke F (2003) Slow Na+ inactivation and variance adaptation in salamander retinal ganglion cells. J Neurosci 23:1506-1516.

Kohn A, Movshon JA (2003) Neuronal adaptation to visual motion in area MT of the macaque. Neuron 39:681-691.

Kremers J, Silveira LC, Kilavik BE (2001) Influence of contrast on the responses of marmoset lateral geniculate cells to drifting gratings. J Neurophysiol 85:235-246.

Liu RC, Tzonev S, Rebrik S, Miller KD (2001) Variability and information in a neural code of the cat lateral geniculate nucleus. Journal of Neurophysiology 86:2789-2806.

Lu SM, Guido W, Sherman SM (1992) Effects of membrane voltage on receptive field properties of lateral geniculate neurons in the cat: contributions of the low-threshold Ca2+ conductance. J Neurophysiol 68:2185-2198.

Ohzawa I, Sclar G, Freeman RD (1985) Contrast gain control in the cat's visual system. J Neurophysiol 54:651-667.

Reich DS, Victor JD, Knight BW, Ozaki T, Kaplan E (1997) Response variability and timing precision of neuronal spike trains in vivo. Journal of Neurophysiology 77:2836-2841.

Reinagel P, Reid RC (2000) Temporal coding of visual information in the thalamus. J Neurosci 20:5392-5400.

Reinagel P, Reid RC (2002) Precise firing events are conserved across neurons. Journal of Neuroscience 22:6837-6841.

Rieke F (2001) Temporal contrast adaptation in salamander bipolar cells. J Neurosci 21:9445-9454.

Ruderman DL, Bialek W (1994) Statistics of natural images: Scaling in the woods. Physical Review Letters 73:814-817.

Sanchez-Vives MV, Nowak LG, McCormick DA (2000) Cellular mechanisms of long-lasting adaptation in visual cortical neurons in vitro. J Neurosci 20:4286-4299.

Schwartz O, Simoncelli EP (2001) Natural signal statistics and sensory gain control. Nat Neurosci 4:819-825.

Shapley R, Enroth-Cugell C (1984) Visual adaptation and retinal gain control. Progress in Retinal Research 3:263-346.

Shapley RM, Victor JD (1978) The effect of contrast on the transfer properties of cat retinal ganglion cells. J Physiol 285:275-298.

Shapley RM, Victor JD (1981) How the contrast gain control modifies the frequency responses of cat retinal ganglion cells. J Physiol 318:161-179.

Shou T, Li X, Zhou Y, Hu B (1996) Adaptation of visually evoked responses of relay cells in the dorsal lateral geniculate nucleus of the cat following prolonged exposure to drifting gratings. Vis Neurosci 13:605-613.

Smirnakis SM, Berry MJ, Warland DK, Bialek W, Meister M (1997) Adaptation of retinal processing to image contrast and spatial scale. Nature 386:69-73.

Solomon SG, Peirce JW, Dhruv NT, Lennie P (2004) Profound contrast adaptation early in the visual pathway. Neuron 42:155-162.

Strong SP, de Ruyter van Steveninck RR, Bialek W, Koberle R (1998) On the application of information theory to neural spike trains. Pac Symp Biocomput:621-632.

Uzzell VJ, Chichilnisky EJ (2004) Precision of spike trains in primate retinal ganglion cells. J Neurophysiol 92:780-789.

van Hateren JH (1997) Processing of natural time series of intensities by the visual system of the blowfly. Vision Res 37:3407-3416.

Victor JD (1987) The dynamics of the cat retinal X cell centre. J Physiol 386:219-246.

Victor JD (1999) Temporal aspects of neural coding in the retina and lateral geniculate. Network-Computation in Neural Systems 10:R1-R66.

Yu Y, Lee T (2005) Adaptive contrast gain control and information maximization. Neurocomputing 65-66:111-116.

Yu Y, Potetz B, Lee TS (2005) The role of spiking nonlinearity in contrast gain control and information transmission. Vision Res 45:583-592.

Zaghloul KA, Boahen K, Demb JB (2005) Contrast adaptation in subthreshold and spiking responses of mammalian Y-type retinal ganglion cells. J Neurosci 25:860-868.

Zaghloul KA, Boahen K, Demb JB (2003) Different circuits for ON and OFF retinal ganglion cells cause different contrast sensitivities. J Neurosci 23:2645-2654.

.

Chapter 5

Contrast adaptation in a non-adapting LGN model

Abstract

Sensory neurons are believed to adapt their gain to match the variance of signals along the dimension they encode. Contrast normalization has been the subject of extensive physiological and theoretical study. We have reported elsewhere that lateral geniculate nucleus (LGN) cells exhibit contrast normalization in their responses to full-field flickering white-noise stimuli, and the extent of normalization was correlated with conserving the rate of transmission of visual information across contrasts. Furthermore, both of these observations could be reproduced in a non-adapting LGN model. In this study we show that these non-adapting model cells recapitulated other contrast dependencies of LGN neurons: decreasing stimulus contrast resulted in an increase in spike-timing jitter, spike-number variability, and response latency. Additionally, the contrast normalization of model cells depends on the model's parameters, so we can speculate which physiological characteristics of LGN cells are necessary for contrast normalization. Moreover, like LGN cells, the model cells exhibit rapid, transient changes in firing rate and information transmission just after changes in contrast. Although intrinsic changes in visual neurons have been demonstrated after changes in contrast, which most likely contribute to coding efficiency, our results suggest how it is that significant functional normalization may arise passively from the nonlinearity of LGN neurons.

Introduction

Natural visual stimuli have a vast dynamic range compared to the modest dynamic range of visual neurons. There would appear to be no transfer function that could respond differentially to the small stimulus differences in low-contrast scenes, yet avoid saturation in responses to high-contrast scenes. A possible solution is suggested by the fact that the dynamic range is much more limited in any spatiotemporally local sample of the visual stimulus. Therefore, neurons could dynamically adapt their transfer functions to match the local stimulus statistics in order to faithfully report stimulus differences within that context. We will refer to this property as contrast normalization.

Neurons in the early stages of vertebrate visual systems have been reported to change their gain or sensitivity as the stimulus contrast changes (Enroth-Cugell and Robson, 1966; Shapley and Victor, 1978; Shapley and Victor, 1979; Shapley and Victor, 1981; Shapley and Enroth-Cugell, 1984; Ohzawa et al., 1985; Shapley, 1997; Benardete and Kaplan, 1999; Sanchez-Vives et al., 2000a, b; Chander and Chichilnisky, 2001; Kim and Rieke, 2001; Rieke, 2001; Baccus and Meister, 2002; Kim and Rieke, 2003; Solomon et al., 2004; Zaghloul et al., 2005). Similarly, motion contrast normalization has been reported in motion sensitive neurons from primates (MT) to flies (H1) (Fairhall et al., 2001; Brenner et al., 2002; Kohn and Movshon, 2003).

Some reports have concluded that changes in ionic conductances play an instrumental role in contrast normalization (Sanchez-Vives et al., 2000b; Kim and Rieke, 2001). Other studies have concluded that resting membrane potentials change

in order to adapt to different contrasts (Carandini and Ferster, 1997; Baccus and Meister, 2002). On the other hand, recent theoretical findings have suggested that neurons could exhibit contrast normalization without actively changing either of these properties. Instead, intrinsic nonlinear properties of the cell (such as the threshold and saturation) are sufficient to reproduce contrast normalization (Borst et al., 2005; Yu and Lee, 2005; Yu et al., 2005).

In Chapter 4, we demonstrate that a non-adapting model can exhibit contrast normalization comparable to that found in LGN cells. Here we investigate whether this model is able to reproduce other contrast dependencies of the LGN, including spike-count variability, precision, and latency. We also investigate how contrast normalization depends on model parameters, and whether the model is able to exhibit transient changes after the stimulus contrast is changed.

Methods

Model Parameters. Models were implemented as described in Keat et al. (2001) by systematically varying the model parameters. We created model cells by using all possible combinations of the following parameters: $\theta = 0.1$ or 0.2; B = 3, 5, or 7; τ_P = 20, 35, or 50; $\tau_A = 20$; σ_a = 0.01, 0.16, 0.31, or 0.61, σ_b = 0.02, 0.15, or 0.28; $F = F_X$ or F_Y. The filter functions, F_X and F_Y, were taken from the X ON and Y OFF cat LGN data in Figure 8C of Keat et al. (2001).

Because latency depended strongly on filter shape, in Figure 5.4C, we also varied the filter shape. For each of 200 model cells, the values of θ, B, τ_P, τ_A, σ_a, and σ_b were randomly selected from the values listed above. The filter function was described by a summation of Gaussians with a positive peak between 20 and 40 ms and a negative peak of half the amplitude between 35 and 65 ms. The widths of the first and second peaks were randomly chosen to be between 7 and 15 ms and between 15 and 24 ms, respectively. We required the filter function at time $t = 0$ to be less than .05 of the maximum filter amplitude. All filter functions were ON type; calculations using OFF-type filters showed similar results (not shown).

Experimental Data. Model results are compared to data recorded from LGN neurons, as described elsewhere (Chapter 4). Experimental methods were essentially as per Reinagel and Reid (2000). Briefly, cats were anesthetized with sodium pentothal (2-4 mg * kg^{-1} * h^{-1}, i.v.). Animals were ventilated using an endotracheal tube. Electrocardiogram, electroencephalogram, temperature, expired CO_2, and oxygen in blood were continually monitored. All surgical and experimental

procedures were in accordance with National Institutes of Health and United States Department of Agriculture guidelines and were approved by the UCSD Institutional Animal Care and Use Committee. Parylene-coated tungsten electrodes (AM Systems, Everett, WA) were inserted through a 0.5 cm diameter craniotomy over the LGN. Waveforms were analyzed offline to isolate single unit responses (Fee et al., 1996). Stimuli were spatially uniform random binary flicker presented on a custom-built photopic LED array at 125 frames/s. The same binary pattern was scaled about the mean to obtain 11%, 33%, and 100% contrast, where contrast is defined as the standard deviation of the luminance over the mean. Only steady-state responses (after 5 s at fixed contrast) are shown.

Gain Calculations. First we estimated the filter at each contrast as the spike-triggered average. The filters for the three contrasts were normalized to the amplitude of their first peaks. The stimulus at each contrast was convolved by its corresponding filter to estimate the instantaneous stimulus strength. The input-output function was defined as the relation between the observed probabilities of spiking and the instantaneous stimulus strength. For each cell, we fit the input-output function to the data from the 100% contrast condition to the following sigmoidal equation:

$$y = \exp(A - e^{-Gx+S}) \qquad \text{Eq. 1}$$

In this equation, the variables *A*, *G*, and *S* describe the amplitude, slope, and horizontal offset of the nonlinear function, respectively. We then fit the input-output functions at the other two contrasts holding *A* constant. (Estimates of *A* were noisy at low contrasts, and fitting *A* did not improve the quality of fits.) We excluded a data

set from our analysis if there were less than 100 spikes in the response or if the R^2 value associated with this fit was less than 0.90. We define the Gain and Offset as *G* and *S* from the sigmoidal fits.

Spike-count Variability Measure. In Figure 5.6D, we report the trial-to-trial variability in spike count by calculating the Allan Factor (*AF*). The Allan Factor is equal to the average squared difference in spike counts (*N*) between consecutive trials divided by twice the mean spike count (υ) across trials.

$$AF = \frac{< (N_i - N_{i-1})^2 >}{2\mu} \qquad \text{Eq. 2}$$

In our model simulations, the expected spike count in a given time window does not drift from trial to trial, and therefore the Allan Factor is identical to the Fano Factor (variance/mean spike count). For real LGN data the Allan Factor can differ from the Fano Factor and thus we use the Allan Factor for both. Spike counts were analyzed in non-overlapping 5-ms bins of the repeated stimulus, and we report the average Allan Factor across time bins. (Trends were qualitatively the same using 10, 50, 100, 250, 500, and 1000 ms bins, not shown.)

Spike-timing jitter measures. We measured the trial-to-trial jitter in spike timing by the width of the peak of the average cross-correlation between sequential trials. We defined the jitter as the half-width of this peak at half maximum. We considered this measure invalid if the peak was not at $t = 0$, or if the peak was not smooth. Specifically, we smoothed by a 5-ms moving average and required that the cumulative square difference between the raw and smoothed curves be <25%.

Response Latency. Spike-triggered averages (STAs) were computed from responses of each model cell to each contrast. The latency was defined as the time to the shortest latency peak of the STA. In a separate analysis (not shown) we replicated the results of Figure 5.6F using two event-based methods. First, we computed STAs instead from the times of discrete firing events (PSTH peaks) as per Berry et al. (1997), where the time of each event was defined as the average time of the first spike in the event. Second, we compared the times of all firing events that were shared across both contrast conditions, as described above. Both calculations yielded similar trends (not shown). We note that the trends in latency observed in the model did not depend on the sign of the filter (not shown).

Information Calculations. We represented the model responses as time-binned spike trains, using a fixed bin size of $\delta\tau$ = 2 ms. Due to the after-potential, it was rare to observe two spikes within one bin. The value of a bin was defined to be zero if no spikes occurred within the bin or one if any spikes occurred. We calculated the visual information from spike trains by using the direct method (Strong et al., 1998), implemented exactly as in Reinagel and Reid (2000). For steady-state information calculations (Figure 5.5), entropies were measured for words of length L = 1 bin (2 ms), though trends were the same as we varied the bin length. We calculated both the average noise entropy, $<H_{noise}>$, which estimates the trial-to-trial variability of responses during fixed stimuli, and the average total entropy, $<H_{total}>$, which estimates the variability of responses across all stimuli in the ensemble. Entropy values were averaged across time points during the steady-state stimulus (from t=5 s to t=10 s relative to a change in stimulus contrast). The mutual

information was defined as the difference in these entropies: $I = H_{total} - H_{noise}$. We correct for finite data size according to the method of (Strong et al., 1998). Specifically, we fit a second-order polynomial to 1/(fraction of data) versus the entropy estimates, and evaluate the polynomial at 1/(fraction of data) = 0. We require that the total correction for finite data size was <10% and the second-order term of this correction was <1%.

Analysis of responses as a function of time after contrast change. We define a stimulus sequence as a 40 s stimulus in which contrast changes every 10s, transitioning from high to medium to low to medium contrast in that order. Different sequences differ in the binary flicker pattern, but not the contrast transition pattern. We presented one model cell with 216 different stimulus sequences (each shown once) and 686 additional stimulus sequences (each repeated 512 times). The time-varying firing rates were calculated by averaging the firing rate in each time bin over the 216 unique stimulus sequences (Figure 5.7A). Results shown are from averaging in overlapping boxcar windows of length 8 ms.

In order to compute the information rate following a contrast change, the variability of spiking responses both to repeated stimulus sequences and unique stimulus sequences needed to be estimated within small time windows. Estimates in small time windows are problematic because of the sparse nature of the responses. For steady state analysis we overcome this by averaging noise entropy across time; for time-locked analysis we average within a small time window across many different repeated stimulus sequences.

We calculated the time-varying noise entropy separately from each of the 686 repeated stimulus sequences and averaged the entropies across stimulus sequences. We calculated the time-varying total entropy separately from each of 128 blocks of 512 unique sequences, and averaged the entropies across blocks. Entropies and information were calculated for words of length L = 1 bin, for every 2-ms time step relative to the time of contrast change. Results shown are from averaging the information rates in overlapping boxcar windows of 12 bins (24 ms).

Results

When an LGN neuron is presented with stimuli of different contrasts, its responses exhibit contrast normalization. We recently reported that contrast normalization for white noise stimuli was correlated with preservation of information at low contrasts and that both of these phenomena were also observed in a non-adapting model (Chapter 4). Here, we explore why contrast normalization occurs in this model. Additionally, we show that the non-adapting model also exhibits several other properties of LGN responses, some of which have previously been thought to give evidence of active adaptation.

A generative model for spike trains

Responses of LGN neurons can be compactly described by a nonlinear model with few parameters (Figure 5.1; Keat et al., 2001). This model has been shown to successfully reproduce responses of LGN neurons to white noise stimuli, including the reliability and precision of spikes. This is only one of several nonlinear models that can produce contrast normalization with fixed model parameters, but it was the only model we tested that also exhibited changes in spike timing (precision and latency) with contrast, as discussed further below.

The model first convolves the stimulus with a linear filter. The generator potential is equal to the convolved stimulus plus noise; the amplitude and time-constant of this noise are defined by the model parameters σ_a and τ_A, respectively. A spike is generated whenever the generator signal crosses a threshold, θ. Each time a

spike occurs, a negative after-potential is added to the generator potential, such that the threshold is crossed repeatedly during sustained excitatory stimuli. The amplitude, time-constant, and variability in the amplitude of the negative after-potential are defined by the model parameters B, τ_P, and σ_b, respectively.

To test the effects of contrast in this model, we used a temporal binary white noise stimulus. The stimulus was shown repeatedly at each of three contrasts. Responses of a model cell to 100%, 33%, and 11% contrast stimuli are shown in Figure 5.2A, 5.2B, and 5.2C, respectively. Responses to all contrasts were generated using a single set of fixed model parameters. In the following sections we will describe the responses of fixed-parameter model cells in terms of contrast normalization and information transmission, as well as the contrast dependence of response reliability, precision, and latency. We will compare the qualitative trends in the model to previous results from real LGN neurons.

Model cells can exhibit contrast normalization

Although this model has fixed parameters at all contrasts, it could exhibit contrast normalization due to its nonlinearity. To measure the gain of the model we fit a linear-nonlinear cascade to the responses at each contrast condition, a method routinely used to characterize gain of visual neurons (Sakai et al., 1995; Chander and Chichilnisky, 2001; Kim and Rieke, 2001; Baccus and Meister, 2002; Zaghloul et al., 2005). Briefly, the data are fit by a filter and an input-output function. The filter is defined as the spike-triggered average, which is taken as an approximation of the stimulus feature to which the neuron is sensitive. The similarity of the stimulus to the

filter is evaluated at each time step of the stimulus; this can be thought of as the stimulus strength. An input-output function is defined as the average probability of spiking as a function of the stimulus strength. Differences in gain at different contrasts can be measured by comparing the amplitudes of the recovered filters (if the input-output function is fixed), or by the recovered input-output functions (if the filter amplitude is normalized). We have analyzed our model responses in both ways.

Here, we show the latter approach in which we scaled all of the model cell's recovered filters to the same amplitude (Figure 5.3A), such that gain changes were contained within differences in the input-output functions. The observed input-output function is steeper for lower contrast stimuli than for higher contrasts (Figure 5.3B). We fit a sigmoid equation to the input-output function at each contrast in order to calculate the gain (see Methods). For this model cell the gain at low, medium, and high contrast is equal to 0.100, 0.079, and 0.054, respectively. Therefore the model cell exhibits contrast normalization, despite the fact that the same parameters were used to generate responses to all contrasts. We note that the model also shows changes in filter shape, to be discussed below.

Next, we simulated model responses using many different sets of parameters (see Methods) to generate a large representative population of model cells. For any given model cell the parameters were fixed for all contrasts. We compared the gain of each model cell at 100% contrast to its gain at either 33% or 11% contrast (Figure 5.4A).

As reported in Chapter 4, for some model cells, the responses showed little or no contrast normalization: the gain was relatively independent of contrast (purple

symbols near thick line). For other model cells, the gain increased by nearly the same factor that the contrast decreased (red triangles near dashed line, and red circles near thin line).

We express the extent of contrast normalization by κ:

$$\kappa = \frac{G_{lower} / G_{higher} - 1}{C_{higher} / C_{lower} - 1} \qquad \text{Eq. 3}$$

where C is the stimulus contrast and G is the gain (Chapter 4). If the gain increases by the same factor that the contrast decreases, the contrast normalization κ is equal to one. If the gain does not change with contrast, the contrast normalization κ is equal to zero. We note that κ could in principle be less than zero (gain paradoxically increased at high contrast) or greater than one (gain increased by more than stimulus contrast decreased), but for real LGN neurons these values are rarely observed.

The population of model cells exhibited a range of contrast normalizations (κ broadly distributed between zero and one (Figure 5.4B). The extent of the contrast normalization depended strongly on the amplitude of the noise added to the convolved stimulus, σ_a (compare symbols of different colors in Figure 5.4A and 5.4B). The dependence of κ on model parameters will be described further below. The model cell population exhibits contrast normalization comparable to the range reported in LGN neurons, (Chapter 4; data reproduced in Figure 5.4A and 5.4B, black symbols).

"Contrast Gain Control" refers to a specific process in the early visual system that has other properties in addition to contrast normalization (Shapley and Victor,

1979). For example, Contrast Gain Control in visual neurons is accompanied by a decrease in latency with increasing contrast. Although we have not explored other features of Contrast Gain Control in detail, we did observe changes in latency with contrast, but see Appendix to Chapter 4. We measured the response latency for all our model cells at each contrast by determining the time of the first peak of the spike-triggered average (see Methods). By this measure, model cells had both shorter latency and shorter duration at higher contrasts (Figure 5.4C, see also Figure 5.2D), consistent with results from neurons (Shapley and Victor, 1978; Benardete et al., 1992; Smirnakis et al., 1997; Chander and Chichilnisky, 2001). Recall that for any given model cell, the linear filter used to generate responses was fixed at all contrasts. Nevertheless the shape of the empirically recovered spike triggered average can change as a function of contrast due to effects of the nonlinearity (Pillow and Simoncelli, 2003).

Effects of contrast and changing coding characteristics on information

We report in Chapter 4 that in LGN neurons, contrast normalization was significantly and positively correlated with the preservation of information transmission across contrasts. For LGN and model neurons with large gain changes, the mutual information between neural responses and the stimulus was relatively constant across contrasts. This did not follow automatically, because information rates depend on details of the spiking response which are not trivially related to the gain of the response. Therefore, it is important to investigate the effect of contrast on the

reliability and precision of responses and to examine how changes in these variables effect changes in information transmission.

Most model cells showed at least some decrease in information transmission at lower contrast (Figure 5.5A and Chapter 4). This might be attributable to changes in spike-count variability and/or temporal jitter of spiking responses. Indeed, the spike-count variability and temporal jitter of LGN responses both increased as stimulus contrast decreased. Though the model we have implemented was designed to replicate the spike-count and spike-timing variability of neural data for any stimulus with the same statistics (including contrast) as the stimulus used to fit the parameters (Keat et al., 2001), it had not been shown whether this model, with fixed parameters, would show similar changes in spike-count variability and temporal jitter with changes in contrast.

We quantified the spike-count variability of model responses to repeated stimuli by calculating the Allan Factor (see Methods). The Allan Factor is high if the spike count is highly variable. We report that in model responses, the spike-count variability increases as the stimulus contrast decreases (Figure 5.5B), as is the case for LGN neurons (Chapter 4). The Allan Factor associated with a Poisson spike train is equal to one. Like LGN cells, the model responses often exhibit sub-Poisson spike-count variability. The supra-Poisson spike-count variability occasionally observed in LGN neurons is likely caused by bursting, which is not replicated by this model.

The temporal precision of model responses degraded as contrast decreased (see Figure 5.2). We measured the jitter in spike timing by the width of the peak in the cross-correlation between responses of consecutive trials (see Methods). As the

stimulus contrast decreased, the temporal jitter increased (Figure 5.5C), as was also found in LGN data (Chapter 4). Our model cells had spike-timing jitter of a few milliseconds, well within the range of values measured under identical conditions from LGN cells. Although the parameter values we tested did not replicate the complete range of temporal jitter observed in the LGN, it remains possible that other parameter combinations could produce more or less jitter than found in these model cells.

In Chapter 4, we reported that the preservation of information was correlated with the extent of contrast normalization for both LGN (R^2=0.67; p<0.01) and model cells (R^2=0.87; p<0.01) (Figure 5.5D). We did not examine whether information was also better preserved when the spike-count variability or temporal jitter remained relatively constant across contrasts.

As before, we calculate the information ratio as the information rate in bits per spike during the lower contrast divided by that at the higher contrast, such that if the information rate is constant across contrasts, the information ratio is equal to one. We compare this to the Allan Factor ratio, which is the Allan Factor at the higher contrast divided by that at the lower contrast. Therefore, if the Allan Factor (spike-count variability) increases as the contrast decreases, the Allan Factor ratio will be less than one. There was a very weak but significant correlation between the Allan Factor ratio and the information ratio for model cells (Figure 5.5E, black symbols; R^2=0.093; p<0.01) and no correlation for LGN cells (Figure 5.5E, red symbols; R^2=-0.10; p=0.46).

Similarly, we calculated the Jitter ratio as the temporal jitter at the higher contrast divided by that at the lower contrast. Therefore, if the jitter increases as the contrast decreases, the Jitter ratio will be less than one. For model cells, the jitter ratio was strongly and significantly correlated with the information ratio (Figure 5.5F, black symbols; R^2=0.85; p<0.01), but for LGN cells, these variables were uncorrelated (Figure 5.5F, red symbols; R^2=0.23; p=0.11).

How model parameters influence contrast normalization

To determine which parameters are important for contrast normalization in the model, we separately varied each parameter holding all other parameters at fixed values (see Methods). We find that the contrast normalization depends most strongly on the generator potential's noise term, σ_a (Figure 5.6E; also compare symbols of different colors in Figure 5.4B). The contrast normalization is also weakly dependent on parameters of the negative after-potential, including its amplitude (B), time constant (τ_P), and noise (σ_b) (Figure 5.6B, 5.6C, and 5.6F, respectively). The mechanism of contrast normalization in the model will be further considered in the Discussion.

Models with fixed parameters exhibit transitory changes

Sensory neurons exhibit transitory changes in their response properties immediately after an abrupt change in contrast. These gradual changes suggest an active adaptation process. We note, however, that transitory effects on the timescale of

integration time of the filter are expected even in a fixed, linear system. Like LGN neurons, our model cells contained a biphasic linear filter that integrated stimuli for up to 100 ms (e.g., see Figure 5.3A). Thus it is not surprising that model cells exhibit smoothing of transitions as well as overshooting and ringing following abrupt changes in contrast (Figure 5.7). In particular, the firing rate overshoots the steady state when contrast changes (Figure 5.7A), and the information rate dips below the eventual steady state particularly for transition from high to medium contrast (Figure 5.7B). Slow changes, on the order of seconds, occur in neurons but not in our model.

Discussion

Contrast normalization without parameter change

Many sensory neurons exhibit contrast normalization. Often this is cast in the vocabulary of adaptation, as if neurons are actively changing their properties in response to the contrast of recent stimuli in order to optimize information coding. Numerous investigations in several systems have searched for these changing properties, including changes in gain of membrane voltage (Sanchez-Vives et al., 2000b; Rieke, 2001; Baccus and Meister, 2002; Kim and Rieke, 2003; Zaghloul et al., 2005), shifts in mean membrane potential relative to threshold (Carandini and Ferster, 1997; Zaghloul et al., 2005), and recruitment of inhibitory circuitry (Chance et al., 2002; Murphy and Miller, 2003; Prescott and De Knoninck., 2003).

We show here that at least one class of model cell with fixed parameters can qualitatively account for contrast normalization across the range observed in LGN neurons. This is consistent with the fact that contrast normalization is rapid or instantaneous in the early visual system (Shapley, 1997). Our results do not establish the mechanisms of contrast normalization in the LGN, but they show that some effects of contrast may arise automatically from either linear filtering or the nonlinear nature of spike generation.

Why do the model cells exhibit contrast normalization?

To understand how contrast normalization arises in this model, we illustrate a short sample of response generation in a model cell in Figure 5.8. For high contrast stimuli (red curves in Figure 5.8), the generator potential $h(t)$ tends to cross threshold

well before the peak of the filtered stimulus *g(t)*. The negative after-potential causes repetitive firing (i.e. *h(t)* crosses threshold again) for the strongest stimulus events. Nevertheless, the cumulative effect of the negative after-potential is to truncate responses, such that the number of spikes during the peak in *g(t)* increases much less than linearly with the size of the peak. The majority of the time bins with supra-threshold values of *g(t)* do not contain spikes. Therefore if we measure the average probability of a spike given *g(t)* in the range indicated by the shaded region, the probability is low (0.067). For low contrast stimuli, on the other hand (blue curves in Figure 5.8), the peaks in *g(t)* are rarely large enough to enter this saturating range, such that the majority of the time bins with supra-threshold values of *g(t)* do contain spikes. If we measure the average probability of a spike given *g(t)* in the indicated range, the probability is higher (0.082). We note that the calculation of the gain depends only on the relation of *g(t)* to spikes (Figure 5.3); the noise and after-potentials included in *h(t)* are unobserved variables in real experiments.

After-potential effect

In this context, we can rationalize the dependence of contrast normalization on model parameters. The after-potential reduces the probability of repeated firing within peaks of *g(t)* and, to a lesser extent, reduces the probability of firing a spike in subsequent peaks of *g(t)*. As we decrease the amplitude or duration of the after-potential, the gain increases at both contrasts, but the effect is larger for high contrast. Therefore the difference in gain becomes smaller, such that contrast normalization decreases (Figure 5.6B and 5.6C). When the after-potential is small and fast

compared to fluctuations of *g(t)*, the responses at both high and low contrast are approximately linear with the size of the peak in *g(t)*, and contrast normalization is low.

Why would this gain change result in equalizing information rates across contrasts? Refractoriness increases reliability in the retina, LGN, and primary visual cortex (Kara et al., 2000), in that the number of spikes elicited during an epoch of repetitive spiking is more reliable when a refractory period is implemented. In our model, as the amplitude and duration of the negative after-potential increase, we expect that the reliability should increase across all contrasts, and indeed we find that the information rate in bits/spike increases (not shown). Still, because epochs of repetitive firing are less common for lower-contrast responses, we do not expect the reliability to increase as much as for higher-contrast stimuli. Therefore it makes sense that the information ratio in bits/spike decreases as the amplitude and duration of the after-potential increase (data not shown).

Sub-threshold Noise

The noise parameter σ_a had by far the strongest correlation with contrast normalization among our model cells. Other modeling results have suggested that a balanced change in both the excitatory and inhibitory background firing rates can serve as a gain control mechanism (Chance et al., 2002). In the context of our model, adding noise to *g(t)* increases the probability that a just-sub-threshold stimulus will evoke a spike in a given trial, but decreases the probability that a just-super-threshold stimulus will evoke a spike. Therefore the gain decreases (the slope of the input-output

function becomes shallower) with noise σ_a. In the low-contrast case, where noise fluctuations are large relative to stimulus-induced fluctuations, this effect is strong and the reduction in gain is large. In the high contrast case, peaks in *g(t)* are often far above and below threshold, so the same amount of noise has less effect on the gain. Consequently, the gains at the two contrasts become more similar, and there is less contrast normalization.

How does this translate to information transmission? For low contrast stimuli, noise can dominate the times of threshold crossings, which decreases the mutual information about the stimulus in bits/spike. For high contrast stimuli the same noise has relatively little effect on the threshold crossings, and thus little effect on information transmission. Thus the low noise condition, where low contrast stimuli can elicit spikes only at very strong peaks in *g(t)*, corresponds to a relatively high information rate at low contrast, at least in bits/spike.

Contrast normalization versus Contrast Gain Control

In the early visual system, contrast normalization is just one aspect of the well-defined phenomenon known as Contrast Gain Control. In addition to normalization, in Contrast Gain Control the dynamics of the cell change with stimulus contrast (Shapley and Victor, 1978, 1981; Victor, 1987; Benardete and Kaplan, 1999; Chander and Chichilnisky, 2001; Kim and Rieke, 2001; Baccus and Meister, 2002; Zaghloul et al., 2005). We generated model responses using a fixed filter at all contrasts and find that the latency of the recovered filters depends on the stimulus contrast (Figure 5.4C). We attribute this to the positive threshold-crossing structure of the model (Figure 5.1),

which effectively introduces a derivative of the filter into the generation mechanism. We have not tested for other hallmarks of Contrast Gain Control and it remains possible that active adaptive mechanisms are required to account for the full observed phenomenon. Additionally, it has been shown that spike-triggered covariance techniques is more accurate than spike-triggered average techniques in recovering the true filter (Schwartz et al., 2002). Therefore, it will be important to determine whether the covariance technique finds the same latency effects reported above.

Transient changes after contrast shifts

Recent research has emphasized the time course of neural characteristics following a change in stimulus contrast. After the stimulus contrast is changed, the firing rate of neurons in the early visual system quickly changes and then gradually converges to their steady-state values (Smirnakis et al., 1997; Brown and Masland, 2001; Chander and Chichilnisky, 2001; Baccus and Meister, 2002; Solomon et al., 2004; Zaghloul et al., 2005). These dynamic changes in firing rate include both a fast and a slow component (Smirnakis et al., 1997; Chander and Chichilnisky, 2001; Baccus and Meister, 2002). The fast component occurs within 100 milliseconds of a change in stimulus contrast (Victor, 1987). The slow component of the firing rate adaptation occurs on the order of 1-10 seconds (Smirnakis et al., 1997; Brown and Masland, 2001; Chander and Chichilnisky, 2001; Baccus and Meister, 2002; Solomon et al., 2004), and this time constant depends on the duration of the contrast periods (Zaghloul et al., 2005). The time constants of the slow component have been related

theoretically to Bayesian optimal strategies for detecting that the contrast has changed (DeWeese and Zador, 1998).

Current research is attempting to isolate which of these firing rate trends would require an adaptive mechanism (Shapley, 1997; Smirnakis et al., 1997; Chander and Chichilnisky, 2001). Intracellular studies in the retina concluded that ganglion cell's spiking generation mechanism adapts to stimulus contrast on the timescales of seconds (Kim and Rieke, 2001; Zaghloul et al., 2005). An increased number of sodium channels become inactive after a high contrast stimulus is presented, resulting in a decreased sensitivity to stimulus fluctuations (Kim and Rieke, 2003).

In the fly motion-sensitive neuron H1, Fairhall et al (Fairhall et al., 2001) showed that information transmission efficiency (in bits/spike) dropped transiently just after a decrease in contrast, recovering gradually. This result was highly suggestive that an active adaptation process is required to restore coding efficiency after a change in stimulus statistics. Moreover, that study showed that both gain change and information optimization occurred within tens of ms, much faster than the firing rate adaptation which was on the order of seconds.

Here we show that a model with no adapting parameters is capable of producing the fast component of firing rate change following a change in stimulus contrast (Figure 5.7A). The biphasic nature of the filter is sufficient to reproduce the over-shooting firing rate observed in visual neurons. The duration of the firing-rate transient is limited by the length of the filter, 50-100 milliseconds. In our model cells, gain changes (not shown) and optimization of information transmission (Figure 5.7B)

both occur on this fast timescale and both occur without any change in model parameters.

The model presented here does not account for the slow firing-rate adaptation observed in retinal ganglion and LGN cells (Smirnakis et al., 1997; Brown and Masland, 2001; Chander and Chichilnisky, 2001; Baccus and Meister, 2002; Solomon et al., 2004). This slow form of firing-rate adaptation has been attributed to a gradual change in cells' baseline membrane potentials (Baccus and Meister, 2002; Solomon et al., 2004). Although the model does not replicate the slow component of firing rate adaptation, this component appears to be uncoupled from contrast normalization and information optimization.

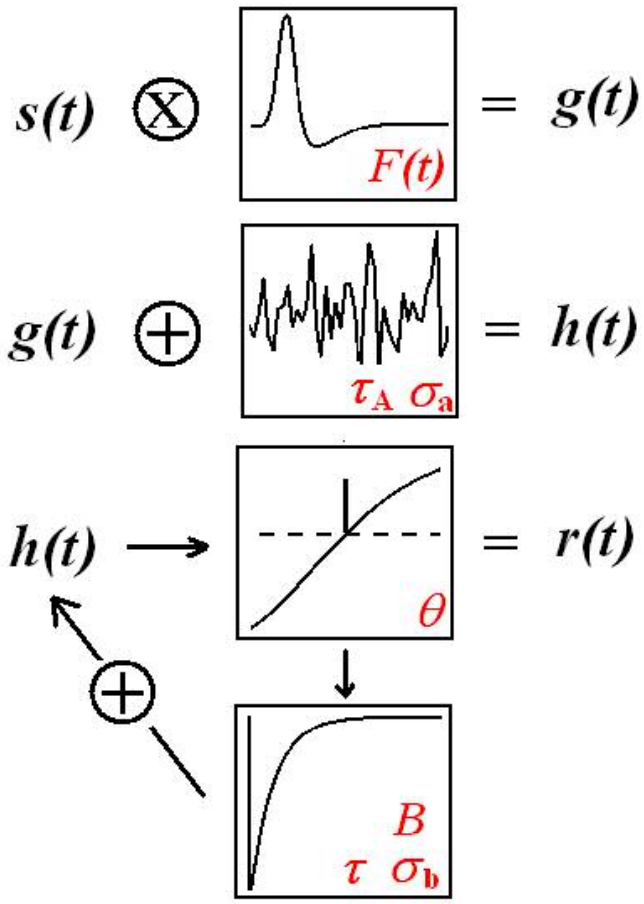

Figure 5.1: Generative model to predict spike trains from stimuli. First row: the stimulus, *s(t)*, is convolved with a filter, *F(t)*, to produce *g(t)*. Second row: a noise signal is added to *g(t)* to produce the generator potential, *h(t)*. The parameters τ_A and σ_a determine the time-constant and amplitude of this noise term. Bottom rows: when the generator potential crosses a threshold, θ, a spike occurs. Each time a spike occurs, a negative after-potential is added to the subsequent generator potential. The parameters B, τ_P, and σ_b determine the amplitude, the time-constant, and variability in the amplitude of the negative after-potential.

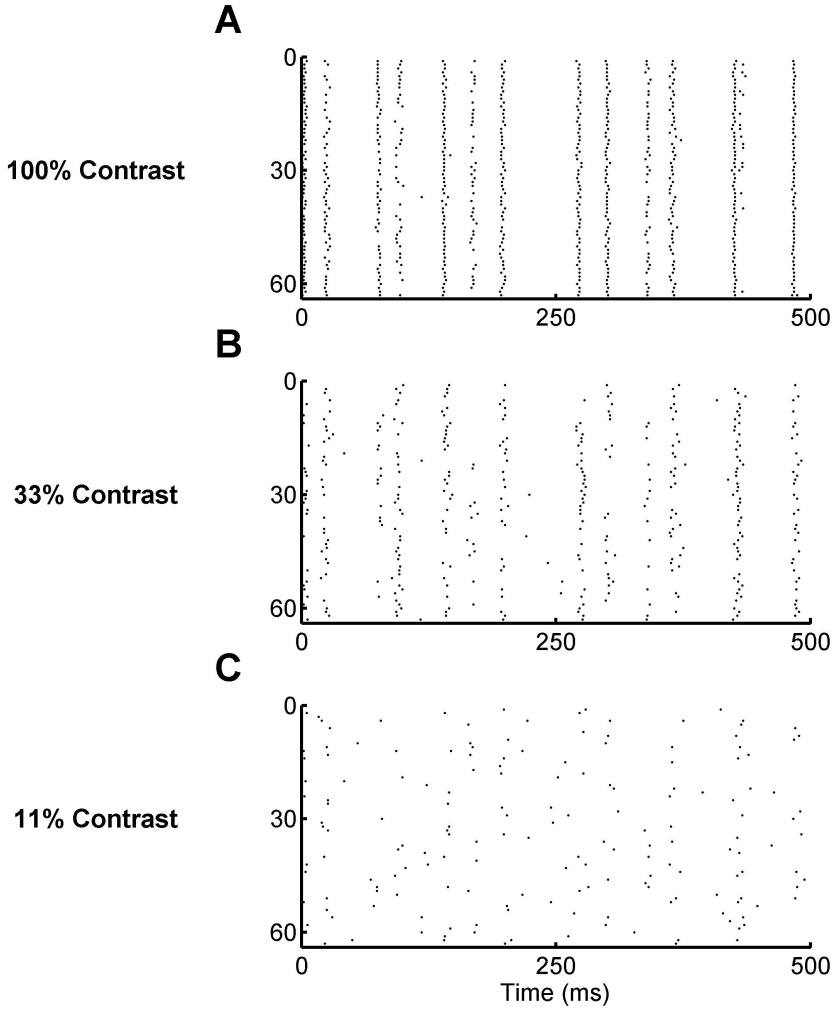

Figure 5.2: Response characteristics from model cell as a function of temporal contrast. Responses of one representative model cell to full-field binary white noise visual stimuli of different contrasts. The parameters for this model cell are: θ =0.4, B=3, τ_P =50, σ_a =0.31, σ_b =0.28, τ_A =20. A, Raster plot for 64 repeats of a repeated stimulus at 100% contrast. Each row represents a trial; each point represents the time of an action potential within that trial. A 500 ms segment from the middle the 5 s trials is shown. B and C, Responses to 64 repeats of the same full-field binary stimulus sequence as in (A), scaled about the mean to 33% and 11% contrast, respectively.

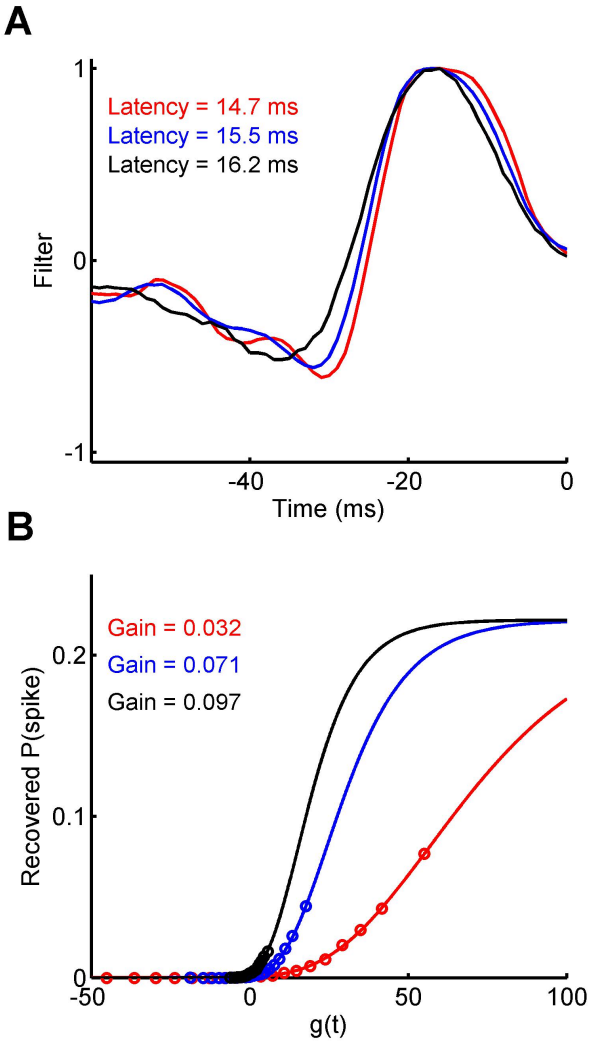

Figure 5.3: Measuring gain from model responses. A, Linear filters from a Linear-Nonlinear cascade, fit to high (red curve) medium (blue curve) and low (black curve) contrast responses from the model cell responses shown in Figure 5.2. The filters were normalized by the amplitude of their first peak. B, Symbols indicate the empirical probability of spiking versus the stimulus strength (see Methods). The points were fit to sigmoid functions (curves). Colors defined as in (A).

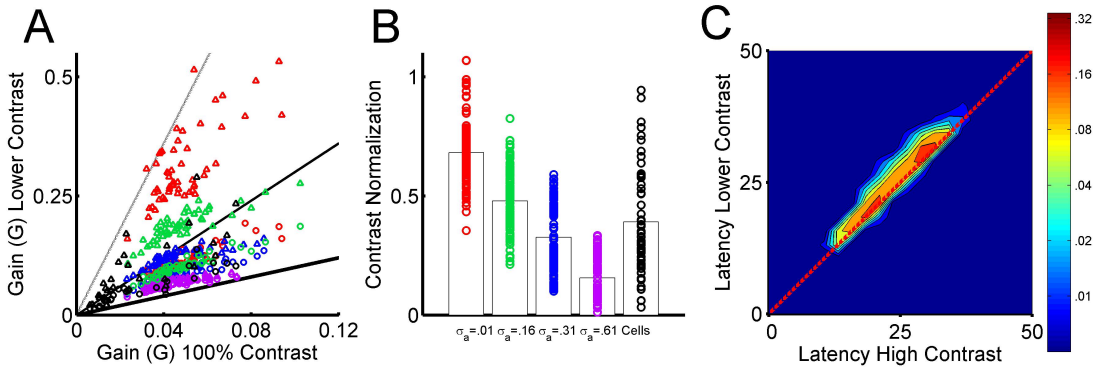

Figure 5.4: Fixed-parameter model cells reproduce range of contrast normalization observed in LGN. A, The gain of each model cell at 100% contrast (horizontal axis) is compared to the gain of the same model cell for 33% contrast (○) and 11% contrast (Δ). In the absence of gain control, gain would be constant (x=y, thick, solid line). Three-fold or nine-fold gain changes correspond to the thin, solid line or the dashed line respectively. Black symbols are data from the LGN, previously published in Chapter 4. Red, green, blue, and purple symbols correspond to model cells in which σ_a was set to 0.01, 0.16, 0.31, and 0.61, respectively. For oth6er parameter values see Methods; for clarity this figure shows results only for θ= 0.2. Results using θ =0.1 show a similar dependence on σ_a. B, Each symbol indicates the contrast normalization (κ, Eq. 3) for a single model cell. Colors as defined in (A). C, Response latency of model cells at 33% or 11% contrast versus 100% contrast for model cells (N=864 including both 100%-33% and 100%-11% comparisons). At each x-y point, the number of model cell results is indicated by color, where red corresponds to the highest density and dark blue to the lowest. The color is scaled as the log of the probability.

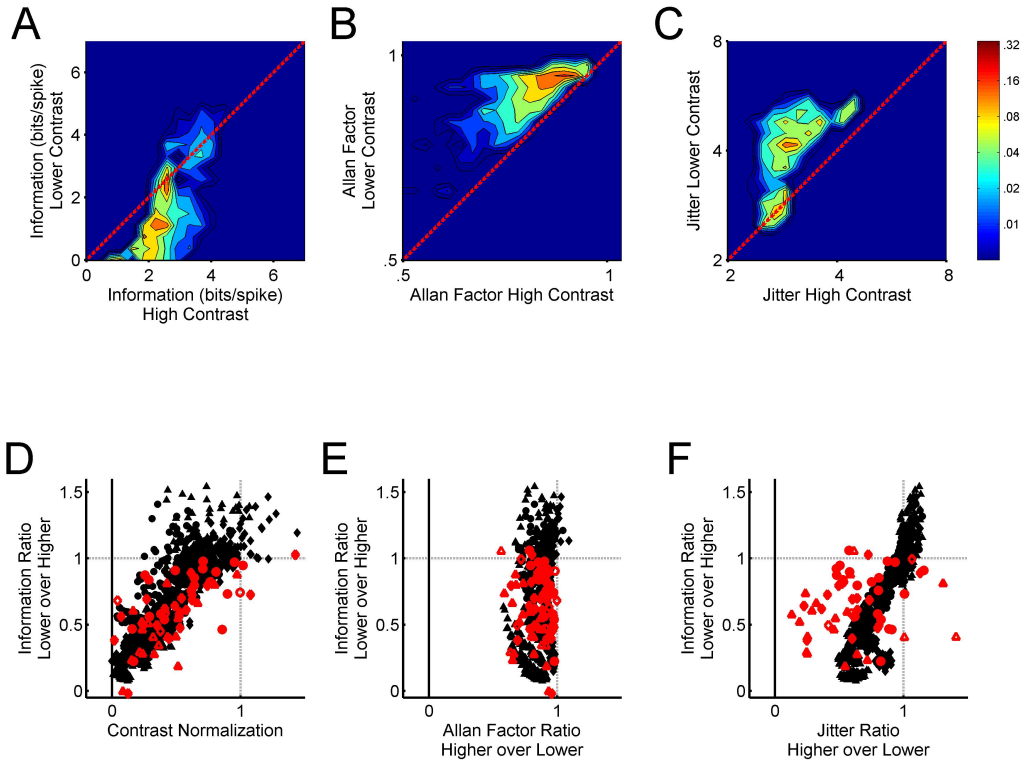

Figure 5.5: Effects of contrast and changing coding characteristics on information. A, The information rate in bits per second at 100% contrast (x-axis) compared to either 33% or 11% contrast (y-axis) for model cells (N=864 including both 100%-33% and 100%-11% comparisons). At each x-y point, the number of model cell results is indicated by color, where red corresponds to the highest density and dark blue to the lowest. The color is scaled as the log of the probability. B, The variability of spike counts at 33% or 11% contrast versus 100% contrast for model cell responses, plotted as in (A). C, Temporal jitter of spike timing at 33% or 11% contrast versus 100% contrast for model cell responses, plotted as in (A). D, The information ratio is calculated as the information (in bits per spike) at the lower contrast divided by that at the higher contrast. Contrast normalization, κ, is as defined in Eq. 3. Each black symbol compares the information ratio to the contrast normalization from responses generated by a model with one set of fixed parameters, evaluated at three different stimulus contrasts. Red symbols are LGN data from Chapter 4. E, The Information ratio versus the Allan Factor ratio, where the Allan Factor ratio is defined as the Allan Factor at the higher contrast divided by that at the lower contrast. Symbols as in (D). F, The Information ratio versus the Jitter ratio, where the Jitter ratio is defined as the jitter at the higher contrast divided by that at the lower contrast. Symbols as in (D).

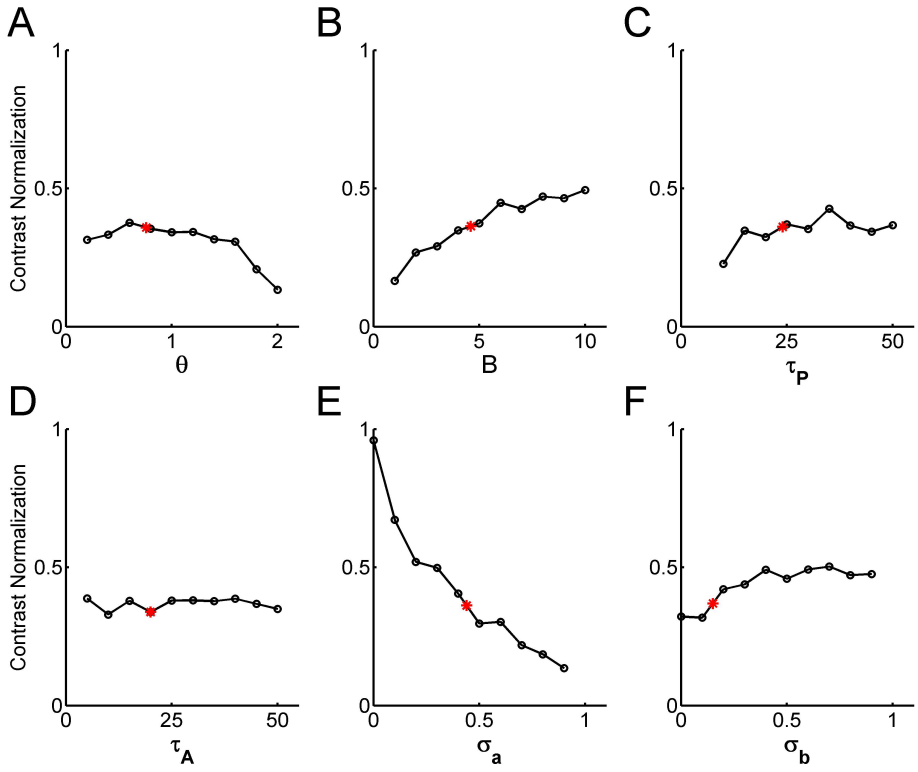

Figure 5.6: Contrast normalization dependence on model parameters. For a reference model cell we used the average parameters for X ON LGN cells as reported in Table 2 of (Keat et al., 2001), which are: θ =0.76, B=4.59, τ_P =24, τ_A =20, σ_a =0.44, and σ_b =0.15. We then varied each one of these parameters separately. The red symbols in each panel show the value along each parameter range that was held constant when other parameters were varied. For each resulting model cell we calculated the contrast normalization from comparison of the responses to high vs. medium contrast. A, Contrast normalization versus the threshold, θ. When the generator potential crosses θ, a spike is elicited. B, Contrast normalization versus the amplitude B of the negative after-potential. C, Contrast normalization versus the time constant τ_P of the negative after-potential. D, Contrast normalization versus the time-constant τ_A of the noise signal that is added to the convolved stimulus. E, Contrast normalization versus the amplitude σ_a of the noise signal added to the convolved stimulus. F, Contrast normalization versus the amplitude σ_b of the noise of the negative after-potential.

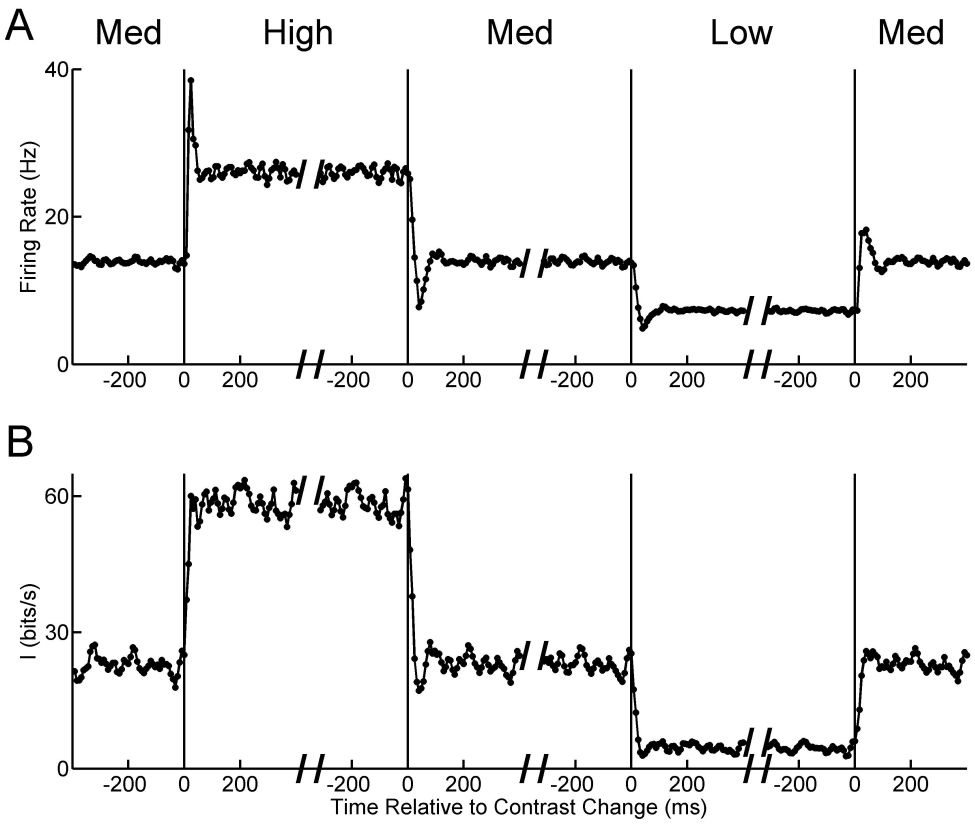

Figure 5.7: Transient changes in model responses following contrast changes. Responses of one model cell (parameters indicated by red points in Figure 6) in a contrast switching experiment. The stimulus consisted of continuous binary white noise that changed contrast every 10 seconds, switching from 100% to 33% to 11% to 33% and then repeating (see Methods). A, Firing rate as a function of time, shown around the times of contrast transitions. B, Information rate in bits per second.

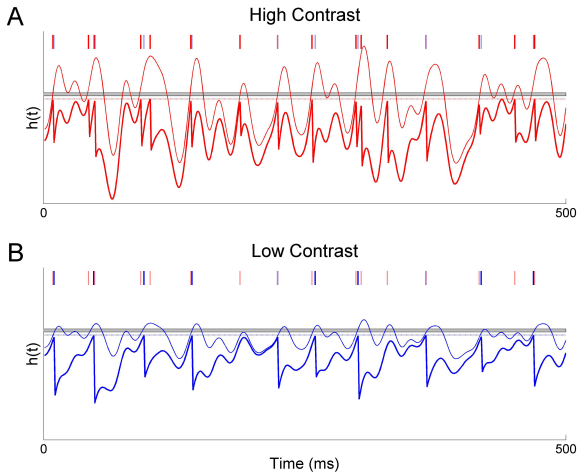

Figure 5.8: Illustration of why the model exhibits contrast normalization. A, The generator potential, *h(t)*, for a high-contrast stimulus from one model cell is shown in the thick red line. The convolved stimulus, *g(t)*, which does not include the negative after-potentials or noise, is shown in the thin red line. Spike times from one trial are shown with the thick, red ticks on top. The thin blue ticks show spike times from the low-contrast stimulus (below), such that spike times can be compared. B, The generator potential, *h(t)*, and the convolved stimulus, *g(t)*, for a low-contrast stimulus are shown by the thick and thin lines, respectively. Spike times for the low-contrast stimulus are shown in the thick blue ticks, while the thin red ticks show the spike times for the high-contrast stimulus.

Chapter 5, in full, is a republication of the material submitted in June of 2006. K.S., Reinagel, P., Contrast adaptation in a non-adapting LGN model. (2006). The dissertation author was the primary investigator and first author of this paper.

Acknowledgements: The authors thank Pamela Magoffin for surgical assistance, Samar Mehta for assistance with spike sorting, and E.J. Chichilnisky for comments on earlier versions of the manuscript. This work was supported by NSF and NSF/IGERT (K.D.) and Alfred P. Sloan Foundation (P.R.).

References

Baccus SA, Meister M (2002) Fast and slow contrast adaptation in retinal circuitry. Neuron 36:909-919.

Benardete EA, Kaplan E (1999) Dynamics of primate P retinal ganglion cells: responses to chromatic and achromatic stimuli. J Physiol 519 Pt 3:775-790.

Benardete EA, Kaplan E, Knight BW (1992) Contrast gain control in the primate retina: P cells are not X-like, some M cells are. Vis Neurosci 8:483-486.

Berry MJ, Warland DK, Meister M (1997) The structure and precision of retinal spike trains. Proc Natl Acad Sci U S A 94:5411-5416.

Borst A, Flanagin VL, Sompolinsky H (2005) Adaptation without parameter change: Dynamic gain control in motion detection. Proc Natl Acad Sci U S A 102:6172-6176.

Brenner N, Agam O, Bialek W, de Ruyter van Steveninck R (2002) Statistical properties of spike trains: universal and stimulus-dependent aspects. Phys Rev E Stat Nonlin Soft Matter Phys 66:031907.

Brown SP, Masland RH (2001) Spatial scale and cellular substrate of contrast adaptation by retinal ganglion cells. Nat Neurosci 4:44-51.

Carandini M, Ferster D (1997) A tonic hyperpolarization underlying contrast adaptation in cat visual cortex. Science 276:949-952.

Chance FS, Abbott LF, Reyes AD (2002) Gain modulation from background synaptic input. Neuron 35:773-782.

Chander D, Chichilnisky EJ (2001) Adaptation to temporal contrast in primate and salamander retina. J Neurosci 21:9904-9916.

DeWeese M, Zador A (1998) Asymmetric dynamics in optimal variance adaptation. Neural Computation 10:1179-1202.

Enroth-Cugell C, Robson JG (1966) The contrast sensitivity of retinal ganglion cells of the cat. J Physiol (Lond) 187:517-552.

Fairhall AL, Lewen GD, Bialek W, de Ruyter Van Steveninck RR (2001) Efficiency and ambiguity in an adaptive neural code. Nature 412:787-792.

Fee MS, Mitra PP, Kleinfeld D (1996) Automatic sorting of multiple unit neuronal signals in the presence of anisotropic and non-Gaussian variability. J Neurosci Methods 69:175-188.

Kara P, Reinagel P, Reid RC (2000) Low response variability in simultaneously recorded retinal, thalamic, and cortical neurons. Neuron 27:635-646.

Keat J, Reinagel P, Reid RC, Meister M (2001) Predicting every spike: A model for the responses of visual neurons. Neuron 30:803-817.

Kim KJ, Rieke F (2001) Temporal contrast adaptation in the input and output signals of salamander retinal ganglion cells. J Neurosci 21:287-299.

Kim KJ, Rieke F (2003) Slow Na+ inactivation and variance adaptation in salamander retinal ganglion cells. J Neurosci 23:1506-1516.

Kohn A, Movshon JA (2003) Neuronal adaptation to visual motion in area MT of the macaque. Neuron 39:681-691.

Liu RC, Tzonev S, Rebrik S, Miller KD (2001) Variability and information in a neural code of the cat lateral geniculate nucleus. J Neurophysiol 86:2789-2806.

Murphy BK, Miller KD (2003) Multiplicative gain changes are induced by excitation or inhibition alone. J Neurosci 23:10040-10051.

Ohzawa I, Sclar G, Freeman RD (1985) Contrast gain control in the cat's visual system. J Neurophysiol 54:651-667.

Pillow JW, Simoncelli EP (2003) Biases in white noise analysis due to non-Poisson spike generation. Neurocomputing 52:109-115.

Prescott SA, De Knoninck Y (2003) gain control of firing rate by shunting inhibition: roles of synaptic noise and dendritic saturation. PNAS 100:2076-2081.

Reinagel P, Reid RC (2000) Temporal coding of visual information in the thalamus. J Neurosci 20:5392-5400.

Rieke F (2001) Temporal contrast adaptation in salamander bipolar cells. J Neurosci 21:9445-9454.

Sakai HM, Wang JL, Naka K (1995) Contrast gain control in the lower vertebrate retinas. J Gen Physiol 105:815-835.

Sanchez-Vives MV, Nowak LG, McCormick DA (2000a) Membrane mechanisms underlying contrast adaptation in cat area 17 in vivo. J Neurosci 20:4267-4285.

Sanchez-Vives MV, Nowak LG, McCormick DA (2000b) Cellular mechanisms of long-lasting adaptation in visual cortical neurons in vitro. J Neurosci 20:4286-4299.

Schwartz O, Chichilnisky EJ, Simoncelli EP (2002) Characterizing neural gain control using spike-triggered covariance. Advance in Neural Information Processing Systems 14:269-276.

Shapley R (1997) Retinal physiology: adapting to the changing scene. Curr Biol 7:R421-423.

Shapley R, Victor JD (1979) The contrast gain control of the cat retina. Vision Res 19:431-434.

Shapley R, Enroth-Cugell C (1984) Visual adaptation and retinal gain control. Progress in Retinal Research 3:263-346.

Shapley RM, Victor JD (1978) The effect of contrast on the transfer properties of cat retinal ganglion cells. J Physiol 285:275-298.

Shapley RM, Victor JD (1981) How the contrast gain control modifies the frequency responses of cat retinal ganglion cells. J Physiol 318:161-179.

Smirnakis SM, Berry MJ, Warland DK, Bialek W, Meister M (1997) Adaptation of retinal processing to image contrast and spatial scale. Nature 386:69-73.

Solomon SG, Peirce JW, Dhruv NT, Lennie P (2004) Profound contrast adaptation early in the visual pathway. Neuron 42:155-162.

Strong SP, de Ruyter van Steveninck RR, Bialek W, Koberle R (1998) On the application of information theory to neural spike trains. Pac Symp Biocomput:621-632.

Victor JD (1987) The dynamics of the cat retinal X cell centre. J Physiol 386:219-246.

Yu Y, Lee T (2005) Adaptive contrast gain control and information maximization. Neurocomputing 65-66:111-116.

Yu Y, Potetz B, Lee TS (2005) The role of spiking nonlinearity in contrast gain control and information transmission. Vision Res 45:583-592.

Zaghloul KA, Boahen K, Demb JB (2005) Contrast adaptation in subthreshold and spiking responses of mammalian Y-type retinal ganglion cells. J Neurosci 25:860-868.

Chapter 6

Concluding Remarks

Work presented here describes how fixed, nonlinear properties in the LGN neuron can help these neurons to encode information about the broad range of visual stimuli. First, we show that the T-type calcium channel present in LGN neurons is de-ianctivated during only a subset of stimuli. In this state, an excitatory stimuli causes the cell to elicit a burst of spikes rather than a single spike. Therefore, distinguishing between these two responses can provide visual information (Chapter 2). Because de-inactivation of the channels require sustained hyperpolarization, a burst response could indicate that an excitatory stimulus occurred after a period of un-excitatory stimuli.

In Chapter 3, we demonstrate why it is important to use our state-information measure rather than other measures that we considered. Further, we show that burst structure depends on the stimulus, such that distinguishing bursts with different numbers of spikes can provide additional visual information. Physiologically, bursts and spikes could be distinguished, because bursts have been shown to be more effective in driving downstream neurons.

Next, we found that LGN neurons exhibit contrast normalization, such that relationship between neurons' firing rates and the stimulus depends on the stimulus contrast. The extent of contrast normalization varied across cells, and we postulated that cells that were characterized by larger contrast normalization would be better able to preserve the information transmitted across contrasts. However, information rates depend on reliability and precision in addition to firing rate, and both of the qualities degrade as the contrast decreases. Still, we found that cells with stronger contrast normalization better preserved their information rates across contrasts (Chapter 4).

Although contrast normalization might be a result of the cell actively adapting to the new contrast, we investigated whether a model with fixed parameters could reproduce the contrast normalization in the LGN. In Chapter 4, we show that the model also exhibits contrast normalization and the associated preservation of information. This suggests that a fixed nonlinearity is sufficient to produce contrast normalization and that this phenomenon provides useful coding advantages.

Contrast normalization is but one characteristic of the classically-described Contrast Gain Control, but in Chapter 5 we show that the model cell responses include yet another characteristic of Contrast Gain Control: the latency of the increases as contrast decreases. Furthermore, we demonstrate that after a change in stimulus contrast, there are transient changes in model cell responses. These results demonstrate that changes in response properties do not imply that neurons actively adapted to changes in contrast. Neurons, instead, appear to be equipped with fixed nonlinear properties that better enable them to encode the variety of stimulus conditions present in natural scenes.